T-3147

ANALYZING INJECTIVITY OF NON-NEWTONIAN FLUIDS: AN APPLICATION OF THE HALL PLOT

by

R. Scot Buell

T-3147

A thesis submitted to the Faculty and the Board of Trustees of the Colorado School of Mines in partial fulfillment of the requirements for the degree of Master of Science (Petroleum Engineering).

Golden, Colorado
Date: 5/16/86

Signed: R. Scot Buell
R. Scot Buell

Approved: Fred H. Poettmann
Fred H. Poettmann
Thesis Advisor

Golden, Colorado
Date: May 16, 1986

Craig W. Van Kirk
Craig W. Van Kirk
Professor and Head,
Department of
Petroleum Engineering

ABSTRACT

The Hall plot was originally developed for the evaluation of waterflood injection wells. It has also been applied to the injection of non-Newtonian fluids, which is quite different from the conditions for which the Hall plot was originally developed. A two-phase numerical reservoir simulator in radial coordinates was developed to model the injectivity of non-Newtonian fluids in porous media. The simulator was used to verify the Hall plot for non-Newtonian fluids. Analytical methods were also used where appropriate to evaluate the injectivity of non-Newtonian fluids. The simulator was applied to hypothetical examples and also used to history match field injectivity data. Based both on the field injectivity data and the hypothetical examples analyzed with the simulator, guidelines are presented for the preparation and analysis of non-Newtonian injectivity data using the Hall plot.

TABLE OF CONTENTS

LIST OF FIGURES

LIST OF TABLES

ACKNOWLEDGMENTS

I thank the Gas Research Institute, Potential Gas Agency, and the Sloan Foundation for their financial support. I thank Dr. Fred Poettmann, who originally suggested and supervised this work. I am indebted to Dr. Hossein Kazemi whose guidance was instrumental to the development of the reservoir simulator. Drs. James Crafton and John Wright were helpful with their comments and suggestions. I wish to thank my parents and my wife for their moral and financial support. Finally, I thank Rebecca and my Bullmastiffs for their patience.

NOMENCLATURE

A = adsorption, milligram/gram

A_m = maximum adsorption, milligram/gram

B = formation volume factor, dimensionless

c = compressibility, psi^{-1}

C = polymer concentration, PPM

C_s = wellbore storage coefficient, ft^3/psi

e = 2.718282, dimensionless

f_w = fractional flow of water, dimensionless

F_c = inacessible pore volume factor, dimensionless

g = gravitational constant, 32.2 ft/sec^2

h = formation thickness, feet

k = absolute permeability, md

k_r = relative permeability, dimensionless

k_{wi} = initial virgin absolute permeability to water, md

K = consistency index for power law fluid, cp

K_a = adsorption coefficient, ppm^{-1}

L = hole depth, feet

m = slope of the Horner or injection plot, psi/cycle

m_H = slope of the Hall plot, (psia-days)/barrel

M = mobility ratio, dimensionless

n = rheological slope parameter, dimensionless

N_{ca} = Capillary number, dimensionless

N_e = Ellis number, dimensionless

p = pressure, psia

p_{cwo} = capillary pressure, water-oil, psi

p_e = pressure at the external drainage radius, psia

p_i = initial reservoir pressure, psia

p_{wf} = bottomhole injection pressure, psia

p_s = surface tubing pressure, psia

q = rate, barrels/day

Q = cumulative injection, barrels

R_{rf} = residual resistance factor, dimensionless

R_f = resistance factor, dimensionless

r = radius, feet

r_{b1} = radius, bank one, feet

r_{b2} = radius, bank two, feet

r_e = external drainage radius, feet

r_w = wellbore radius, feet

S = saturation, dimensionless

s = skin, dimensionless

T = transmissibility, $feet^5/lbf\text{-}day$

t = time, days or hours

u = interstitial velocity, feet/day

v = Darcy velocity, feet/day

Greek Symbols

Δp_f = pressure loss due to friction, psi

γ = shear rate, s^{-1}

$\Gamma(x)$ = Gamma Function, $\int_0^\infty t^{x-1}e^{-t}\,dt, \quad x>0$

γ_r = rock specific gravity, dimensionless

λ = Carreau rheological parameter, sec

Π = 3.141593, dimensionless

ρ = fluid density, lbm/ft^3

ϕ = porosity, dimensionless

σ = surface tension, dynes/cm

τ = shear strss, $dynes/cm^2$

θ_t = characteristic fluid time, sec

μ = viscosity, cp

μ_a = apparent viscosity, cp

μ_e = effective viscosity, cp

μ_∞ = apparent viscosity at an infinite shear rate, cp

μ_0 = apparent viscosity at zero shear rate, cp

Subscripts

c = capillary pressure

d = displacing phase

e = external drainage radius

e = effective viscosity

i = initial, investigation

o = oil

p = injection time or polymer

r = relative permeability

w = water, wellbore radius

wf = injecting pressure at r_w

wi = water initial

ws = shut in pressure at r_w

CHAPTER 1

INTRODUCTION

Aqueous polymer and micellar solutions are currently used for the enhanced recovery of oil from porous media. Polymer floods, micellar-polymer floods, and injectivity or productivity profile modification treatments are the most common applications of polymer and micellar solutions. The behavior of polymer and micellar solutions in porous media is complex because the solutions have non-Newtonian rheological properties. Adsorption/retention and permeabilty reduction also occur with polymer and micellar solutions, which also cause additional complexities. Polymer solutions tend to deviate more from Newtonian behavior than micellar solutions. There are usually other phases present beside polymer, such as oil, which are an additional complication.

The interpretation of injection pressures and rates associated with polymer and micellar solution injection are important to the efficient application of the solutions. In theory, the determination of reservoir plugging, fracturing, fluid viscosity changes, and permeability changes can be made from the fluid pressures and rates. The economic success of enhanced oil recovery projects is very dependent on how rapidly additional oil recovery occurs. The rate of

oil recovery is directly related to the rate of enhanced recovery fluid injection. Therefore, it is essential that injectivity be maintained at optimum rates to ensure the economic success of enhanced oil recovery projects. The Hall plot (Hall 1963) is a useful tool for evaluating performance of injection wells.

The Hall plot is one method for analyzing injection pressures and rates. It was originally developed for single phase, steady state, radial flow of Newtonian liquids. Since the advent of polymer and micellar solutions for enhanced oil recovery, the Hall plot has also been applied to the injection of these solutions. Several of the assumptions made in the original development of the Hall plot are violated for polymer and micellar solutions. The Hall plot was not derived for non-Newtonian or multiphase flow. When polymer and micellar solutions flow through porous media, adsorption and retention occur which reduces permeability. In addition, the flow of the fluids is non-Newtonian. Multiphase flow may also occur. This work will verify the validity of the Hall plot for the injection of polymer and micellar solutions. The Hall plot is a steady-state approach, and is therefore not valid for transient flow conditions. However, it will be demonstrated in Chapter 6 that the transient period is relatively short for

most polymer and micellar solution injection situations, and therefore does not significantly influence the Hall plot.

Because of the complex nature of polymer and micellar solution flow through porous media, exact analytical solutions are generally not possible. However, some relatively simple approximate analytical solutions can be developed. To realisticly analyze polymer or micellar solution injection, a two-phase, radial, numerical, reservoir simulator was developed. The simulator includes the following phenomena and effects: transient and steady state flow, two-phase (oil-aqueous phase) flow, non-Newtonian rheology, adsorption/retention, residual resistance factors, concentration effects, skin, and well bore storage. The simulator is designed to consider all the important phenomena and effects which occur when polyacrylamide or polysaccharide polymer solutions are injected in porous media. It should be noted that the interfacial phenomena occurring when micellar solutions are injected are not considered in the simulator. Even with this simplification, the simulator still does an adequate job as will be shown in Chapter 5.

The simulator was used to history match several field injectivity data sets. Once a good history match was obtained, the in-situ viscosities and resistance factors are

known. If the Hall plot is a valid method for analyzing injectivity of polymer and micellar solutions, it should be possible to calculate permeabilities, resistance factors, and in-situ viscosities from the Hall plot which closely agree with those found in the reservoir simulation history match. This is the methodology which was employed to verify the Hall plot.

This thesis is composed of six chapters. Chapter 2 develops the physical relations which exist when non-Newtonian solutions flow through porous media. The mathematical representations of the phenomena is given where appropriate. The following physical relations are discussed in Chapter 2: rheology, adsorption/retention, shear rate-velocity relations, polymer degradation, resistance factors, and inaccessible pore volume. Chapter 3 reviews alternatives to the Hall plot for analyzing injection well pressure data for both Newtonian and non-Newtonian fluids using falloff tests, type curves, and reservoir simulation. The Hall plot is derived in Chapter 4. Chapter 4 also develops simple approximate analytical methods for injection of non-Newtonian solutions based on theoretical considerations. Chapter 5 presents the results from the simulator for three wells. Two of the wells are field tests and one is a hypothetical example. Various methods of

integrating the Hall plot are presented. Simulator results are compared with the approximate analytical solutions. Chapter 6 presents conclusions regarding the validity of the Hall plot and the best methods of preparing and analyzing the Hall plot.

Appendix A presents the development of the reservoir simulator which forms the basis for the history matching and conclusions. The equations used in the simulator are presented and then given in finite difference form. The procedure for solving the finite difference equations, and the assumptions and limitations of the simulator are reviewed. Methods used to test and verify the simulator are also presented. Appendices B, C, and D summarize the data used in the three wells simulated. To understand how injection well analysis fits into the operational scheme in enhanced oil recovery, a brief review of polymer and micellar-polymer flooding follows.

1.1 Polymer Flooding

Polymer flooding is often referred to as an improved waterflooding process. Polymer flooding is quite similar to waterflooding, the principle difference being that the injected fluid has been made more viscous by a high molecular weight polymer. The increase in viscosity of the

injected fluid improves the mobility ratio. Some polymer solutions reduce permeabilty, which also improves the mobility ratio. The mobility ratio is defined in equation (1.1), where "d" denotes the displacing phase.

$$M = \frac{k_d k_{rd} \mu_o}{k_o k_{ro} \mu_d} \qquad (1.1)$$

It should be noted that when adsorption/retention occurs, as with polymer, that k_d may not be equal to k_o. An improvement (reduction) in the mobility ratio results in increased areal and vertical sweep efficiency. It is primarily through improved sweep efficiency that polymer flooding recovers additional oil. Figure 1.1 illustrates the relation between mobility ratio and areal sweep efficiency.

In general, polymer flooding does not significantly reduce residual oil saturation. Polymer flooding does not mobilize large amounts of residual oil, making recoveries from polymer flooding relatively small as a percentage of the remaining oil-in-place when compared with other enhanced oil recovery processes.

There are two polymer types which are in wide use in enhanced oil recovery. One polymer is synthetic polyacrylamide, which is typically used in concentrations of

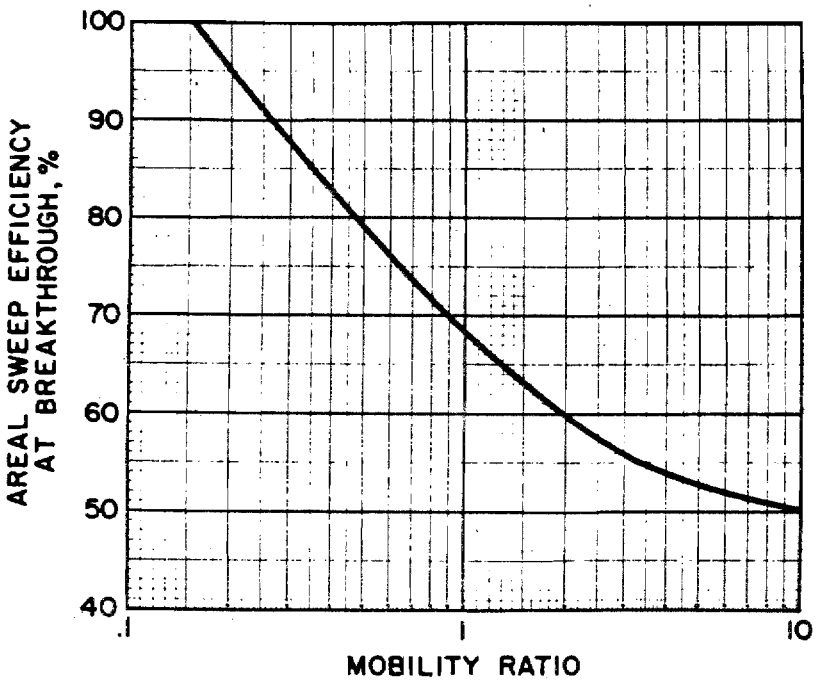

Figure 1.1

Areal Sweep Efficiency at Breakthrough, Five-Spot Pattern

(Craig, F. F., 1971, The Reservoir Engineering Aspects of Waterflooding, Society of Petroleum Engineers, Dallas, p.122)

250 to 2000 ppm in aqueous solutions. The mean molecular weight of polyacrylamide is usually on the order of several million. The standard deviation and the mean of the molecular-weight frequency-distribution significantly influences the properties of the polymer. In general narrow (small standard deviation) molecular weight distributions are desired. Polyacrylamide typically has about 30 percent hydrolysis, and is thus referred to as partially hydrolyzed polyacrylamide (PHPA). PHPA improves the mobility ratio by increasing viscosity and by permeability reduction. The second and less commonly used polymer is polysaccharide, the biopolymer made from xanthan gum. Biopolymers do not significantly reduce permeability, but do decrease the mobility ratio primarily by increasing the displacing phase viscosity.

1.2 Micellar-Polymer Flooding

Micellar solutions are typically composed of a petroleum sulfonate, water, a cosurfactant (usually an alcohol), a hydrocarbon, and electrolytes or salts. The micellar solution is usually displaced by a mobility buffer, i.e., a polymer solution. Figure 1.2 illustrates the micellar-polymer displacement process. The mobility buffer is then displaced by water. The micellar solution is capable of solubilizing fluids it contacts. A micelle on

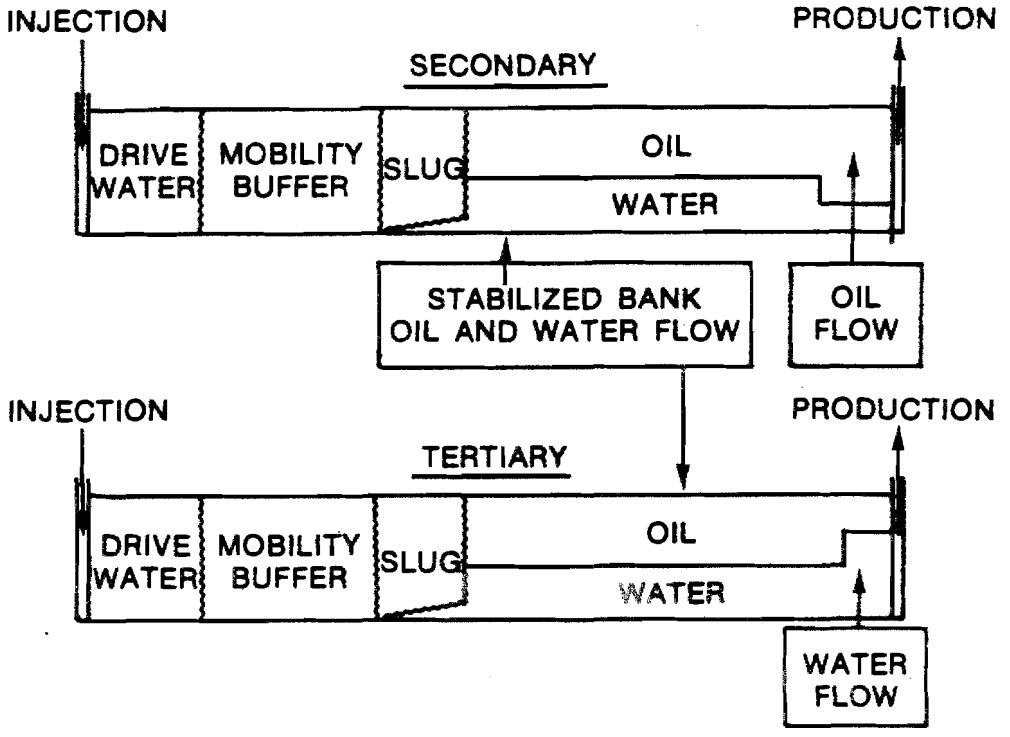

Figure 1.2

Microemulsion Flooding

(Poettmann, F. H., 1983, Improved Oil Recovery, Interstate Oil Compact Commission, Oklahoma City, p. 175.)

the order of 10^{-8} meters in size when it has solubilized a fluid (Poettmann 1983). When the fluids contacted by the micellar solutions are solubilized, the micellar polymer flood is, in effect, a miscible displacement process. After dissipation of the micellar slug, it may no longer miscibly displace the contacted fluid, but will instead immiscibly displace the fluids at greatly reduced interfacial tension. A significant reduction in interfacial tension will also mobilize large amounts of residual oil. The amount of residual oil left by a displacement process is related to the capillary number. The higher the capillary number, the less the residual oil saturation. It can be seen from equation (1.2) that a large reduction in interfacial tension can greatly increase the capillary number.

$$N_c = \frac{v\mu}{\sigma} \qquad (1.2)$$

Micellar-polymer flooding, in contrast to polymer flooding, has the ability to greatly reduce residual oil saturations. Micellar-polymer flooding has the capability to produce large portions of the remaining oil in place by improved vertical and areal sweep efficiency and by reducing residual oil saturations.

CHAPTER 2

BEHAVIOR OF NON-NEWTONIAN SOLUTIONS IN POROUS MEDIA

2.1 Rheological Models

A Newtonian fluid exhibits constant viscosity for steady-state, isothermal shearing, which means for any shear rate the viscosity does not change. Throughout this work all processes are assumed to be isothermal, so changes in temperature do not cause changes in viscosity. The classical definition for a Newtonian fluid is given in equation (2.1).

$$\tau = \mu \frac{dv}{dx} \tag{2.1}$$

The term dv/dx is referred to as the shear rate, and will be denoted by γ from here on. The viscosity of a Newtonian fluid is μ. For non-Newtonian fluids, the apparent viscosity is not constant, but a function of shear rate. Polymer solutions used in enhanced oil recovery are aqueous solutions. Concentrations of polymer also affect viscosity. In general, increasing concentration results in increased apparent viscosity, all other things remaining equal. Micellar solutions can form oil or water external emulsions and liquid crystals. The concentration of surfactants and cosurfactants, and the structure of the micellar solution influence the apparent viscosity. The viscosities of

polymer and micellar solutions are a function of both composition and shear rate. Figure 2.1 illustrates the relation between a Newtonian fluid and various types of non-Newtonian fluids. The majority of polymer and micellar solutions applied in enhanced oil recovery are pseuodoplastic (shear thinning). This means that most polymer solutions have less viscosity at higher shear rates.

There are three rheological models which have been widely used to describe polymer and micellar solutions. The models are the Ostwald-de Waele, Ellis, and Carreau, each named after the respective developer. It should be remembered throughout the discussion of the rheological models that follow, that all model parameters are functions of concentration. The Ostwald-de Waele is more commonly known as the power law. The Ostwald-de Waele is a two-parameter model and the Ellis is three-parameter model. The Carreau model is based on four parameters. The theoretical basis for each of these models is weak, and it is appropriate to think of them as empirical models.

2.1.1 Ostwald-de Waele Model

The most popular rheological model used in enhanced oil recovery is Ostwald-de Waele. The model is given in equation (2.2).

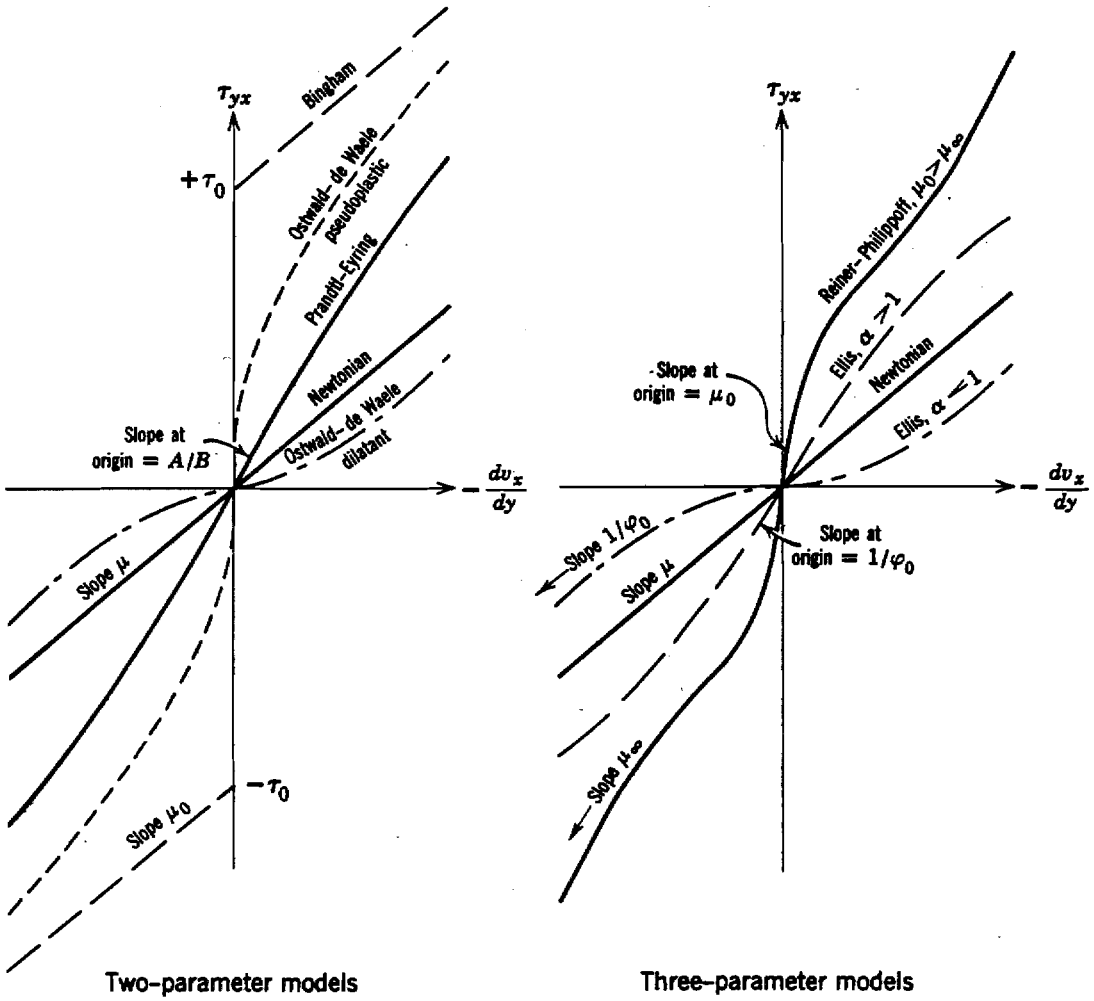

Figure 2.1

Rheograms for Some Non-Newtonian Rheological Models

(Bird, R. Byron; Stewart, Warren E.; and Lightfoot, Edwin N., 1960, Transport Phenomena, John Wiley, New York, p. 10.)

$$\tau = K \gamma^n \tag{2.2}$$

The coefficient, K, is referred to as the consistency of the fluid. The larger the value of K the more viscous the fluid. The exponent n is a quantitative measure of the degree of non-Newtonian behavior; the larger the deviation from 1.0, the more non-Newtonian the fluid behavior. Pseudoplastic fluids have n values between zero and 1.0, while dilatant fluids have n values larger than 1.0.

For most reservoir engineering computations, the apparent viscosity of the non-Newtonian fluid is the value required. Apparent viscosity can be defined for a non-Newtonian fluid by equation (2.3).

$$\tau = \mu_a \gamma \tag{2.3}$$

where μ_a is the apparent viscosity at a particular shear rate. For a pseudoplastic fluid, μ_a will decrease with increasing shear. By substituting equation (2.3) into equation (2.2), the apparent viscosity for a power law fluid can be defined by equation (2.4).

$$\mu_a = K \gamma^{n-1} \tag{2.4}$$

For flow-through porous media, it is sometimes useful to define an effective viscosity for use in a modified Darcy's law. It should be noted that effective and apparent viscosities are not the same. Apparent viscosity is the shear stress divided by the shear rate at any point on a

rheogram. Effective viscosity is defined so as to satisfy some form of Darcy's law. The definition of effective viscosity is different for each rheological model, while the definition of apparent viscosity is always given by equation (2.3) regardless of the rheological model. The effective viscosity is a constant for power-law fluids at any shear rate and is defined (Chistopher and Middleman 1965) as

$$\mu_e = (K/50)\ (12/n)^n\ (150k\phi)^{(1-n)/2} \qquad (2.5)$$

The modified Darcy's law can be written as in equation (2.6) for power-law fluids.

$$v = \left[\frac{k\ \Delta p}{\mu_e\ L}\right]^{1/n} \quad \text{power law fluids} \qquad (2.6)$$

Both Vogel and Pusch (1981) and Huh and Snow (1985) have pointed out that the power law model is inadequate to describe accurately the rheology of polymer solutions. One of the obvious problem with the power law is that as the shear rate approachs zero, the apparent viscosity approaches infinity. This is an unrealistic result for polymer and micellar solutions. At very low shear rates, real polymer and micellar solutions have finite viscosities. Figure 2.2 illustrates the rheological behavior of a real polymer solution. Because of the problems as discussed above, the power law is not considered to be a suitable rheological model to have in the reservoir simulator.

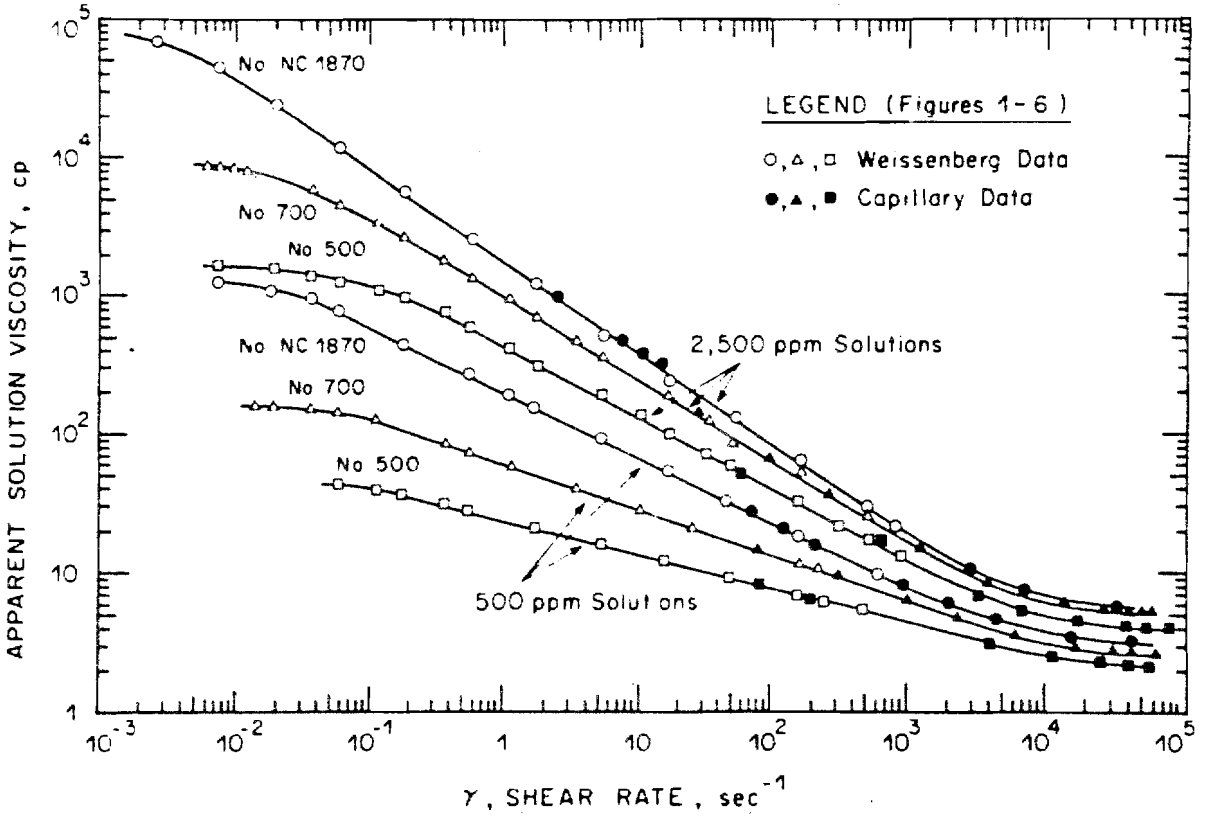

Figure 2.2

Apparent Viscosities of Polyacrylamide Solutions

(Mungan, Necmittin, 1972, "Shear Viscosities of Ionic Polyacrylamide Solutions," Society of Petroleum Engineers Journal, December, p. 471)

2.1.2 Ellis Model

The Ellis rheological model overcomes some of the short-comings of the power law model. The Ellis rheological model is given in equation (2.7).

$$1/\mu_a = (1/\mu_0)[1+ (\tau/\tau_{1/2})^{n-1}] \qquad (2.7)$$

The slope of the power law region is given by n-1. The coefficient μ_0 corresponds to the viscosity at zero shear, and $\tau_{1/2}$ is shear stress where the apparent viscosity has dropped to half of μ_0. Sadowski and Bird (1965) developed a relation for effective viscosity for use in Darcy's law. The effective viscosity for an Ellis fluid is given in equation (2.8).

$$1/\mu_e = 1/\mu_0 \ (1 + (4/(n+3))(\tau_{rh}/\tau_{1/2})^{n-1}) \qquad (2.8)$$

The coefficient τ_{rh} is equal to $R_h\Delta p/L$, where R_h is the mean hydraulic radius. A form of Darcy's law can also be written for the Ellis model using effective viscosity, as shown in equation (2.9).

$$v = \frac{k \ \Delta p}{\mu_e \ L} \qquad \text{Ellis fluids} \qquad (2.9)$$

The general form of the Ellis model is not very convenient for reservoir simulation. To be consistent with other models, it is preferable to have the apparent

viscosity defined in terms of shear rate rather than shear stress. For computational convenience in the reservoir simulator, rather than using the Ellis model directly, a small modification to the power law will result in a rheological model which is quite similar to the Ellis model. Below some specified shear rate, the power law has a constant viscosity. It is this modification of the power law that is used for Ellis fluids in the simulator. The Ellis model still has some shortcomings when applied to real polymer and micellar solutions. As can be seen in Figure 2.2, polymer solutions have a limiting viscosity at very high shear rates. Both Ellis and power law fluids approach zero viscosity at high shear rates.

2.1.3 Carreau Model

The rheological model which most accurately matches the behavior of polymer solutions is the Carreau model (Carreau 1968). The apparent viscosity of Carreau fluid is given by equation (2.10).

$$\mu_a = \mu_\infty + (\mu_0 - \mu_\infty)\,[1 + (\lambda\gamma)^2]^{(n-1)/2} \qquad (2.10)$$

The coefficient, n-1, is the slope of the power law region for a Carreau fluid, μ_0 is the viscosity at zero shear, and μ_∞ is the viscosity at infinite shear. The intersection of the zero shear viscosity and the power law

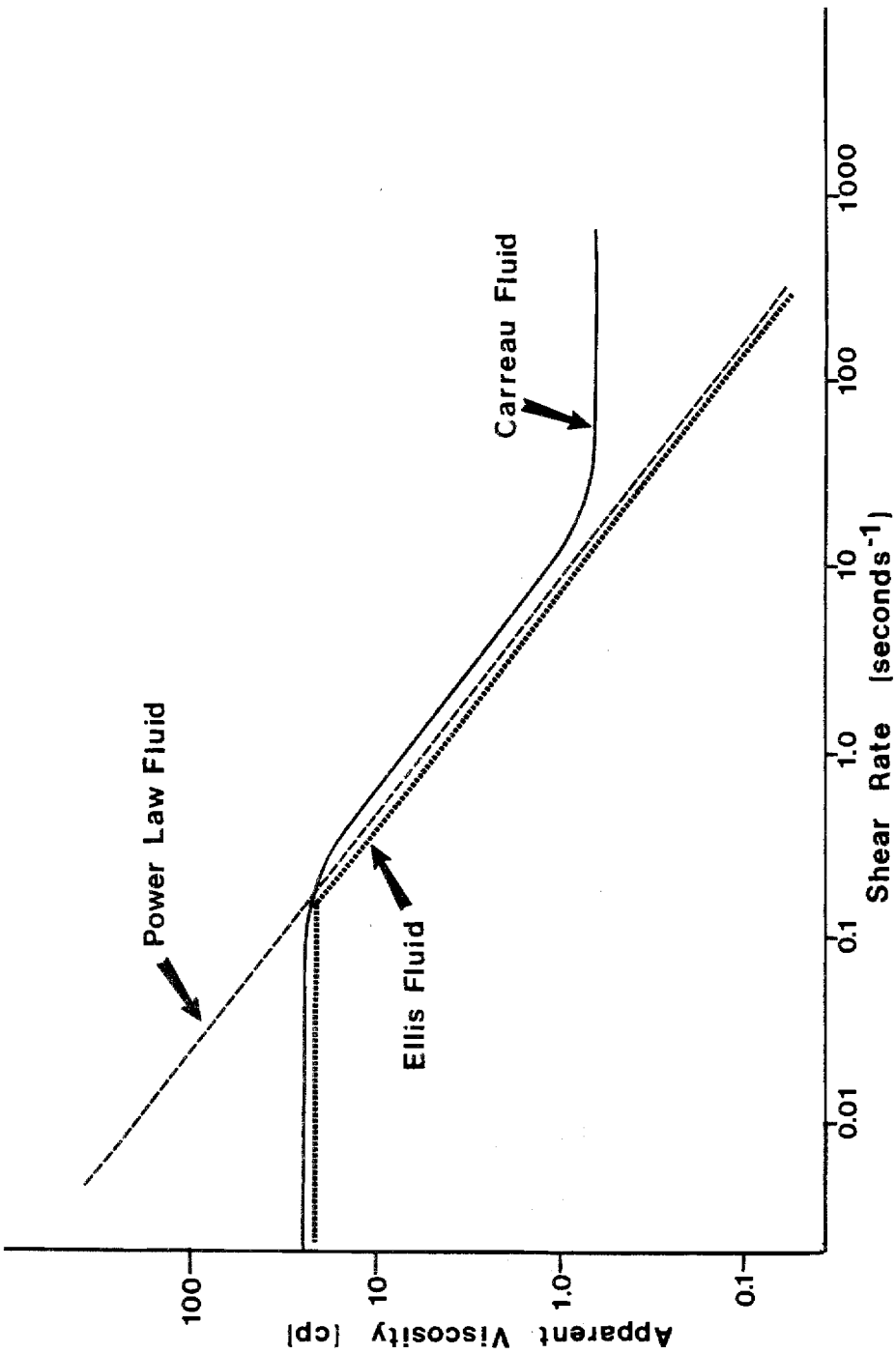

Figure 2.3

Apparent Viscosities as a Function of Shear Rate for Some Rheological Models

region occurs at $1/\lambda$. Figure 2.3 compares the curve shapes for a pseudoplastic fluid using the power law, modified power law, and the Carreau models. It can be seen that the curve shape generated by the Carreau model compares most favorably with the behavior of real polymer solutions as illustrated in Figure 2.2. The Carreau model is the recommended rheological model for polymer and micellar solutions. However, the modified power law (Ellis) is an available rheological option in the program.

It is not possible to easily define an effective viscosity for a Carreau fluid. However, it is possible to write Darcy's law if a shear-rate, velocity relationship is used. For equation (2.11) Savins's (1969) shear-rate, velocity relation was used, this relation is discussed in section 2.2.

$$v = \frac{k}{\mu_\infty+[\mu_0-\mu_\infty]\{1+(\lambda(v/(k\phi)))^2\}^{n-1/2}} \frac{\Delta p}{L} \quad \text{Carreau fluids} \qquad (2.11)$$

2.1.4 Viscoelastic Effects

The rheological models described above assume viscometric flow; that is, no-time dependent elastic effects are considered. If the fluid relaxation time is small compared with the time of deformation, no elastic effects will be observed. The deformation time is approximated by

time required to pass through a constriction in the porous media. The fluid relaxation time is the time required for a fluid to recover from a deformation. Relaxation time is a function of shear and normal stresses and the modulus of elasticity of the fluid. When elastic forces start to become significant in comparison to viscous forces, this is referred to in the literature as the viscoelastic effect. The importance of viscoelastic effects are best determined from the Ellis number, which is defined in equation (2.12).

$$N_e = \frac{\theta_t}{D_p/u} = \frac{\text{characteristic fluid time}}{\text{characteristic flow time}} \qquad (2.12)$$

Characteristic fluid time (θ_t) relations have been published by several researchers, including Truesdell (1964) and Marshall and Metzner (1967). The variable D_p is the diameter of the particles for a packed bed. Viscoelastic effects become significant when N_e exceeds 0.10. The onset of viscoelastic effects results in increased apparent viscosity of polymer and micellar solutions. Viscoelastic effects offset the shear thinning behavior of pseudoplastic fluids. A model to consider viscoelastic effects explicitly is not included in the reservoir simulator. A convenient method to include viscoelastic effects is to input the polymer or micellar solution apparent viscosity in a table as a function of interstitial velocity and

concentration. The simulator can then model viscoelastic effects, even though a rigorous theoretical treatment of viscoelastic effects is not built into the simulator. If the information is available, the input of apparent viscosity as function of interstitial velocity and concentration into the simulator is the most accurate. Laboratory measurements are usually required to generate this data.

2.2 Shear Rate - Interstitial Velocity Relations

The previous section discussed rheological models used in the simulator in terms of shear rates. To apply the rheological models, it is necessary to determine some representative shear rate within the porous media. A number of researchers have published equations that relate interstitial velocity to shear rate. Savins (1969) derived a shear rate-interstitial velocity relation based on a capillary model, which is given in equation (2.13).

$$\gamma = \frac{\phi\, u}{2.828\ (C' k \phi)^{1/2}} \qquad (2.13)$$

The variable u is interstitial velocity and C′ is a constant that varies between 25/12 and 2.5. Gogarty (1967) developed a relation using statistical fit of laboratory data. Gogarty flowed surfactant stabilized water in hydrocarbon dispersions (micellar solutions) through

consolidated sandstone cores to develop his relation. The Gogarty equation is

$$\gamma = \left[\frac{b\,u}{f(k)\ (k/\phi)^{1/2}}\right]^{y} \qquad (2.14)$$

where f(k) is defined as

$$f(k) = m \log\ (k/k_r) + p \qquad (2.15)$$

The constants m and p must be determined for the particular fluid system. The constants B and y must be determined for the particular reservoir rock. Because of the four constants to be determined based on laboratory measurements, the Gogarty equation cannot be applied unless core flow experiments are conducted.

Jennings, Rogers, and West (1971) presented a shear rate-interstitial velocity relation based on a capillary bundle, given in equation (2.16).

$$\gamma = \frac{u}{[1/2\ (K/\phi)]^{1/2}} \qquad (2.16)$$

Chistopher and Middleman (1965) developed a relation for power law fluids based on the Blake-Kozeny equation:

$$\gamma = \frac{3n + 1}{4n}\ \frac{12\ u\ \phi}{(150\ k\phi)^{1/2}} \qquad (2.17)$$

The constant, 12, was determined for a packed bed of uniform spheres; for consolidated porous media the constant is typically taken as 50. The Christopher-Middleman equation

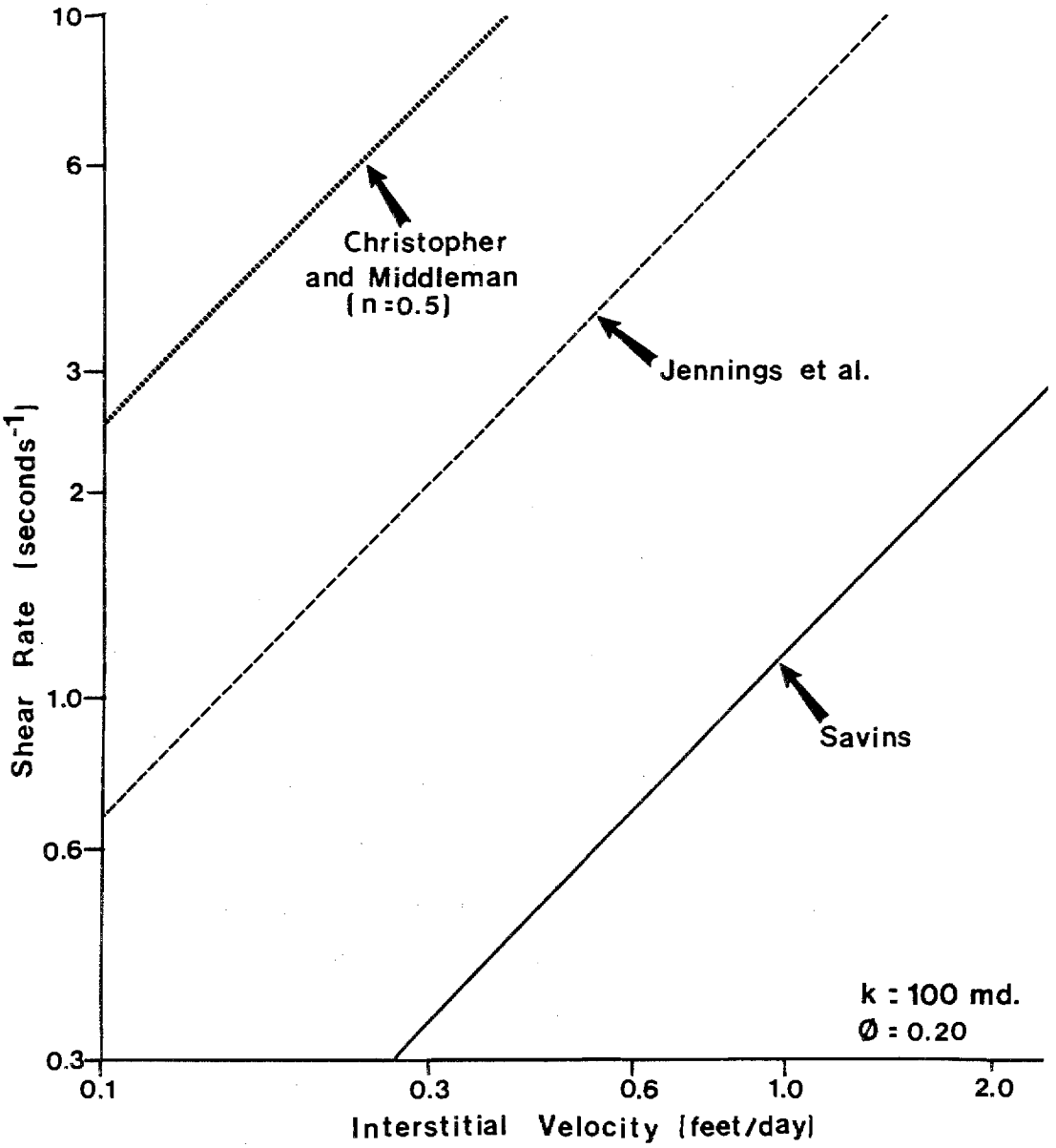

Figure 2.4

Comparison of Shear Rate-Interstitial Velocity Relationships

(2.17) was derived specifically for power law fluids. For a Carreau fluid, it is necessary to use equations (2.13), (2.14), or (2.16). To date there has been nothing published on the subject of which relation yields the most accurate results. The Gogarty equation is probably the most accurate, since it is based on a fit of laboratory data. However, laboratory data is rarely available. Figure 2.4 compares the Savins, Jennings, et al., and the Christopher and Middleman equations. It can be seen in Figure 2.4 that for a given interstitial velocity, the calculated shear rate can vary considerably depending on the relation used.

2.3 Degradation

Degradation, when referring to polymer solutions, means a loss of screen factor and viscosity. The screen factor is defined as the time it takes for the fluid to flow through five 100-mesh stainless screens divided by the time it takes for water to flow through the same screens. The screen factor is a good measure of mechanical degradation. There are four principle types of polymer solution degradation: mechanical, thermal, chemical, and microbial.

Microbial degradation occurs only with the polysaccharides since they have a biologic origin. Polyacrylamides do not experience microbial attack. Microbes present in the injected water simply eat the

polymer. If the polymer is consumed by microbes, there is obviously a loss of viscosity. A well designed polymer application will inhibit microbes using some type of biocide. The removal of oxygen from the injected fluid will also help to minimize microbial attack.

Thermal degradation occurs rapidly for polyacrylamide above 200°F, and for polysaccharide above 160°F. These temperatures are considered to be the safe limit for the application of these polymers (Poettmann 1985). Even at temperatures below the safe limit, there will be some loss of viscosity over a period of weeks and months. Thermal degradation is greatly accelerated by the presence of oxygen, microbes, and divalent ions.

Chemical degradation can occur because of the presence of calcium, sodium, and iron cations. Oxygen and an acidic pH will also accelerate chemical degradation. Polyacrylamide is much more sensitive to cations than is polysaccharide. Polyacrylamide is much more sensitive to divalent cations than to monovalent cations. An acidic pH will greatly reduce viscosity. The result of chemical degradation is to ball up the polymer molecules and reduce viscosity (Chauveteau 1981). To obtain maximum viscosity the polymer chain has to be fully extended.

Mechanical degradation occurs at high pressure

gradients, which causes the polymer molecules to be ripped apart. Polyacrylamide is very sensitive to shear degradation; polysaccharide is not. A number of researchers have published critical shear rate relations. When the critical shear rate is reached, some percentage of the screen factor or viscosity has been lost. The critical shear rate is often set at the point where ten percent of the screen factor has been lost. Maerker (1975, 1976), Seright (1980), Morris and Jackson (1978) have published relations to predict when shear degradation begins. The best way to limit shear and mechanical degradation is by limiting the pressure gradients.

As can be seen from the discussion above, there are many other factors, determining viscosity besides concentration and shear rate. It has been assumed for simplicity that the parameters in the rheological model have been appropriately adjusted for all types of degradation. If the viscosity is defined in a tabular form as a function of interstitial velocity, the appropriate corrections for degradation are also assumed to be made. It should be obvious that these assumptions do not take into account the fact that all types of degradation can be functions of both space and time.

2.4 Adsorption - Retention

When polymer and micellar solutions flow through porous media, some of the polymer or sulfonate will become trapped or lost to the rock. There are three basic causes of losses: adsorption, mechanical entrapment, and hydrodynamic entrapment. Figure 2.5 illustrates mechanical entrapment and adsorption. When mechanical entrapment occurs, the polymer is actually physically trapped. Hydrodynamic entrapment occurs because the pressure gradient in the region of the molecules keeps them trapped.

Adsorption is a surface phenomenon, and is usually modelled with a Langmuir adsorption isotherm. The form of the Langmuir adsorption isotherm is given below.

$$A = \frac{K_a \, C \, A_m}{1 + K_a C} \tag{2.18}$$

The variable A is the amount of adsorption. The coefficient A_m is the maximum amount of adsorption that will occur. The variable C is the concentration, and K_a is a constant. Adsorption is normally expressed in micrograms per gram of rock or in pounds per acre foot of reservoir. Figure 2.6 illustrates a typical adsorption isotherm.

Since data on the various polymer loss mechanisms are usually not available, it is difficult to determine exactly how much each mechanism is contributing to polymer and

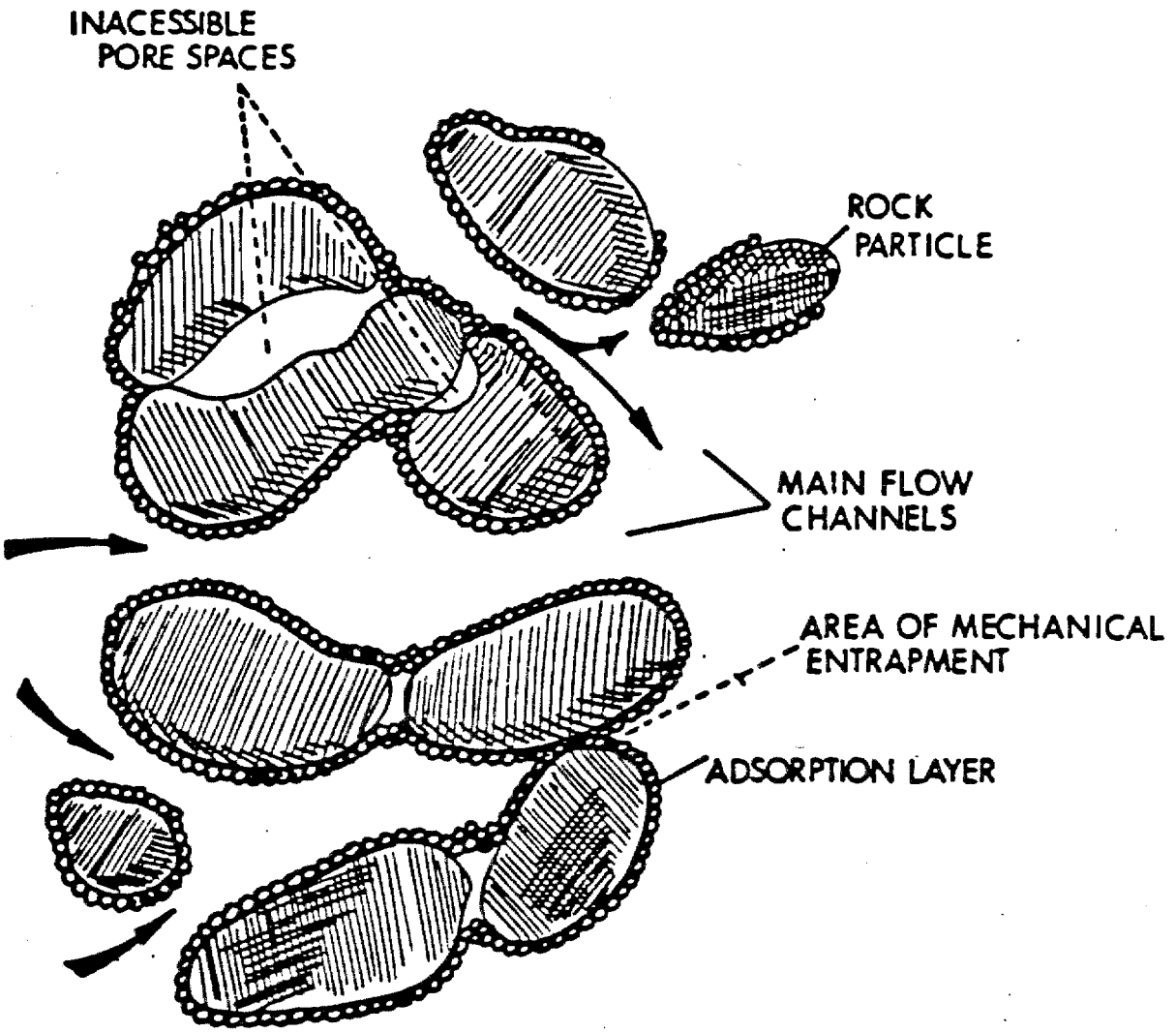

Figure 2.5

Polymer Adsorption and Mechanical Entrapment

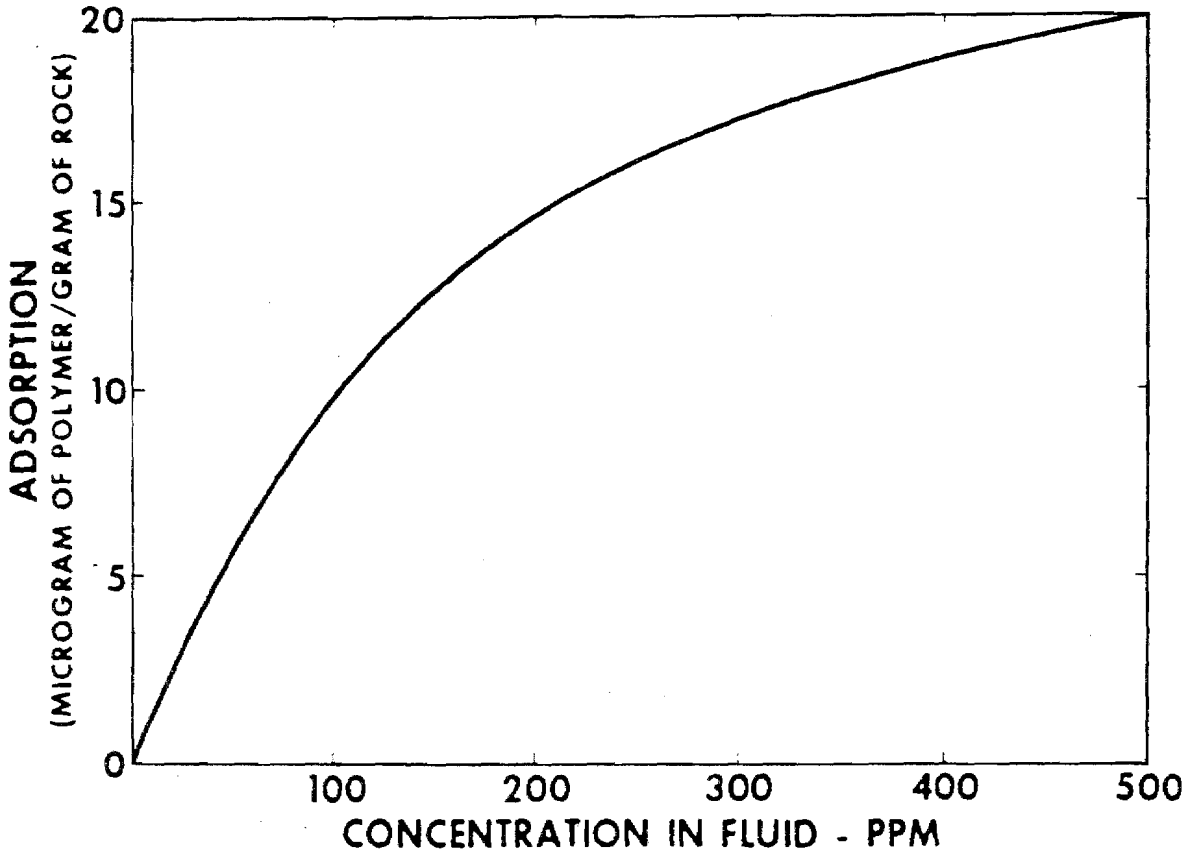

Figure 2.6

Langmuir Adsorption Isotherm

(Dawson, Rapier and Lantz, Ronald B., 1972, "Inaccessible Pore Volume in Polymer Flooding," Society of Petroleum Engineers Journal, October, p. 450)

micellar solution loss. Adsorption and hydrodynamic and mechanical entrapment are therefore, lumped together. Cohen and Christ (1986) have developed an experimental method to distinguish polymer loss due to adsorption versus mechanical and hydrodynamic losses. The Cohen and Christ procedure has been applied to packed sand beds only, and not formation cores. Their experiments on sand packs indicated that 35 percent of the polymer losses were due to adsorption and 65 percent of the polymer losses were due to mechanical and hydrodynamic effects. For computation in the simulator, all polymer losses can be lumped into the Langmuir adsorption isotherm, or polymer loss can be input in a tabular form as a function of concentration. All polymer and micellar solution losses are assumed to occur instantaneously; that is, thermodynamic equilibrium is assumed to be attained immediately.

Adsorption/retention losses of polymer can range from 25 to 500 pounds per acre foot, while sulfonate may exhibit losses up to 1500 pounds per acre foot. Mungan (1969), Hirasaki and Pope (1974), and Cohen (1983) have published results of polymer adsorption studies. Polyacrylamides adsorb much more than polysaccharides (Castagno 1984). All losses to the reservoir rock are also assumed to be irreversible. While some desorption of surfactants may

occur, in reality the amount is usually small. The desorption of polymer is also insignificant (Fanchi 1984). When adsorption and retention occur, the permeability of the rock is reduced. The consideration of permeability reduction is discussed in the next section.

Adsorption/retention denudes the polymer solution or micellar slug of polymer or surfactant at the flood front. Because of the denuding at the flood front, the polymer or surfactant concentration will eventually be reduced to zero at the flood front. Adsorption/retention delays the time to breakthrough of polymer or surfactant.

2.5 Resistance Factors and Residual Resistance Factor

Resistance factors are used to measure the combined change in mobility due to viscosity and permeabilty effects. The resistance factor is defined in equation (2.19).

$$R_f = \frac{\text{Mobility of Water}}{\text{Mobility of Polymer}} = \frac{(k_w k_{rw})/\mu_w}{(k_p k_{rp})/\mu_p} \qquad (2.19)$$

The relative permeability of the water and polymer solution is usually assumed to be the same. The absolute permeability to polymer can be quite different from the absolute permeability of water, due to adsorption. The resistance factor can be related to the improvement in the mobility ratio. Improvement in the mobility ratio increases

conformance as shown in Figure 1.1.

A measure of the permeability alteration due to adsorption and retention of polymer and sulfonate is the residual resistance factor. The residual resistance factor is defined in equation (2.20).

$$R_{rf} = \frac{\text{Water mobility before polymer}}{\text{Water Mobility after polymer}} = \frac{(k_{wi}\ k_{rwi})}{(k_{wp}\ k_{rwp})} \qquad (2.20)$$

The viscosity of water can be omitted from this computation since it remains constant before and after polymer injection. The relative permeabilities are usually assumed to be the same before and after polymer injection. The residual resistance factor is then the ratio of absolute permeabilites before and after polymer injection. For computational purposes in the reservoir simulator, R_{rf} is taken to be a linear function of adsorption/retention, as shown in equation (2.21).

$$R_{rf} = 1 + (R_{rf-max}-1)(A/A_m) \qquad (2.21)$$

The constant R_{rf-max} is the maximum amount of permeability reduction attainable. It should be noted that the amount of permeability reduction is not necessarily the same for oil as it is for the aqueous phase. Equation (2.21) would then be written for each phase if the amount of permeability reduction was different. For a polysaccharide,

R_{rf-max} is quite close to 1.0; for a polyacrylamide the R_{rf-max} may be as high as 15.0. Using equation (2.21), it is possible to calculate the amount of permeability reduction for a given amount of adsorption/retention.

2.6 Inaccessible Pore Volume

The term inaccessible pore volume is considered by many to be a misnomer, but it is a term that has gained common usage. Dawson and Lantz (1974) were the first to propose the inaccessible pore volume theory. Dawson and Lantz prepared cores by flooding the cores with polymer solutions until the effluent concentrations had stabilized, which indicated no more adsorption/retention was occurring. It was neccesary to have no adsorption/retention occurring in the rock because adsorption/retention slows the propagation of the polymer flood front, since the rock strips polymer from solution. They then flooded the cores, in which all adsorption/retention had been completed, and observed that if a polymer solution was prepared with salt water, the polymer breakthrough would occur before the breakthrough of the salt in the water solvent. Dawson and Lantz concluded that the interstitial velocity of the polymer is greater than that of the water solvent. The higher interstitial velocity of the polymer was attributed to a reduced flow area for the polymer molecules because of their larger size.

That area unavailable to flow for the polymer is called the inaccessible pore volume.

While this phenomenon was originally attributed to inaccessible pore volume, it is now recognized that it is also due to several other phenomena. Lecourtier and Chauveteau (1984) have proposed a pore wall exclusion theory based on thermodynamic considerations to account for the higher interstitial velocity of the polymer. Other researchers have also proposed theories to explain this phenomenon.

In terms of reservoir simulation, the inaccessible pore volume only modifies the polymer flow equation. The inaccessible pore volume factor, denoted by F_c, is equal to 1.0 less the pore volume fraction which is not accessible to polymer. F_c takes on values less than one and increases the interstitial velocity of the polymer. For all cases in this study, F_c has been set to 1.0; that is, the velocity of the polymer has not been increased. The option exists however, to make F_c less than 1.0, and increase polymer velocity.

CHAPTER 3

ALTERNATIVES TO THE HALL PLOT FOR ANALYZING INJECTION WELLS

3.1 Falloff Testing

Falloff tests record the transient pressure behavior of injection wells. A falloff test consists of shutting in an injection well and observing the decrease in pressures as a function of time. The pressures in a falloff test are usually measured down hole at the injecting interval. The method of analysis for Newtonian fluid injection is the same as that used in the buildup analysis of producing wells, except that there are some sign changes. Nowak and Lester (1955) were the first to develop the mathematical expressions for Newtonian fluid injection. They based their development on the work of Horner (1951) and Van Everdingen (1953), and derived equation (3.1).

$$p_{ws} - p_i = \left[\frac{70.6\ qB\mu}{k\ h}\right]\left\{E_i\left(-\frac{948\ r_w^2\phi\mu c}{k\ \Delta t}\right) - E_i\left(-\frac{948\ r_w^2\phi\mu c}{k\ (\Delta t+t_p)}\right)\right\} \qquad (3.1)$$

Equation 3.1 is for analyzing the infinite-acting, transient period, following shutin after an injection period. The value Δt is the time since shutin, and t_p is the injection time. The usual method of analysis of falloff and buildup

tests is the Horner plot which can be developed from equation (3.1). The recorded pressures are plotted versus Horner time, where Horner time is $(t_p+\Delta t)/\Delta t$, on semi-logarithimic scales. The slope of the straight line portion of the plot is defined by equation (3.2).

$$m = \frac{162.6\ qB\mu}{k\ h} \tag{3.2}$$

The sign convention that injection is positive will be used throughout the thesis. The skin factor from the Horner plot can be determined from equation (3.3).

$$s = 1.151\left\{ \left(\frac{P_{wf(\Delta t=0)} - P_{ws(\Delta t)}}{m}\right) + \log\left(\frac{\phi\mu c_t r_w^2}{k\ \Delta t}\right) + \log\left(\frac{t_p + \Delta t}{t_p}\right) + 3.23 \right\} \tag{3.3}$$

The term $\log\{(t_p+\Delta t)/t_p\}$ is usually negligible and omitted. Injection wells can also be tested by measuring injection pressures when injection is commenced from a stabilized condition. This is analogous to the drawdown in producing wells, and will be referred to as a injection test for injection wells. The injection test can be analyzed by plotting the flowing bottom hole pressure versus the logarithim of time. Equation (3.2) still applies to the straight line portion of the injection test but the skin

factor is calculated using equation (3.4).

$$s = 1.151 \left\{ \left(\frac{p_{wf(\Delta t)} - p_i}{m} \right) + \log\left(\frac{\phi \mu c_t r_w^2}{k \, \Delta t} \right) + 3.23 \right\} \qquad (3.4)$$

The analytical equations (3.1)-(3.4) are developed in detail in the well testing literature (Matthews and Russell 1967; Earlougher 1977; Smith 1978; Lee 1982). The equations as discussed above are valid for the time period when the reservoir is still infinite acting during both the injection and shut-in periods, i.e. the transient has not yet reached the drainage radius. The equations assume the wellbore storage period is over. It is also assumed in these equations that the reservoir is homogeneous and there is single phase, Newtonian flow. Equations (3.1)-(3.4) are useful for testing and verifying the reservoir simulator as shown in Appendix A.

Researchers have also developed analytical expressions for transient, non-Newtonian, single-phase liquid flow. Odeh and Yang (1979) and Ikoku and Ramey (1979, 1980) have developed analytical expressions for the transient pressure behavior when power law fluids are injected in porous media. Van Poollen and Jargon (1969) were some of the first researchers to investigate transient non-Newtonian flow in porous media. Odeh and Yang derived the following partial differential equation for the flow of power law liquids

through porous media.

$$\frac{\partial^2 p}{\partial r^2} + (1 - 1/n)\,\frac{1}{r}\,\frac{\partial p}{\partial r} = r^{1/n} B\,\frac{\partial p}{\partial t} \tag{3.5}$$

B is defined in equation (3.6).

$$B = \frac{\mu_{eff}\phi^{(1 + 1/2n)}c_h^{1/n}}{k^{(1 - 1/2n)}\,q^{(1/n)}} \tag{3.6}$$

Odeh and Yang solved equation (3.5) for an injection test, assuming a single, homogeneous, power-law fluid bank extending to the drainage radius. The result is given in equation (3.7).

$$p_{wf} = p_i + \left[\frac{70.6\,q\mu}{k\,h}\right]\left[\frac{n^{(2n-1)/(2n+1)}\,(2n+1)^{2/(2n+1)}\,t^{1/(2n+1)}}{\Gamma\{2n/(2n+1)\}\;r_w^{(1/n)}\;B^{1/(2n+1)}} - n\right] \tag{3.7}$$

Where $\Gamma\{x\}$ is the gamma function. For injection tests a plot of p_w-p_i versus $t^{1/(2n+1)}$ will yield a straight line with a slope given by equation (3.8).

$$m = \left[\frac{1}{2\pi\;\Gamma(2n/2n+1)}\right]^{2n+1} \left[\frac{\mu_{eff}^{2n}\,q^{(2n-1)}\,n^{(2n-1)}\,(2n+1)^2}{(hk)^{(2n-1)}\,c}\right]^{1/(2n+1)} \tag{3.8}$$

The slope of the straight line portion of the plot for a

falloff test with a power law fluid is also given by equation (3.8). The falloff test is plotted with $(p_{ws}-p_{wf})$ versus $[(t+\Delta t)^{1/(2n+1)} - \Delta t^{1/(2n+1)}]$. Since the in-situ value of n is usually unknown, it is usually necessary to iterate on the value of n until a straight line is obtained. It can be seen that this procedure would become rather time-consuming if attempted by hand. Ikoku and Ramey went through a development which is quite similar to that of Odeh and Yang, although their results are in a slightly different form. The work of Ikoku and Ramey and Odeh and Yang both assume there is single-phase flow of a power law fluid. While their work is theoretically correct, it is often difficult to unambiguously apply it to field data sets. Their work also fails to account for multiphase flow and multiple fluid banks.

The falloff and injection test provide information on the reservoir at an instant in time, since most of the transient data is obtained over less than a day for polymer and micellar solution injection. The Hall plot, in contrast, provides information about the reservoir on a continuous basis. However, to effectively apply the Hall plot it is necessary to have information that is best obtained from a falloff or injection test. For example, the Hall plot can identify a combined change in transmissibility

and skin factor, but cannot identify how each has changed. For water injection, the transmissibility usually remains relatively constant, but the skin factor may change. Polymer and micellar solution injection may change both the transmissibility and skin factor. It is therefore necessary to run an injection or falloff test periodically to determine the skin factor and transmissibility. It is then possible to determine how each parameter is changing from the Hall plot.

3.2 Type Curves

Type curves accomplish the same result as the falloff or injection test. Rather than making a Horner or injection plot, the field data is compared with dimensionless plots. For non-Newtonian fluids, a dimensionless non-Newtonian pressure is usually plotted versus a non-Newtonian dimensionless time to generate a type curve. The field pressures are then matched with the type curve. Based on a match point, it is possible to calculate various reservoir or fluid parameters. Lund and Ikoku (1980) and Gencer and Ikoku (1984) presented type curves for non-Newtonian /Newtonian composite reservoirs. Vongvuthipornchai and Raghavan (1984) presented type curves for the injection of power-law fluids into vertically fractured wells. Vongvothipornchai and Raghavan (1985) also presented type

curves for wells dominated by skin and storage. The type curves are an alternative method of analyzing injection and falloff data. However, additional complexities can be considered in the type curve approach that are not considered in falloff and injection test analysis methods of the previous section. If a suitable type curve is available, parameters obtained from a type curve match can effectively complement the Hall plot.

3.3 Reservoir Simulation

Reservoir simulation can be used to predict and history match the performance of a reservoir when non-Newtonian solutions are injected. When a suitable history match is obtained with field data, the simulator parameters should reflect the in-situ reservoir parameters. Reservoir simulation has the distinct advantage of considering all important phenomena occurring when non-Newtonian fluids are injected into the reservoir. The assumptions which are made in the analytical solutions and type curves often do not reflect what occurs in the field. Uniform polymer concentrations, no adsorption, and specific rheological models are the assumptions typical of the analytical and type curve solutions for non-Newtonian fluid injection. These types of assumptions are usually invalid for field

injectivity situations, and are not necessary in reservoir simulations. In general, reservoir simulations have the potential to more accurately determine reservoir parameters than type curves and analytical solutions. The principle disadvantage of reservoir simulation is that it is by far the most time and capital intensive of the analysis techniques. Also, a reservoir simulator may not always be available.

Bondor, et al., (1973) presented one of the first reservoir simulators for polymer flooding. Huh and Snow (1985) presented a simulator that will automatically find a "best fit" history match. Fanchi (1985) developed a reservoir simulator for the Department of Energy to simulate polymer and micellar polymer flooding. Where appropriate, the simulator developed in this study has drawn on the simulation work done by these authors.

CHAPTER 4

DEVELOPMENT AND ANALYSIS OF THE HALL PLOT

4.1 Derivation and Development of the Hall Plot

A less common way to analyze injectivity data is the Hall plot. The Hall plot was originally proposed to analyze the performance of waterflood injection wells (Hall 1963). Hall simply used Darcy's law for steady-state flow of a well centered in a circular reservoir, which is given in equation (4.1). Equation (4.1) also assumes single phase, Newtonian flow. Hall integrated both sides with respect to time (equation [4.2]) to obtain equation (4.3).

$$q = \frac{kh\,(p_{wf} - p_e)}{141.2\,B\mu\,(\ln(r_e/r_w) + s)} \tag{4.1}$$

$$\int q\,dt = \frac{kh\,\int(p_{wf} - p_e)dt}{141.2\,B\mu\,(\ln(r_e/r_w) + s)} \tag{4.2}$$

$$Q = \frac{kh\,\int(p_{wf} - p_e)dt}{141.2\,B\mu\,(\ln(r_e/r_w) + s)} \tag{4.3}$$

Separating the integral of equation (4.3), Hall then rearranged equation (4.4) to get equation (4.5).

$$Q = \frac{kh}{141.2\,B\mu\,(\ln(r_e/r_w) + s)}\,\{\int p_{wf}dt - \int p_e dt\} \tag{4.4}$$

$$\int p_{wf}dt = \frac{141.2\ B\mu\ (\ln(r_e/r_w) + s)}{kh} Q + \int P_e dt \qquad (4.5)$$

Hall made a number of very important assumptions in deriving the Hall plot. Equation (4.6) defines the relation between surface and bottomhole pressures for steady-state vertical flow. Where L is the depth of the well and Δp_f is the pressure loss due to friction.

$$p_{wf} = p_s - \Delta p_f + \rho g L \qquad (4.6)$$

Hall substituted equation (4.6) into equation (4.5) to arrive at equation (4.7).

$$\int p_s dt = \frac{141.2\ B\mu\ (\ln(r_e/r_w) + s)}{kh} Q + \int [P_e + \Delta p_f - \rho g L]\ dt \qquad (4.7)$$

Hall simply dropped the second term on the right hand side of equation (4.7) and plotted the integral of wellhead pressures with respect to time versus cumulative injection. This is what has come to be known as the "Hall plot." What Hall observed by plotting in this format was that if an injection well was stimulated, there would be a decrease in slope, and if a well was damaged, the slope would increase. While Hall's conclusions are valid regarding changes in slope, the second term on the right hand side of equation (4.7) is often not negligible in comparison to the other

terms and therefore cannot usually be dropped. The pressure at the drainage radius and the hydrostatic head of the injection column are usually a significant percentage of the bottomhole injection pressure. If the sum of the hydrostatic pressure, friction pressure, and external drainage radius pressure are small when compared to the bottom hole injection pressure, then quantitative calculations can be made from the slopes of the Hall plot as originally proposed by Hall. DeMarco (1968) and Moffitt and Menzie (1978) have used the Hall plot as originally proposed by Hall to analyze injection well performance.

Injection data must be plotted in the form of equation (4.4) to make valid quantitative calculations, or some correction must be made to the analysis method. There are two correction procedures which will be developed in the next section of this chapter to allow quantitative analysis of the Hall plot to be made when the Hall integrals $\int p_s dt$ or $\int p_{wf} dt$ are used. If no corrections are made, $\int (p_{wf}-p_e)dt$ must be plotted versus cumulative injection. The slope of the plot from equation (4.4) is then given by equation (4.8).

$$m_H = \frac{141.2\ B\mu\ (\ln(r_e/r_w) + s)}{k\ h} \qquad (4.8)$$

Equation (4.8) assumes there is a single-phase, homogeneous

fluid bank that extends to the drainage radius. Equation (4.8) may not be appropriate when multiple fluid banks with significantly different properties exist in the reservoir.

The Hall plot is a steady-state analysis method, whereas the falloff tests, injection tests, and type curve analysis are transient methods. As stated previously the transient pressure analysis methods determine the reservoir properties at a point in time. The Hall plot is more of a long term monitoring method; that is, reservoir properties are measured over a period of weeks and months. The Hall plot can therefore help to identify when some change in injectivity has occurred, such as plugging or near well bore damage or fracturing.

Hall's method has several advantages. Integrating the pressure data with the Hall method has a smoothing effect on the data. Smoothing the injection data over several weeks or months results in more accurate answers, as opposed to taking a single instant in time to calculate reservoir properties. Acquisition of the data for the Hall plot is inexpensive, since all that is required is the recording of cumulative injection and surface pressures. The surface pressures are then converted to bottomhole pressures, correcting for hydrostatic head and friction losses. Injection and falloff tests normally require running gauges

to the bottom of the hole on wireline, which is an additional expense. The analysis of a Hall plot is relatively simple. The Hall plot can be used to qualitatively interpret what is happening in the reservoir when changes occur in the slope of the plot. The greatest disadvantage of the Hall plot is that the skin and transmissibility are lumped together in the slope obtained from the plot, which can make quantitative calculations difficult. That is why it is necessary to run a falloff or injection test periodically to determine the transmissibility and skin.

4.2 Qualitative Analysis of the Hall Plot

The Hall plot has been prepared several ways by various investigators (Hall 1963; DeMarco 1968; Moffitt and Menzie 1978). The most common method for preparing the Hall plot is to plot the integral of surface pressure, $\int p_s dt$, versus cumulative injection. Bottomhole pressure, or bottomhole pressure less pressure at the external drainage radius, can also be integrated and plotted versus cumulative injection. For qualitative analysis, the objective is to recognize that a change has occurred in the injective capacity of a well. The change could be due to a change in the transmissibility or a change in the skin. A change in the injective capacity of a well is recognized by a change in slope of the Hall

plot.

If the integrals, $\int p_s dt$ or $\int p_{wf} dt$, are plotted versus cumulative injection, erroneous conclusions can be drawn based on changes in the slope of the Hall plot. Figure 4.1 is a Hall plot based on the data for well A, where the integral $\int p_{wf} dt$ has been plotted versus cumulative injection. Several changes in slope can be seen on the plot, but there has been no change in transmissibility or skin. The changes in slope are due to changes in rate. The changes in slope occur because the integral, $\int p_e dt$ has been ignored. The changes in slope can be understood as follows: with a pressure at the external drainage radius of 1000 psia and a bottomhole injection pressure of 1500 psia, there would be some rate X. If the bottomhole injection pressure was increased to 2000 psia then the injection rate would increase to 2X. When $\int p_{wf} dt$ is plotted versus cumulative injection, a doubling of the injection rate results in only a 33 percent increase in the pressure integral. At higher injection rates, the slope of the Hall plot will decrease, and the Hall plot slope will increase at lower injection rates. Plotting other than $\int (p_{wf}-p_e) dt$ versus cumulative injection will violate the proportionality inherent in Darcy's law.

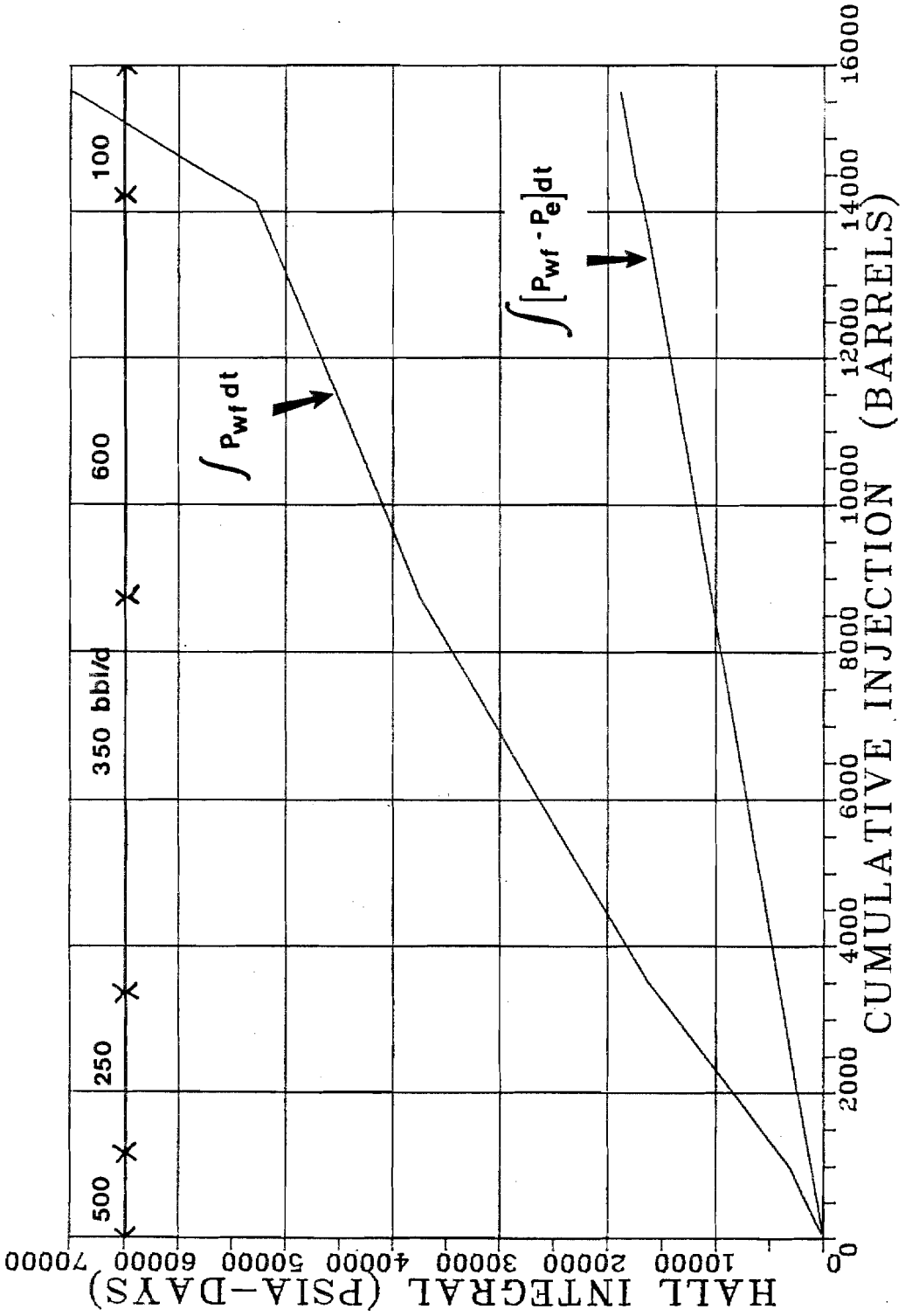

Figure 4.1

Comparison of Hall Integration Methods, Well A, P_{re}=1000 psi

In field situations, plotting the $\int p_s dt$ or $\int p_{wf} dt$ versus cumulative injection has been found to work satisfactorily. There are two reasons why these plots will work in field situations. First, if the injection rates are relatively constant, no changes in slope will occur unless the transmissibility or skin change. Second, if the $\int p_e dt$ is negligible in comparison to the $\int p_{wf} dt$, no changes in slope will occur unless the transmissibility or skin change. When plotting $\int p_s dt$ versus cumulative injection, then $\int (p_e + \Delta p_f - \rho g L) dt$ must be neglible. The value Δp_f is the pressure loss due to friction, and $\rho g l$ is hydrostatic pressure. Figure 4.2 is for the same data set as shown in Figure 4.1, but the pressure at the external drainage radius has been decreased to 100 psia from 1000 psia. The integral $\int p_e dt$ is now smaller in comparison to $\int p_{wf} dt$. It can be seen in Figure 4.2 that the changes in slope due to rate are now smaller. The plot using $\int p_{wf} dt$ versus cumulative injection agrees more closely with the plot of $\int (p_{wf} - p_e) dt$ versus cumulative injection.

Figure 4.3 is a plot prepared by Moffitt and Menzie (1978) for the Bradford field using $\int p_s dt$. The various slopes indicate changes in transmissibility. It can be see from Figure 4.3 that an increase in viscosity of the

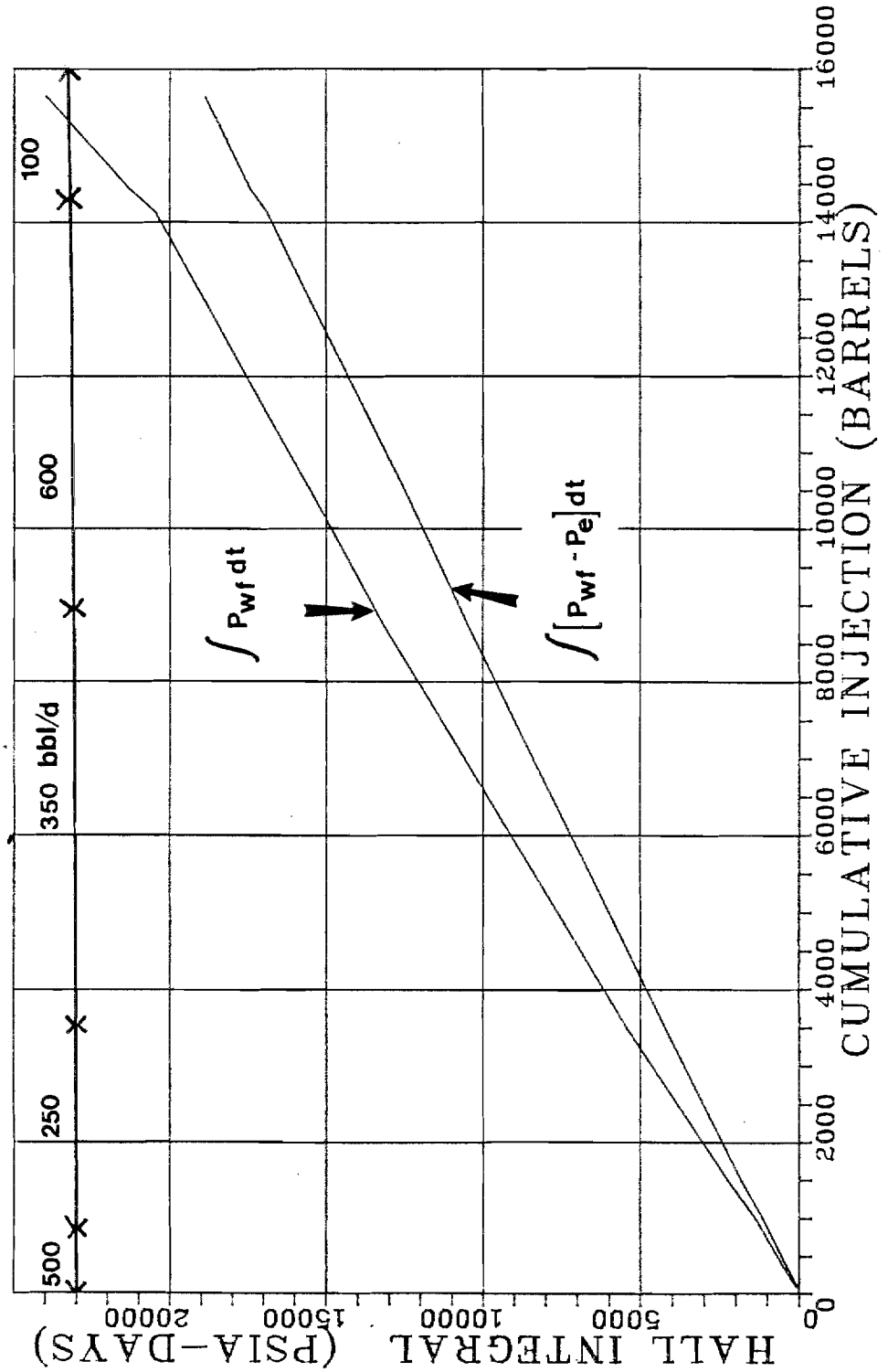

Figure 4.2

Comparison of Hall Integration Methods, Well A, p_{re}=100 psia

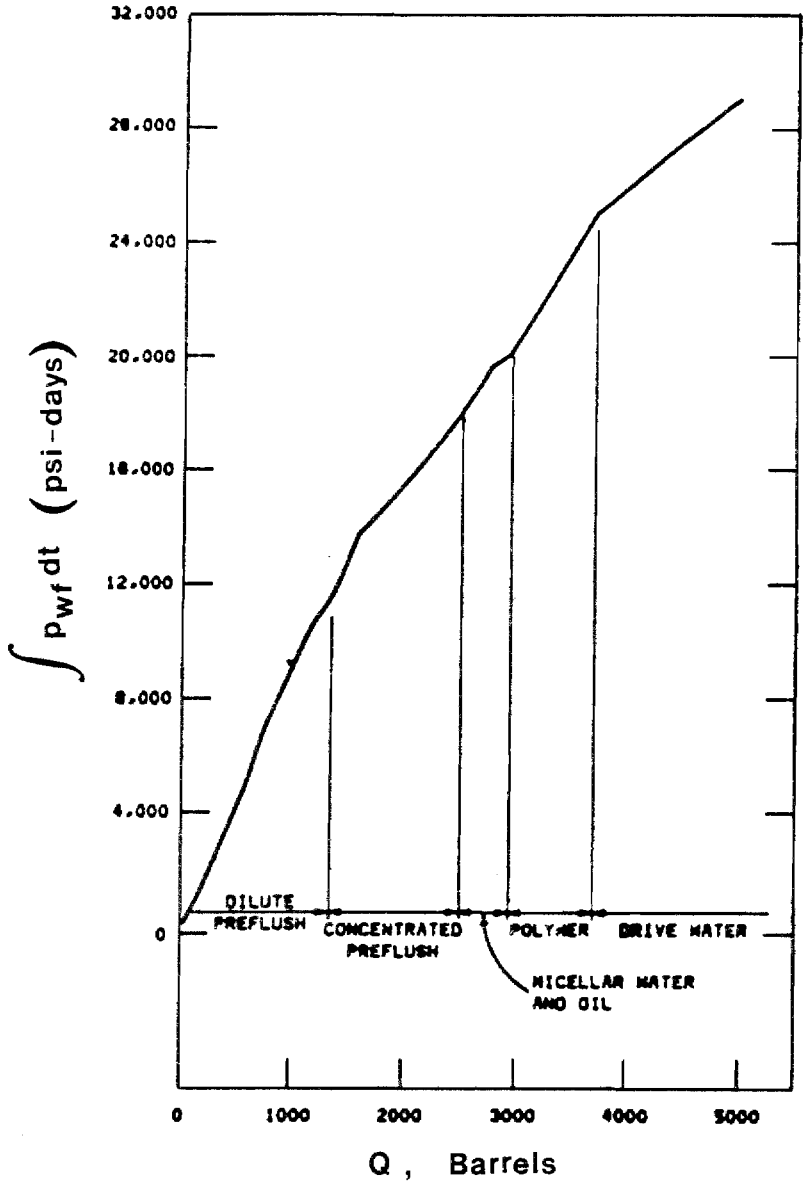

Figure 4.3

Hall Plot for the Bradford Field

(Moffitt, Paul D. and Menzie, Donald E., 1978, "Well Injection Tests of Non-Newtonian Fluids," Society of Petroleum Engineers, paper no. 7177.)

injected fluid results in an increase in the slope of the Hall plot.

To correctly interpret a change in the Hall plot slope, $\int(p_{wf}-p_e)dt$ must be plotted versus cumulative injection. If one of the other plotting methods is used, then one of assumptions as discussed in the previous paragraphs must be satisfied or a correction to the Hall integral must be made. To make quantitative calculations when $\int p_s dt$ or $\int p_{wf} dt$ is plotted versus cumulative injection, it is necessary to correct the integrations. One method to correct the Hall integrals is to simply subtract that term which was omitted in the original integration. To correct $\int p_s dt$, the quantity $\int(p_e+\Delta p_f-\rho gL)dt$ needs to be subtracted from the integral. For most problems the quantity $\int(p_e+\Delta p_f-\rho gL)dt$ can be estimated by $(p_e+\Delta p_f-\rho gL)\Delta t$ to correct the integral, since for most situations the integrand is relatively constant with time. The same logic can be applied to $\int p_{wf} dt$, the correction to be subtracted being $p_e\Delta t$.

An alternative method to correct the Hall plot, is to correct the slope directly, since the slope is the quantity used in most quantitative calculations. When the integral plotted is $\int p_{wf} dt$, it can be easily shown that the corrected slope is equal to equation (4.9).

$$m_H = m'_H - \frac{p_e(t_1 - t_2)}{Q_1 - Q_2} \qquad (4.9)$$

The slope m'_H is the Hall plot slope calculated using the integral $\int p_{wf}dt$. The slope m_H is the corrected slope, which is equivalent to using $\int(p_{wf}-p_e)dt$.

A similar correction scheme can easily be developed using for the Hall integral, $\int p_s dt$, as given in equation (4.10).

$$m_H = m'_H - \frac{(p_e - \Delta p_f + \rho gL)\ (t_1 - t_2)}{Q_1 - Q_2} \qquad (4.10)$$

It has been assumed in equation (4.9) that p_e is constant with respect to time for the period of slope correction and likewise for equation (4.10) that p_e, Δp_f, and ρgL are constant with respect to time for the period of slope correction. From this point on, all Hall plots will be assumed to be suitably plotted ($\int(p_{wf}-p_e)dt$ versus Q) for quantitative analysis unless otherwise stated.

An increase in the slope of the Hall plot indicates a decrease in transmissibility and/or an increase in skin. A decrease in the slope of the Hall plot indicates an increase in transmissibility and/or a decrease in skin. The next two sections will develop methods to quantitatively interpret the Hall plot.

4.3 Quantitative Analysis of the Hall Plot for Newtonian Fluids

When $\int(p_{wf}-p_e)dt$ is plotted versus cumulative injection, the slope of the Hall plot is equal to equation (4.8). This slope assumes single-phase flow with only one fluid bank. It is also possible to analyze the Hall plot using the concept of multiple fluid banks. Analysis methods for the Hall plot using the concept of multiple fluid banks will be developed in this and the following section. Based on the slope of the Hall plot, if the skin is known, the transmissibility can be calculated, and if the transmissibility is known, the skin can be calculated. For single-phase flow, the transmissibility will not change significantly with time; therefore, any change in the slope of the Hall plot will be due to skin effects. Assuming no change in transmissibility, the new skin can be calculated as follows for water injection if the transmissibility is already known. The subscript 1 denotes the old slope and the subscript 2 the new slope.

$$s_2 = s_1 + \frac{k\, k_{rw}\, h}{141.2\ \ B_w\, \mu_w}\,(m_{H1} - m_{H2}) \qquad (4.11)$$

When a waterflood is commenced, there will be two-phase flow in the near wellbore region. The development presented in section 4.1 assumed there was single-phase flow of a homogeneous fluid. As the water moves away from the

wellbore, a water bank and oil bank form. A simplified method to analyze this situation is to apply Darcy's law in a series manner. If the reservoir and fluid properties are assumed to be constant within each bank, then the slope of the Hall plot is given by equation (4.12).

$$m_H = (141.2/kh)\left\{\underbrace{\frac{\mu_w B_w(\ln(r_{b1}/r_w) + s)}{k_{rw}}}_{\text{(water bank)}} + \underbrace{\frac{\mu_o B_o \ln(r_e/r_{b1})}{k_{ro}}}_{\text{(oil bank)}}\right\} \quad (4.12)$$

Since the oil displacement is governed by the Buckley-Levrett (1942) equation, the saturations and relative permeabilities are not constant within each fluid bank. The interface between the oil and water bank is r_{b1}. The interface of the oil and water banks can be estimated using equation (4.13), which results from the Buckley-Leverett equation.

$$r_{b1}^2 = \frac{5.615\ Q}{\phi\ \pi\ h}\left(\frac{\partial f_w}{\partial S_w}\right)_F + r^2_w \quad (4.13)$$

The quantity $(\partial f_w/\partial S_w)_F$ is the derivative of the fractional flow curve at the flood front. The water saturation and the derivative of the fractional flow curve at the flood front are determined using Welge's method (1952). Additional development of the Buckley-Leverett equation is given in Appendix A. Since the saturations and

relative permeabilities in the fluid banks are not constant, results from equation (4.12) will only be approximate. As the oil bank is pushed away from the wellbore the water bank term will dominate in equation (4.12) and the single phase flow solution can be used.

4.4 Quantitative Analysis of the Hall Plot for Non-Newtonian Fluids

The analysis methods for non-Newtonian fluids are similar to the methods developed in the previous section, except that the non-Newtonian rheology and permeability reduction must be considered. All equations developed in this section will degenerate to single fluid bank equations when the terms for banks away from the wellbore are dropped, and the fluid bank in contact with the wellbore is assumed to extend to the drainage radius. Equation (4.14) is for an injection sequence of polymer and then water. The reservoir is assumed to be initially oil saturated. Three fluid banks will be created: oil, polymer, and water.

$$m_H = 141.2 \left\{ \underbrace{\frac{\mu_w B_w (\ln(r_{b2}/r_w) + s)}{h\, k_{wp}\, k_{rw}}}_{\text{(water bank)}} + \underbrace{\frac{\mu_p B_w \ln(r_{b1}/r_{b2})}{h\, k_p\, k_{rw}}}_{\text{(polymer bank)}} + \underbrace{\frac{\mu_o B_o \ln(r_e/r_{b1})}{h\, k_{wi}\, k_{ro}}}_{\text{(oil bank)}} \right\} \qquad (4.14)$$

Equation (4.14) can be rewritten with just one absolute permeability and one aqueous phase viscosity after the introduction of resistance factor (R_f) and residual resistance factor (R_{rf}). Since residual resistance factor and resistance factor are useful in the evaluation of polymer performance, equation (4.14) has been rewritten in equation (4.15).

$$m_H = 141.2 \left\{ \underbrace{\frac{R_{rf}\mu_w B_w (\ln(r_{b2}/r_w) + s)}{h\, k_{wi}\, k_{rw}}}_{\text{(water bank)}} + \underbrace{\frac{R_f \mu_w B_w \ln(r_{b1}/r_{b2})}{h\, k_{wi}\, k_{rw}}}_{\text{(polymer bank)}} + \underbrace{\frac{\mu_o B_o \ln(r_e/r_{b1})}{h\, k_{wi}\, k_{ro}}}_{\text{(oil bank)}} \right\} \qquad (4.15)$$

In general, the bank in contact with the wellbore will dominate the other terms. When the bank in contact has moved out a substantial distance, the other terms, in some situations, can be dropped; and the bank in contact with the wellbore can be assumed to extend to the drainage radius without substantial error in the calculations. When the fluid bank in contact with the wellbore has moved out a short distance, the dropping of the terms for the other banks can result in large errors. In Chapter 5, calculations will be made to determine the amount of error resulting in dropping all but the nearest wellbore term.

The calculations assume the bank at the wellbore extends all the way to the external drainage radius.

If the original transmissibility and skin are known prior to polymer injection, when polymer injection is commenced the in-situ resistance factor can be calculated. When water injection is commenced, the resistance factor is known and the residual resistance factor can be calculated. The terms in equation (4.15) can be rearranged to account for any injection sequence. The position of each fluid bank can be located by using equation (4.13), or the fluid bank position can be approximately located by assuming piston displacement. In equations (4.14) and (4.15) the apparent viscosity of the polymer bank is assumed to be constant in space. There will be less shear-thinning away from the wellbore, and the apparent viscosity of the polymer will increase if the concentration is constant. It is possible to take into account the variation of apparent viscosity in space by applying equations (2.6), (2.9), or (2.11) to Darcy's law in the same series manner used to develop equations (4.14) and (4.15). For the simple case of a power-law fluid bank occupying the whole reservoir, the Hall plot would be altered to the $\int(p_{wf}-p_e)dt$ versus $\int q^{1/n}dt$. The slope of the Hall plot would be be given by equation (4.16), where μ_e is defined by equation (2.5).

$$m_H = \frac{141.2\ B_w \mu_e\ (\ln(r_e/r_w) + s)}{k_p\ k_{rw}\ h} \qquad (4.16)$$

The addition of the non-Newtonian rheology makes the equations more difficult to handle for hand computations, particularly for multiple fluid banks. It will be demonstrated in chapter 5 that the variation in apparent viscosity through space is relatively small for the actual field behavior of polymer solutions, and a constant viscosity approximation for the polymer bank is reasonable.

The Hall plot could also be used to analyze transient flow. The transient flow period can be viewed as a series of steady-state flows. When the Hall plot is applied to the transient flow period the current radius of investigation must be used for r_e. The radius of investigation is defined in equation (4.17), for t in hours.

$$r_i = \left[\frac{k\ t}{948\ \phi\ \mu\ c_t}\right]^{1/2} \qquad (4.17)$$

While it is possible in theory to analyze the transient flow period with the Hall plot, this is not recommended. The falloff and injection testing methods presented in section 3.1 are much better suited to analyzing the transient flow period. Once the pressure transient reaches the drainage radius, a pseudo steady-state or steady-state flow condition

is reached, depending on the boundary condition at the drainage radius.

For most field situations where a reservoir is under water, polymer, or micellar-polymer flooding, the transient period usually does not last more than a day or two. During the transient flow period, the slope of the Hall plot is changing, given constant reservoir properties. Using real field data, it is usually not possible to observe this changing slope period on the Hall plot. The reason that the transient period is not usually observed on the Hall plot is that pressures in the field are typically recorded only once or twice per day. Since the transient period lasts only a few days it is difficult to observe in field data with such infrequent pressure readings. It is possible to observe the transient flow period on the Hall plot when pressures and rates are recorded frequently at early times. The transient flow period will be examined in additional detail in chapter 5 using field examples.

CHAPTER 5

HALL PLOT ANALYSIS RESULTS

This chapter will analyze simulator results for three wells in which non-Newtonian fluids and water were injected. Well A is a hypothetical example; wells B and C are actual wells. Each of the field examples has three months of daily injection data. The two field examples have been history matched with the reservoir simulator. Based on these three wells, the effect of transient flow , multi-phase flow, shear thinning, and permeability reduction on the Hall plot are investigated. The analysis methods developed in chapter 4 will be applied to the examples in this chapter. Results obtained by analysis with the reservoir simulator will be compared with the analysis methods of chapter 4. Based on this comparison, the validity and accuracy of the methods developed in chapter 4 will be evaluated.

5.1 Analysis of Well A (Hypothetical)

Well A is a hypothetical example. The data for Well A is given in Appendix B. Figure 5.1 illustrates the injection history of the well. Water was injected for 51 days, then injection of 1000 ppm polymer solution commenced and continued for the remainder of the injection.

Figure 5.2 illustrates the Hall plot for the transient

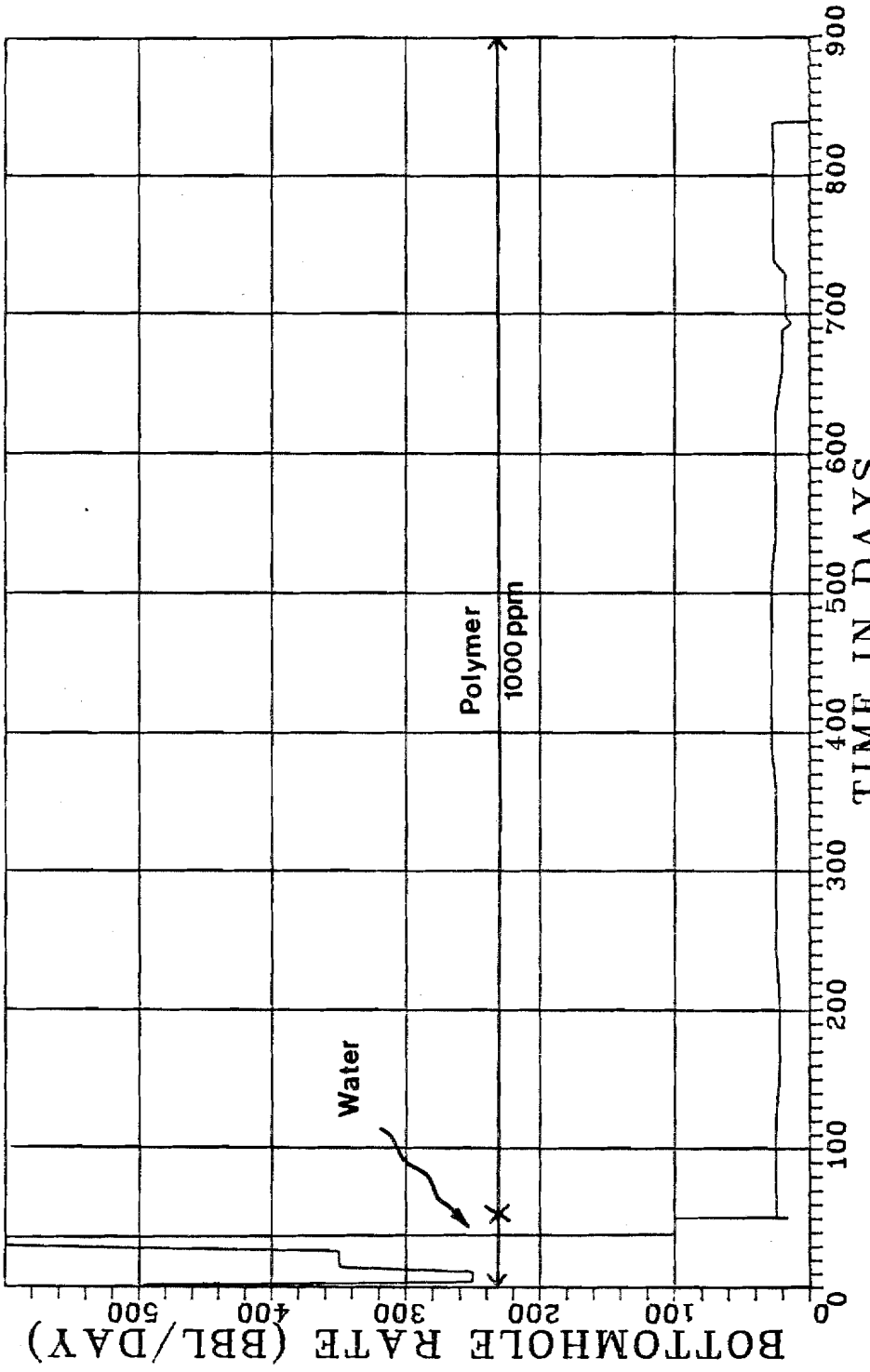

Figure 5.1

Bottomhole Injection Rate Versus Time, Well A

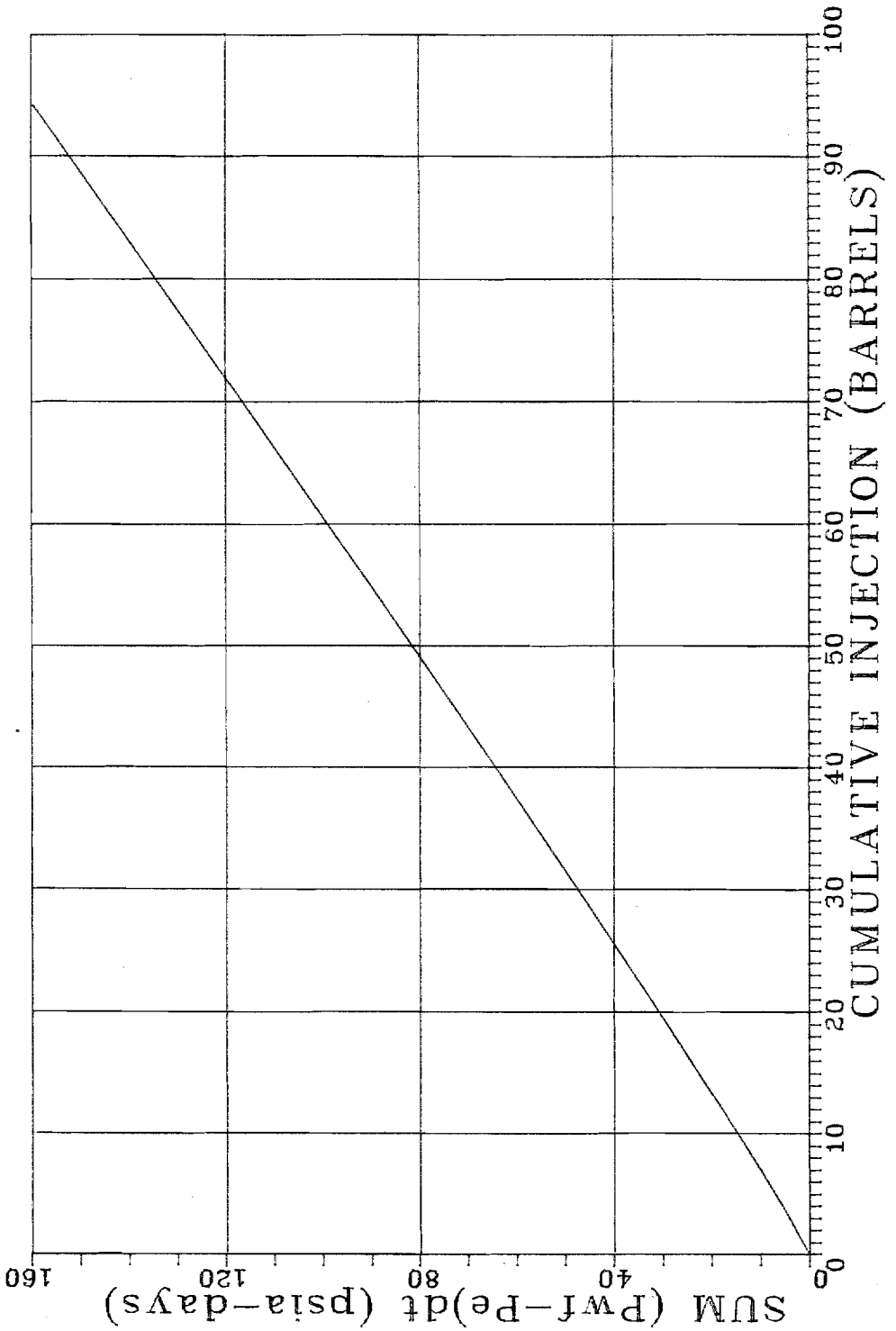

Figure 5.2

Hall Plot, Well A, Single Phase Transient Flow Period

flow period. The injection rate during this period is 500 STB/day. The oil saturation was set at residual, so the plot is for single-phase flow. The wellbore storage period ends after 25 minutes, i.e. wellbore storage ends after 3 barrels of fluid have been injected into the formation and 9 barrels have been injected at the surface. The time to steady state flow is 24 hours using equation (4.17). For this case the end of the transient period occurs when 494 bbl have been injected. It can be seen that there is a slow continuous curve in Figure 5.2 because of the changing radius of investigation. When 50 STB have been injected, the time is 2.7 hours and the radius of investigation is 333 feet. The slope of the Hall plot will be given by equation (5.1) during the transient period.

$$m_H = \frac{141.2\ B\mu_w\ (\ln(r_{ei}/r_w) - 0.5 + s)}{k\ k_{rw}\ h} \qquad (5.1)$$

It should be noted that -0.5 has been added to the equation since the flow is no longer a true steady state, but what is referred to in the literature as pseudo-steady state. Using 333 feet for r_{ei}, it should be possible to back calculate the permeability taking the slope of the curve at a cumulative injection of 50 bbl. The slope of Figure 5.2 at a cumulative injection of 50 STB is 1.77 (psia-days)/STB. The calculated permeability to water

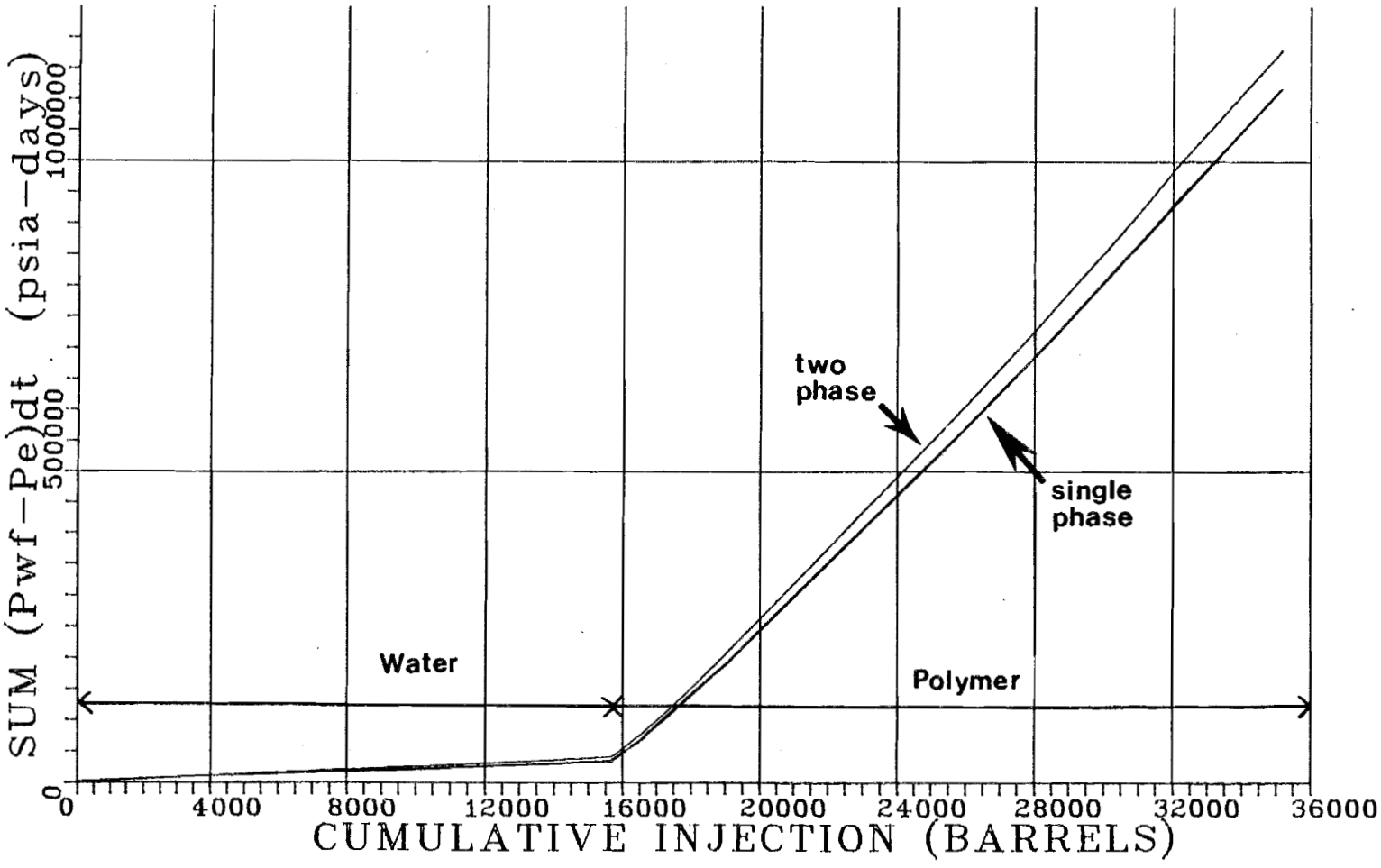

Figure 5.3

Hall Plot, Well A, Comparison of Single and Two Phase Flow

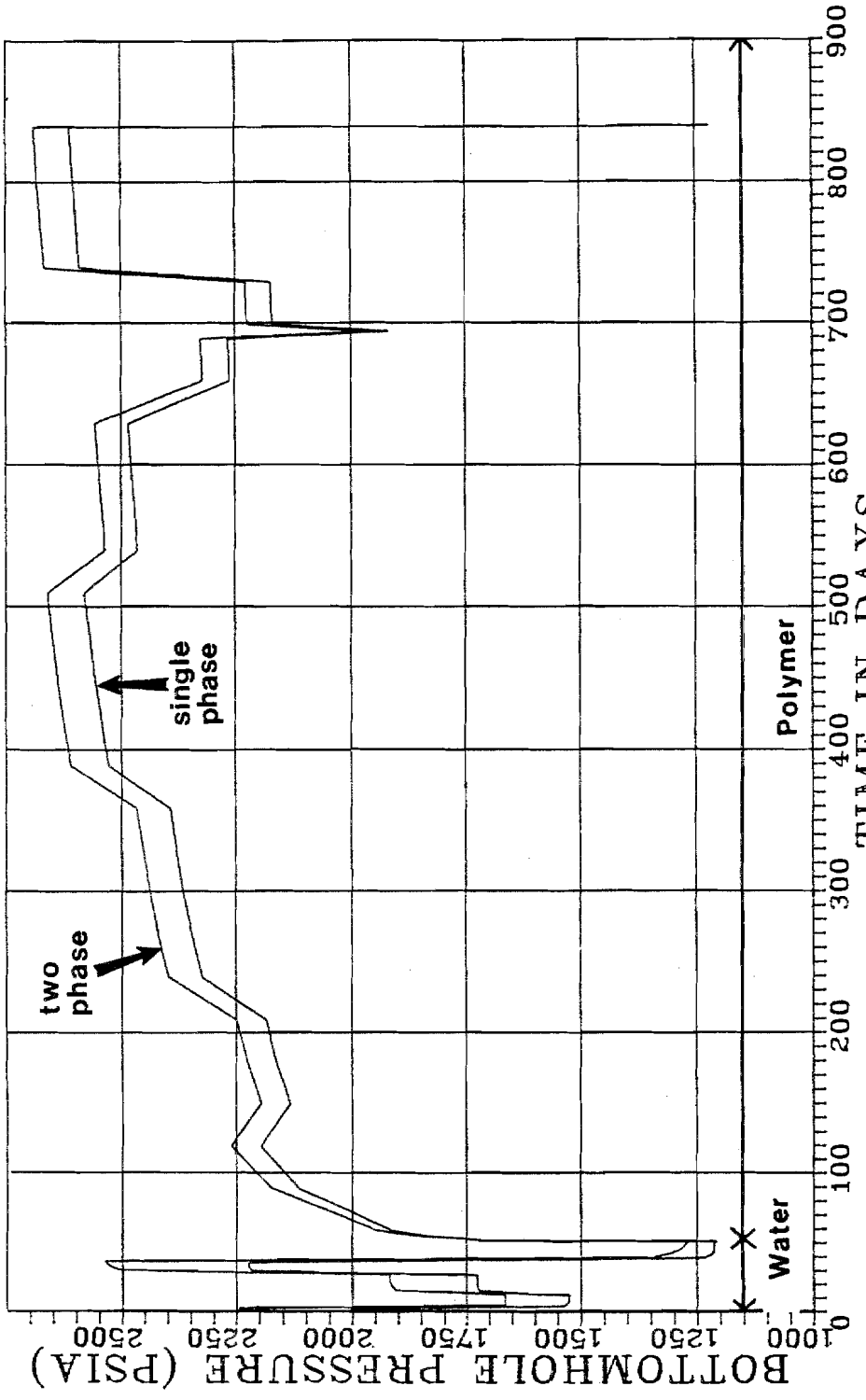

Figure 5.4

Bottomhole Pressure versus Time, Well A, Single and Two Phase Flow

slope calculation for two-phase flow. The Hall plot still generates a straight line for water injection when two-phase flow is occurring in the reservoir.

At the end of the polymer injection, the slope of the Hall plot is 58.1 (psia-days)/STB for single-phase flow. The curve for two-phase flow has a slope of 63.1 (psia-days)/STB. The difference between the two slopes is 8.6 percent. As time continues, the slope to the two-phase Hall plot curve will approach the slope of the single-phase curve. These curves illustrate that for situations where the mobility contrast is not too great two-phase flow effects can be neglected without appreciable error in the Hall plot slope. As the oil bank is pushed farther from the wellbore, there will be less error with the single-phase flow assumption.

5.2 History Matching and Analysis of Well B

Well B is based on the data published by Milton, Argabright, and Gogarty (1981). The data was used to evaluate a reservoir in the Big Horn Basin, Wyoming, for polymer flooding. The Milton, et al., data set was selected because they provided detailed reservoir data, daily pressures and rates, and rheological data. The injection pressures and rates were also controlled to prevent excessive fracturing. Two falloff tests were also run to

determine skin and permeability. The data provided by Milton, et al., is summarized in Appendix C.

The polymer injection sequence consisted of water injection followed by polyacrylamide polymer solution. The polyacrylamide polymer solution was displaced by water. The details of the injection sequence are given in tables C.4 and C.5. When history matching the performance of this well, all the parameters supplied by Milton, et al., were used as input for the simulation runs, with the exception of two. The rheological data and resistance factor estimates provided by Milton et al., were used as a first approximation, and were then adjusted to obtain the best possible match. All pressure data was recorded at the surface. For history matching purposes, all surface pressures were corrected to bottomhole pressures with the inclusion of friction. Because of the high rates, the pressure drop due to friction was as high as 250 psi.

The laboratory measurement of apparent viscosity of the polymer solution as a function of interstitial velocity and concentration is given in Figure 5.5. The residual resistance factor was originally estimated to be 1.05. To obtain the best possible match with the field data, it was necessary to reduce the polymer solution viscosity and increase the residual resistance factor. The best history

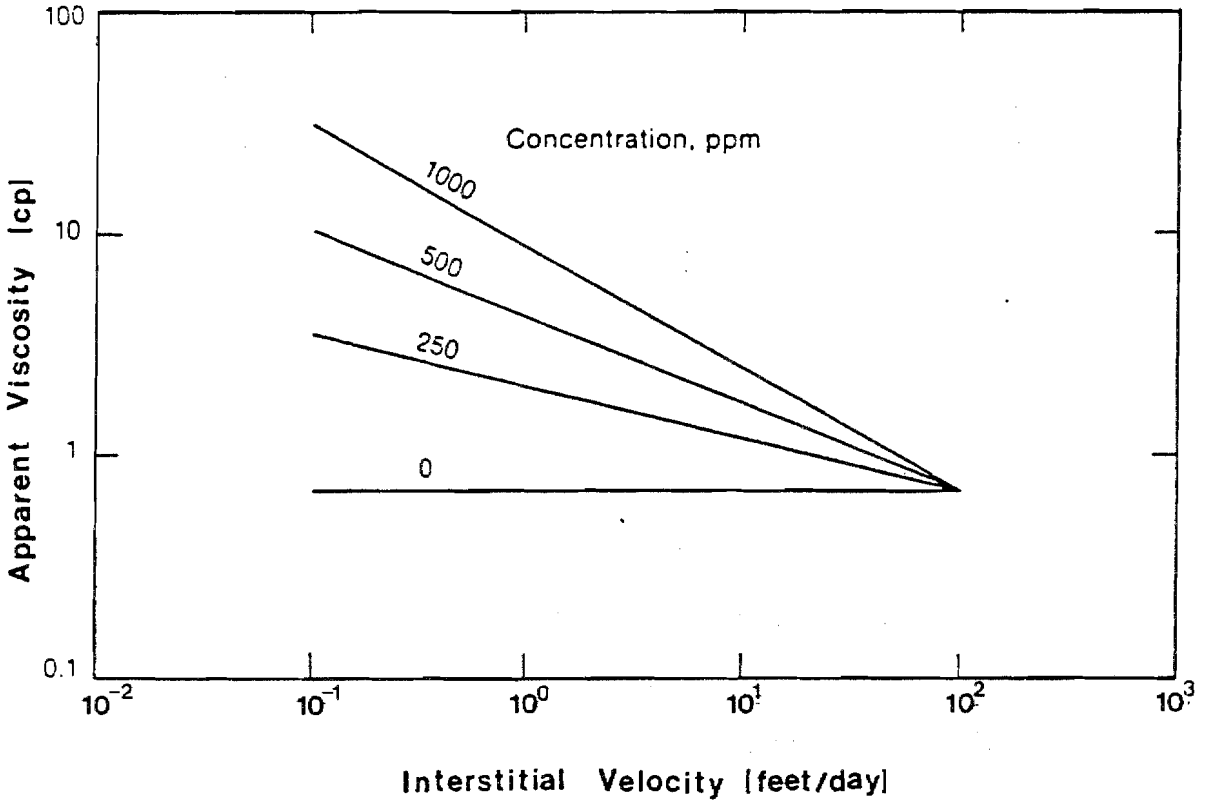

Figure 5.5

Laboratory Apparent Viscosity versus Interstitial Velocity, Well B

match was obtained using the rheology given in Table C.2 and a maximum residual resistance factor of 1.35. Based on the assumed linear relation adsorption/retention isotherm and residual resistance factor, the in situ residual resistance factor is calculated to be 1.33. Table 5.1 compares the laboratory apparent viscosity with the apparent viscosity used in the best history match at a concentration of 1000 and 500 ppm.

Two types of history matching runs were made on Well B. The first type of history matching was done using the rate control (Neumann) boundary condition at the wellbore. The field injection rates were used to predict bottomhole pressures. The history match was obtained by matching field pressures with predicted pressures. The second type of history matching run was made using the pressure control (Dirichlet) boundary condition at the wellbore. The field bottomhole pressures could then be used to predict injection rates. The history matching was then performed by matching field injection rates with simulator predicted rates. The history matching runs used 20 and 50 radial cells. There was no significant difference between the results using 20 and 50 cells. The reservoir had been waterflooded extensively prior to the collection of the Hall plot data. Milton, et al., considered the reservoir to be at residual

Table 5.1

Comparison of Simulator and Laboratory Apparent Viscosities,

Well B

Concentration 1000 ppm

Interstitial Velocity (ft/day)	Laboratory Viscosity (cp)	Simulator Viscosity (cp)
0.01	-	10.0
0.10	38.0	10.0
1.00	9.5	5.5
10.00	3.0	2.0
100.00	0.7	0.7
1000.00	0.7	0.7

Concentration 500 ppm

Interstitial Velocity (ft/day)	Laboratory Viscosity (cp)	Simulator Viscosity (cp)
0.01	-	5.0
0.10	10.0	5.0
1.00	5.0	3.0
10.00	2.0	1.8
100.00	0.7	0.7
1000.00	0.7	0.7

oil saturation at least in the vicinity of the well. The reservoir was therefore modelled using single-phase flow.

Using the rate control (Neumann) boundary condition and matching pressures, Figures 5.6 and 5.7 were obtained. The match based on the Hall plot is quite close except between the injection volumes of 80,000 and 120,000 barrels (Figure 5.6). This interval corresponds to 40 to 70 days on the pressure plot (Figure 5.7). It was not possible to obtain a better match over this interval. One reason for a problem with the match over this interval is due to the fact that both fresh water and brine were injected. The injectivity of fresh water is higher than brine, which can be observed in the injectivity index between 60 and 65 days. The injectivity is calculated in a manner analogous to the productivity index (see equation [5.2]).

$$\text{Injectivity Index} = \text{I.I.} = \frac{q}{p_{wf} - p_e} \qquad (5.2)$$

The injectivity of fresh water is 1.753 bbl/day/psi and the injectivity of brine is 1.367 bbl/day/psi. The simulator is not designed to handle differing injectivity of water due to varying chemical composition. Some type of chemical reaction is occurring due to the water chemistry to cause the change in injectivity. Another problem with the field

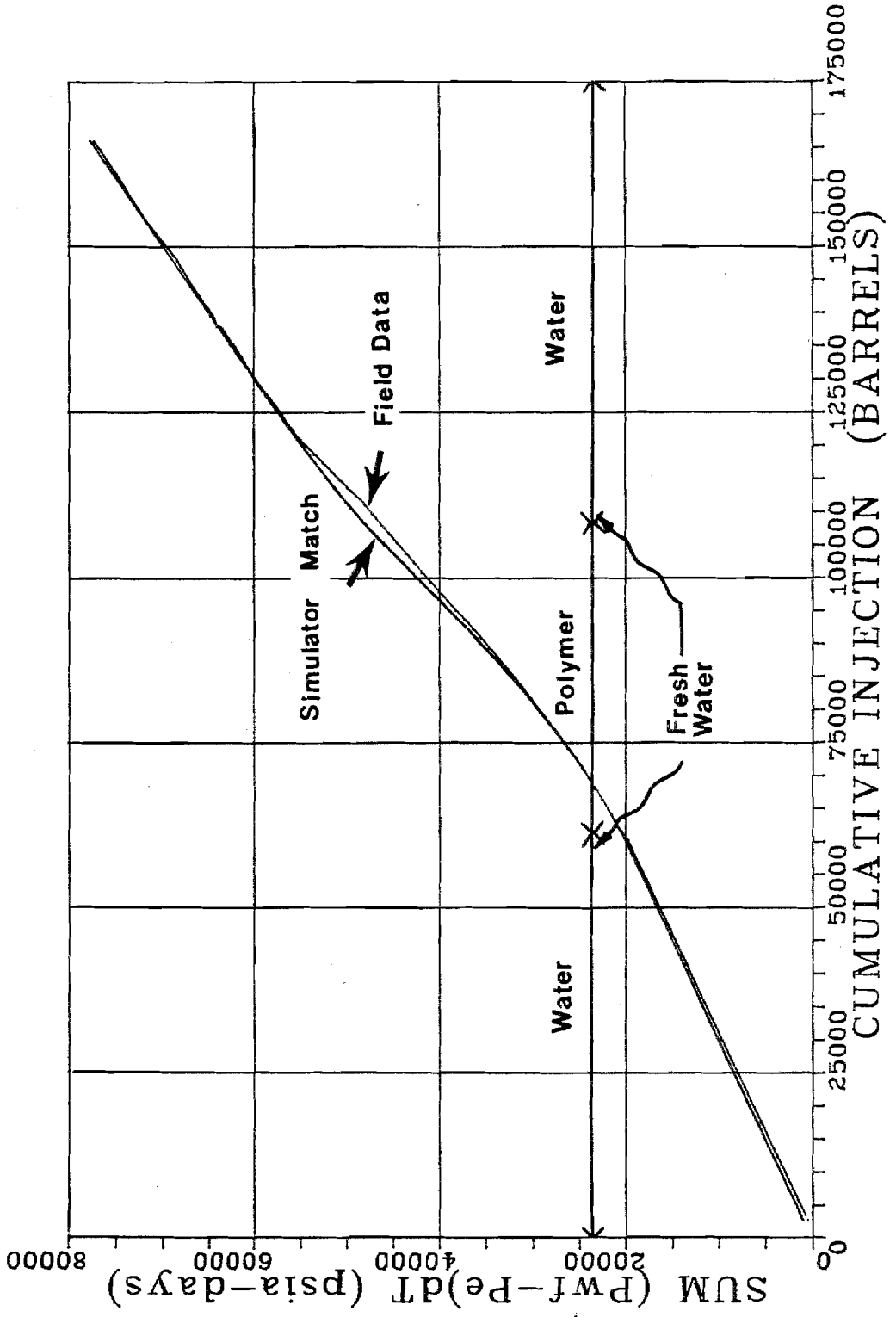

Figure 5.6

Hall Plot, Rate Control History Match, Well B

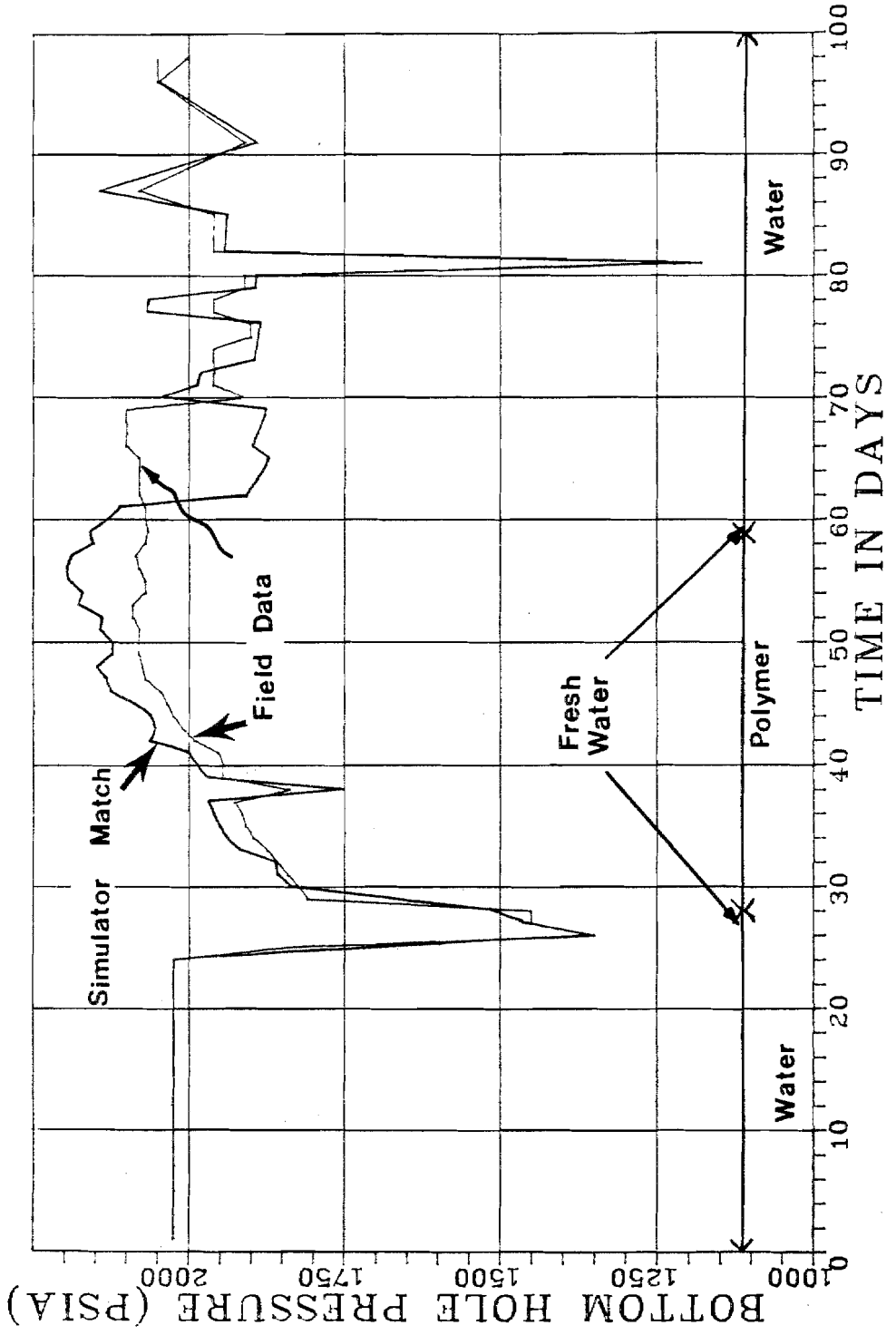

Figure 5.7

Bottomhole Pressure Versus Time, Rate Control History Match, Well B

data is the injectivity of the polymer just prior to water injection is higher than brine injectivity at 1.578 bbl/day/psi. A polymer solution having a higher injectivity than water does not make physical sense. For example it was observed that to obtain a better match in the polymer injection region a poorer match was obtained in the water injection region. The opposite would occur if a better match was obtained in the water injection region.

Figures 5.8 and 5.9 are for a history match using the pressure control (Dirichlet) boundary condition at the wellbore. The same quality of match is obtained using the pressure control boundary conditon as the rate control boundary condition. The error between the two methods is of the opposite sign at any particular point in time.

For example, when using the rate control boundary condition and the history match pressure is too low, a switch in boundary condition to pressure control will result in a rate that is too high. When using the pressure control boundary condition one problem that can occur is that a sudden drop in the wellbore pressure will actually cause the well to backflow into the wellbore. This occurs because the pressure in the wellbore is actually less than the pressure in the first resevoir cell. What this means, is that for history matching, when the well is shutin, the pressures

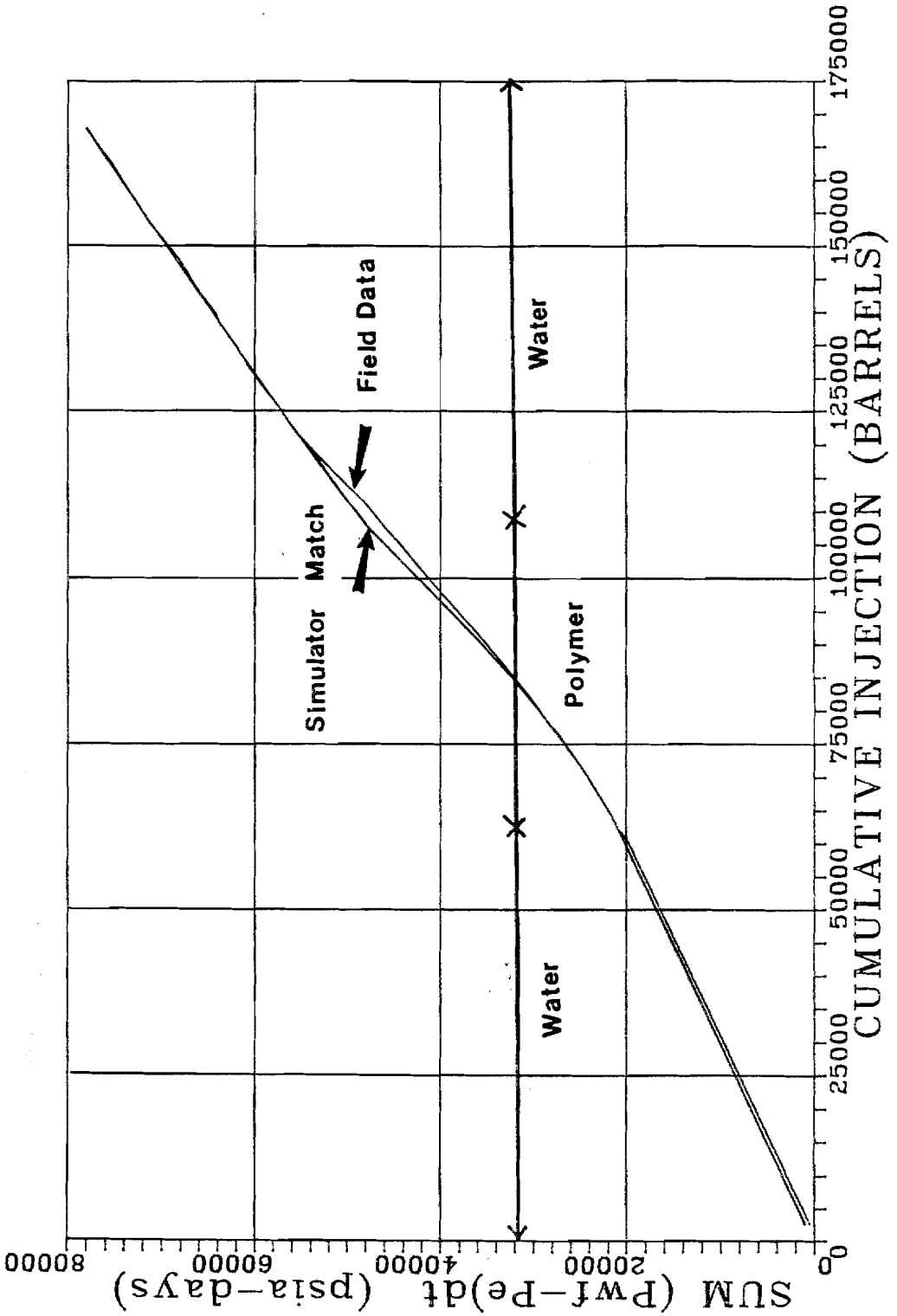

Figure 5.8

Hall Plot, Pressure Control History Match, Well B

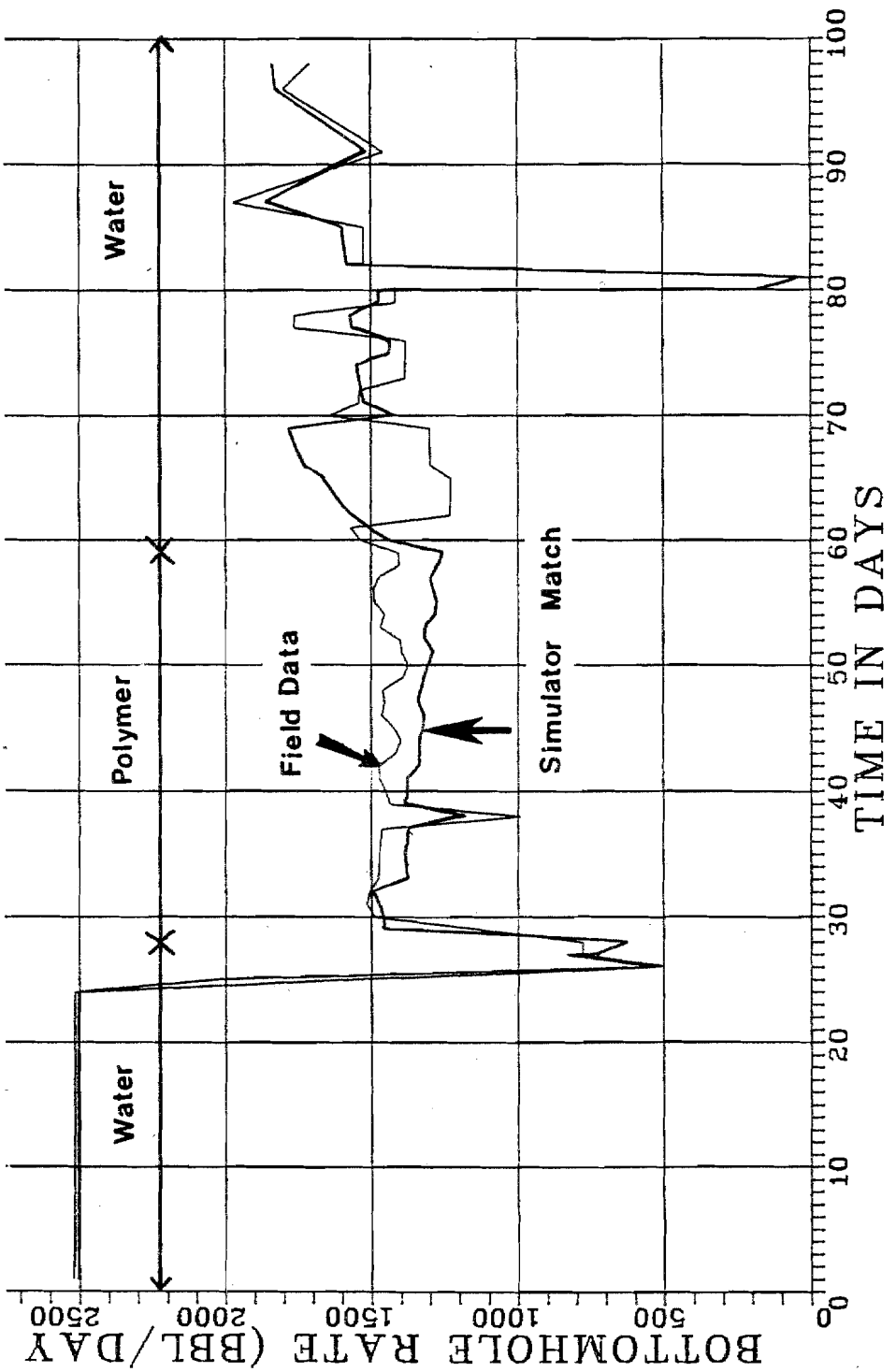

Figure 5.9

Bottomhole Rate Versus Time, Pressure Control History Match, Well B

must be decreased slowly to prevent backflow into the wellbore of the simulator.

In the history matching process, the matching of the initial water injection period was useful for verifing the reservoir properties. The history matching of the polymer injection period was controlled by rheology and residual resistance factor. The history matching of water injection following polymer was controlled by the residual resistance factor.

There was no polymer adsorption/retention data available for this well. Two history matching runs were made at different adsorption/retention levels. The Langmuir adsorption/retention isotherm was estimated to have a maximum adsorption of 0.02 mg/g, and intermediate values were also estimated as a function of concentration to generate a smooth curve. The adsorption/retention was then increased 250 percent to a maximum of 0.05 mg/g. The adsorption isotherms were constructed such that there would be the same in-situ residual resistance factor of 1.33. The two history matching runs are compared in Figure 5.10. It can be seen from Figure 5.10 that changing the adsorption between 0.02 to 0.05 mg/g has no effect on the Hall plot. The residual resistance factor is much more important than the amount of adsorption in determining the pressure

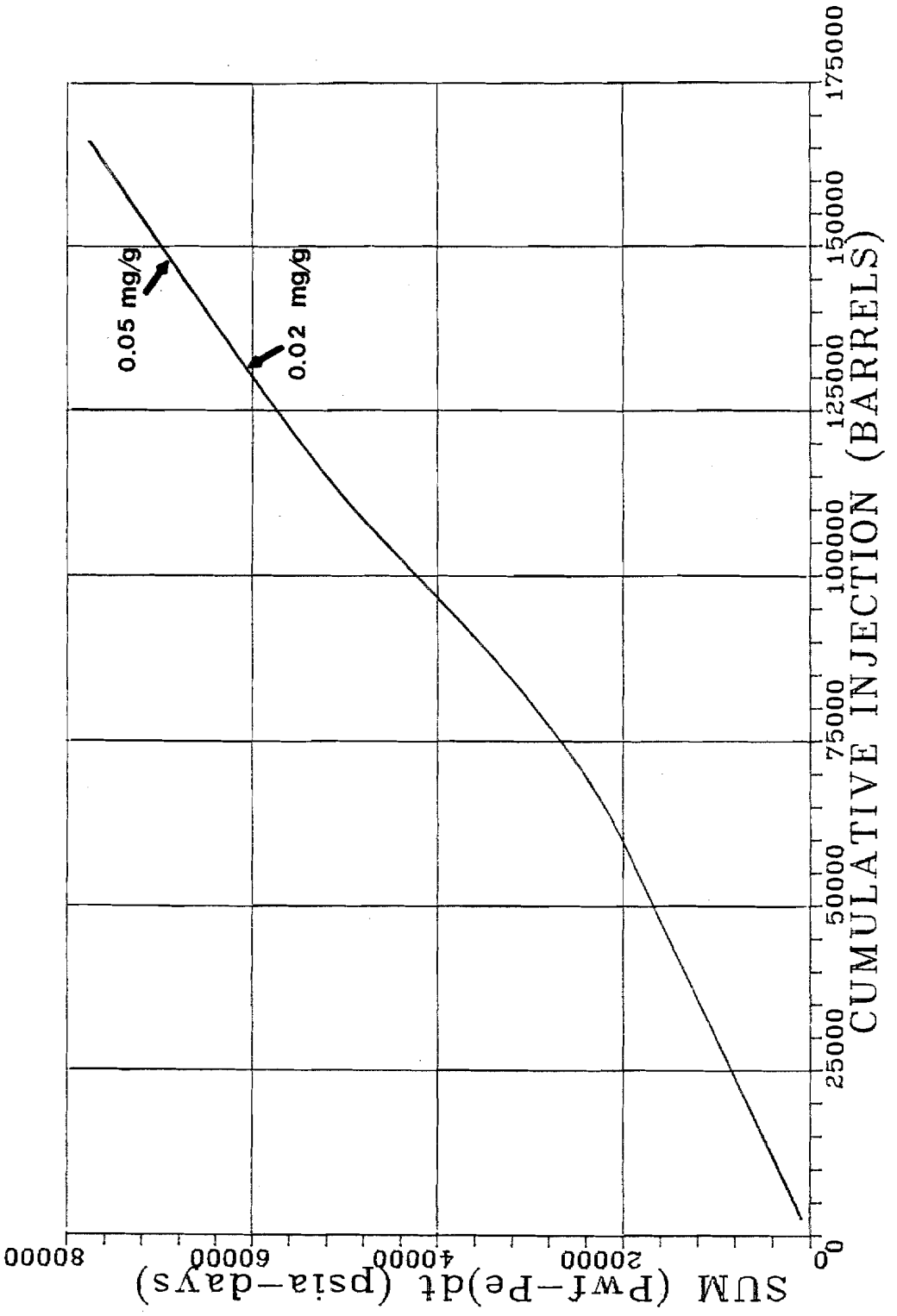

Figure 5.10

Hall Plot, Comparison of Adsorption/Retention Isotherms, Well B

behavior of a well.

Using the Hall plot generated from history matching, the analytical procedures developed in Chapter 5 will now be applied to the Hall plot. The Hall plot shown in Figures 5.6 and 5.8 has three distinct portions: the first section being water, the second section being polymer, and the third section being water injection. Applying Darcy's law in a series manner, an equation can be written for each section. For this example, four unknowns will be assumed: $k_{wi}k_{rw}$, R_{rf}, R_{f1}, and R_{f2}. All other parameters are assumed to be known. It should be noted that R_{f1} and R_{f2} will usually not be equal, principally because adsorption will reduce polymer concentrations as the polymer slug propagates through the reservoir. A reduction in polymer concentration results in less polymer solution apparent viscosity and less permeability reduction. The unknown R_{f1} is the resistance factor of the polymer bank, while polymer solution is being injected. The unknown R_{f2} is the resistance factor of the polymer bank, after polymer injection has stopped and water injection has commenced. The slope of the Hall plot for the first water injection period is given by equation (5.3).

$$m_{H1} = \frac{141.2\ \mu_w B_w\ (\ln(r_e/r_w) + s)}{h\ k_{wi}\ k_{rw}\ \text{(water bank)}} \qquad (5.3)$$

The slope of the Hall plot for the polymer injection period is given by equation (5.4).

$$m_{H2} = 141.2 \left\{ \underbrace{\frac{R_{f1}\mu_w B_w (\ln(r_{b2}/r_w) + s)}{h\, k_{wi}\, k_{rw}}}_{\text{(polymer bank)}} + \underbrace{\frac{\mu_w B_w \ln(r_e/r_{b2})}{h\, k_{wi}\, k_{rw}}}_{\text{(water bank)}} \right\} \qquad (5.4)$$

The slope of the Hall plot for water injection following polymer injection is given by equation (5.5).

$$m_{H3} = 141.2 \left\{ \underbrace{\frac{R_{rf}\mu_w B_w (\ln(r_{b2}/r_w) + s)}{h\, k_{wi}\, k_{rw}}}_{\text{(water bank)}} + \underbrace{\frac{R_{f2}\mu_w B_w \ln(r_{b1}/r_{b2})}{h\, k_{wi}\, k_{rw}}}_{\text{(polymer bank)}} + \underbrace{\frac{\mu_w B_w \ln(r_e/r_{b1})}{h\, k_{wi}\, k_{rw}}}_{\text{(water bank)}} \right\} \qquad (5.5)$$

The permeability of the reservoir can be calculated with equation (5.3). The slope of the Hall plot during the initial water injection period is 0.338 (psia-days)/bbl. From this slope, a permeablity to water of 90.9 md is calculated using a skin of 7.2, where the permeability to water is given by $k_{wi}k_{rw}$. The permeability to water used by the reservoir simulator is 91.0 md. A Darcy skin of 7.2

is used for all time steps by the simulator. Having eliminated one unknown, there are now three unknowns, and only two equations. To solve for all the unknowns it is necessary to have another equation. The residual resistance factor can be estimated by taking the ratio of m_{H1} to m_{H3}. As injection proceeds, the slope m_{H3} will approach the value given by equation (5.6). The contribution from the banks farther away from the wellbore become smaller and smaller as injection continues when using equation (5.5).

$$m_{H3} = \frac{141.2\ R_{rf}\mu_w B_w (\ln(r_e/r_w) + s)}{h\ k_{wi}\ k_{rw}} \qquad (5.6)$$

(water bank)

The latest straight line portion of water injection following polymer is used to estimate m_{H3} so that the influence of the other banks will be at a minimum. By combining equations (5.3) and (5.6) it is possible to solve for R_{rf}. Equation (5.6) is used to estimate the slope given by equation (5.5). The residual resistance factor can be estimated using equation (5.7).

$$R_{rf} = m_{H3}/m_{H1} \qquad (5.7)$$

The latest straight line slope for water injection following polymer is 0.479 (psia-days)/bbl. The residual resistance

factor is computed to be 1.42. The in-situ residual resistance factor calculated in the simulator is 1.33. There are now two equations, (5.4) and (5.5) and two unknowns to find R_{f1} and R_{f2}. Since this problem was simulated using one phase flow, all displacement processes are miscible and therefore, piston-like displacement occurs. The location of the interface between banks can be calculated by volumetric calculations accounting for polymer adsorption. The accuracy of the bank positions is not that important to the computations since the logarithim of the ratio of the radii is taken. At the end of the polymer injection period, the polymer bank has reached a radius of 123 feet. The slope, m_{H2}, taken from the plot is 0.684 (psia-days)/bbl. Substituting numerical values, equation (5.4) becomes

$$0.684 = 0.2843\ R_{f1} + 0.0521 \qquad (5.8)$$

$$m_{H2} = \text{(polymer bank)} + \text{(water bank)}$$

The resistance factor is calculated to be 2.22 for the polymer bank when polymer is being injected. It can be seen that the water bank is less important than the polymer bank, supporting the conclusion that the bank in contact with the wellbore will dominate. The water bank away from the wellbore can be assumed to be negligible, and the single

fluid bank assumption used. Assuming the polymer bank extends to the external drainage radius, equation (5.8) can be rewritten as equation (5.9).

$$0.684 = 0.3319\ R_{f1} \quad (5.9)$$

$$m_{H2} = \text{(polymer bank)}$$

Using the single-fluid bank assumption, the resistance factor is calculated to be 2.06. The single-fluid bank assumption will always underestimate the resistance factor because the polymer bank is assumed to extend to the drainage radius when it actually only extends some fraction of the drainage radius. The apparent viscosity in the simulator varies from 0.70 cp at the wellbore to as high as 4.12 cp at a radius of 63 feet. The residual resistance factor is almost constant at 1.326. The simulator provides pressures for each cell. Using these pressures, it is possible to back calculate an average resistance factor for the polymer bank. The pressure drop across the polymer bank is 846 psi at a rate of 1473 STB/day, when the polymer bank is at 123 feet. The average resistance factor is calculated to be 2.17 for the polymer bank using the simulator data.

The slope of the late time water injection following polymer is 0.479 (psia-days)/bbl and is used to solve equation (5.5). For the late time water injection, the

polymer bank is between 104 feet and 237 feet. Substituting numercial values into equation (5.5) results in

$$0.479 = 0.3774 + 0.0081\, R_{f2} + 0.0441 \quad (5.10)$$

$$m_{h3} = (\text{water bank}) + (\text{polymer bank}) + (\text{water bank})$$

The resistance factor of the polymer bank away from the wellbore is calculated to be 4.19. The pressure drop across the polymer bank is 107 psi at a rate of 1706 STB/day. The average resistance factor of the polymer bank is calculated to be 3.51 using the simulator data. The resistance factor calculated for the polymer bank away from the wellbore can be significantly in error. The reason for the larger errors is that the pressure drop due to the polymer bank, is small away from the wellbore. A small error in the determination of the slope, results in a magnified error in the calculated resistance factor. For example, if the slope was 1 percent in error, and the pressure drop across the polymer bank away from the wellbore was 5 percent of the total pressure drop across the system, the calculated resistance factor would be 25 percent in error. Table 5.2 compares the approximate analytical methods with the simulator results. The analytical methods developed in Chapter 5 give reasonable estimates of the in situ parameters.

Table 5.2

Comparison of Analytical Method with Simulator Results, Well B

Parameter	Analytical Method Multiple Banks	Analytical Method Single Bank	Simulator
$k_{wi}k_{rw}$	90.9	90.9	91.0
R_{rf}	1.42	1.42	1.33
R_{f1}	2.22	2.06	2.17
R_{f2}	4.13	--	3.51

Figure 5.11 compares the three different methods of integrating the Hall plot. For each method of integration, the slopes of the curves are quite different. Quantitative calculations can be made with each curve if the appropriate corrections are made. The correction $p_e\Delta t$ must be subtracted from $\int p_{wf}dt$ to yield $\int(p_{wf}-p_e)dt$. The correction $(p_e-\rho gL+\Delta p_f)\Delta t$ must be subtracted from $\int p_s dt$ to yield $\int(p_{wf}-p_e)dt$.

An example correction will be done on the water injection period given in Figure 5.11. The corrected slope of the Hall plot will be calculated using two points, one at a cumulative injection of 125,000 STB and another at 100,000 STB. The pressure at the external drainage radius is constant at 1180 psia. The combined hydrostatic head and

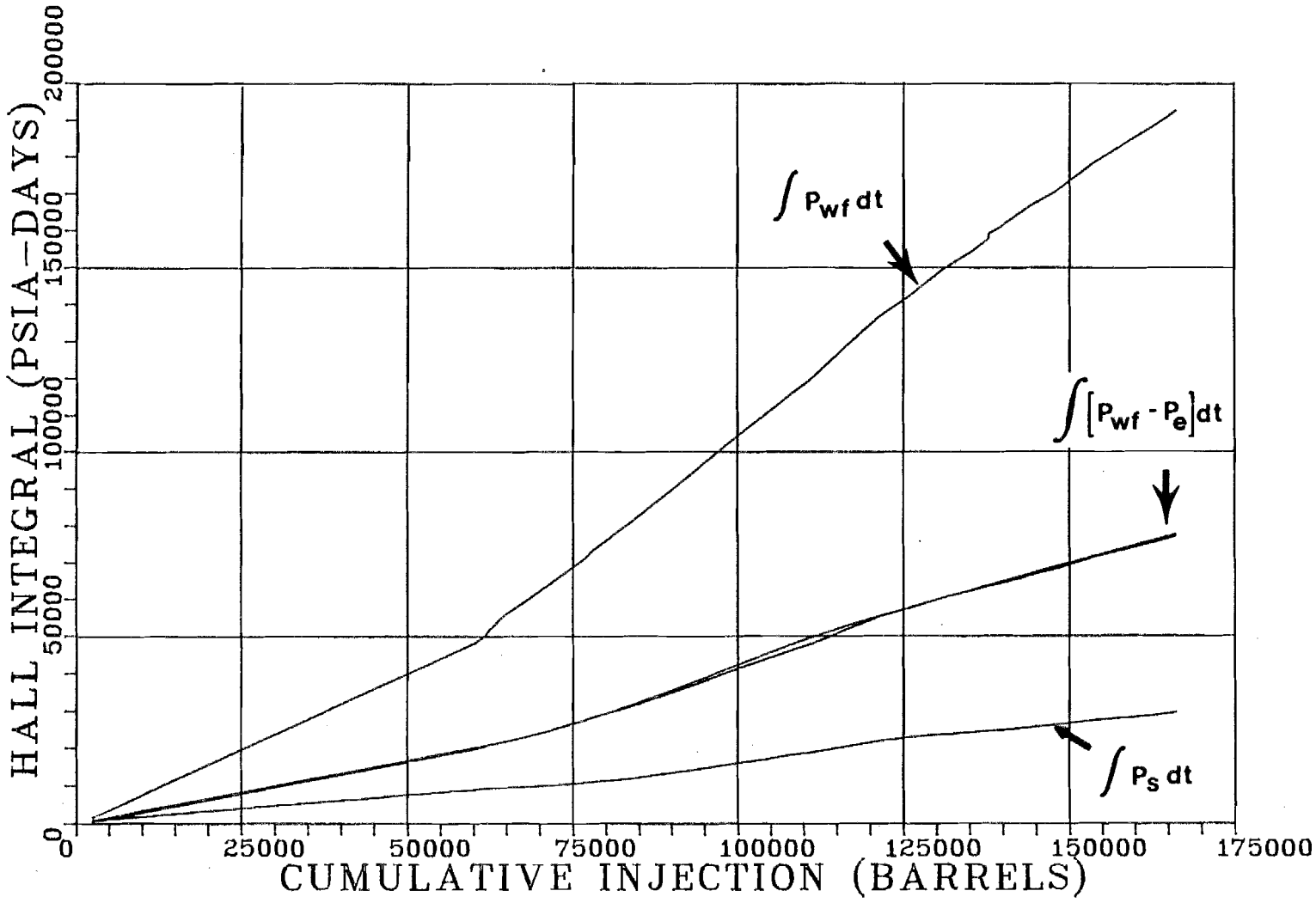

Figure 5.11

Comparison of Hall Integration Methods, Well B

the pressure loss due to friction average about 1700 psi. The data for the Hall plot corrections are given in Tables 5.3 and 5.4. When the corrections have been applied to the other integrations, the corrected values should agree closely with the slope of 0.600 (psia-days)/STB when using $\int(p_{wf}-p_e)dt$. The integral $\int p_s dt$ is corrected to calculate a Hall plot slope of 0.612 (psia-days)/STB, and $\int p_{wf} dt$ is corrected to calculate a Hall plot slope of 0.600 (psia-days)/STB. The difference in the corrected slopes and the slope from $\int(p_{wf}-p_e)dt$ is due to the accuracy with which values can be picked from Figure 5.11. Once the slopes have been corrected, all calculations proceed exactly the same.

Equations (4.9) and (4.10) can also be used to correct the slope directly. When the integral plotted is $\int p_{wf} dt$, equation (4.9) is used. Using the data given in Table 5.4, the slope using $\int p_{wf} dt$ is 1.440 (psia-days)/STB and the slope correction is 0.840. The corrected Hall plot slope, m_H, is calculated to be 0.600 (psia-days)/STB. If the integral $\int p_s dt$ is plotted equation (4.10) is used to correct the slope. The slope m'_H is equal to 0.240 (psia-days)/STB when the integral $\int p_s dt$ is used. The slope correction is calculated to be -0.370 (psia-days)/STB using equation (4.10), which yields a corrected slope of 0.610 (psia-days)/STB.

Table 5.3

Hall Plot Integration Correction Example for $\int p_s dt$, Well B

Cum. Injection (STB)	Time (days)	$\int p_s dt$ (psig-days)	$(p_e - \rho gL + \Delta p_f)$ (psia-days)	Corr. Integral (psia-days)
125,000.0	71.3	21,000	-37,100	58,100
100,000.0	53.5	15,000	-27,800	42,800

$$m_H = \frac{58,100 - 42,800}{125,000 - 100,000} = 0.612 \text{ (psia-days)/STB}$$

Table 5.4

Hall Plot Integration Correction Example for $\int p_{wf} dt$, Well B

Cum. Injection (STB)	Time (days)	$\int p_{wf} dt$ (psig-days)	$p_e \Delta t$ (psia-days)	Corr. Integral (psia-days)
125,000.0	71.3	142,000	84,100	57,900
100,000.0	53.5	106,000	63,100	42,900

$$m_H = \frac{57,900 - 42,900}{125,000 - 100,000} = 0.600 \text{ (psia-days)/STB}$$

5.3 History Matching and Analysis of Well C

Well C was used to evaluate the injectivity of micellar and polymer solutions. The reservoir data and injection history are given in Appendix D. The daily injection data consisted of micellar solution injection followed by polymer solution injection. The polymer solution was displaced with water. The rheological data was limited for the injected fluids. Table 5.5 gives the apparent Brookfield viscosity of the polymer solution at 6 RPM.

Table 5.5

Apparent Viscosity and Screen Factor, Well C

Concentration (PPM)	Apparent Viscosity (cp)	Screen Factor
2300	37.0	11.8
2800	55.0	15.0
3100	70.0	17.5
3430	110.0	18.7

The injection pressures were limited to prevent fracturing of the reservoir. A falloff test was run prior to commencing micellar solution injection, which indicated a water mobility of 27 md/cp and a skin of -1.14. The skin and permeability calculated from the falloff test are used in the simulator. This reservoir had been extensively

waterflooded prior to the injection testing. The reservoir was estimated to be at residual oil saturation, therefore the history match was done using only single-phase flow.

The history match was conducted in the same manner used for Well B. The best history match was obtained by adjusting rheology and resistance factors. All other parameters were input from available data and assumed to be correct. The Carreau model was used to approximate the rheology of the polymer and micellar solution. History matching was done using both the rate and pressure control boundary conditions. For history matching purposes, all surface pressures were converted to bottomhole pressures.

Using the Neumann (rate control) boundary condition, Figures 5.12 and 5.13 were obtained. The overall match is not as good as obtained for Well B. There are several possible reasons for the poorer match. The simulator does not model the interfacial effects which occur with micellar solutions. The rheology of the micellar solution was estimated by assigning a polymer concentration to the micellar solution. The micellar slug was relatively small at 556 STB. The polymer concentrations could have varied with time. The rheology of the polymer solution used to obtain the best match is given in Tables D.3 and D.4 of Appendix D. It can be seen from these tables that if the concentration

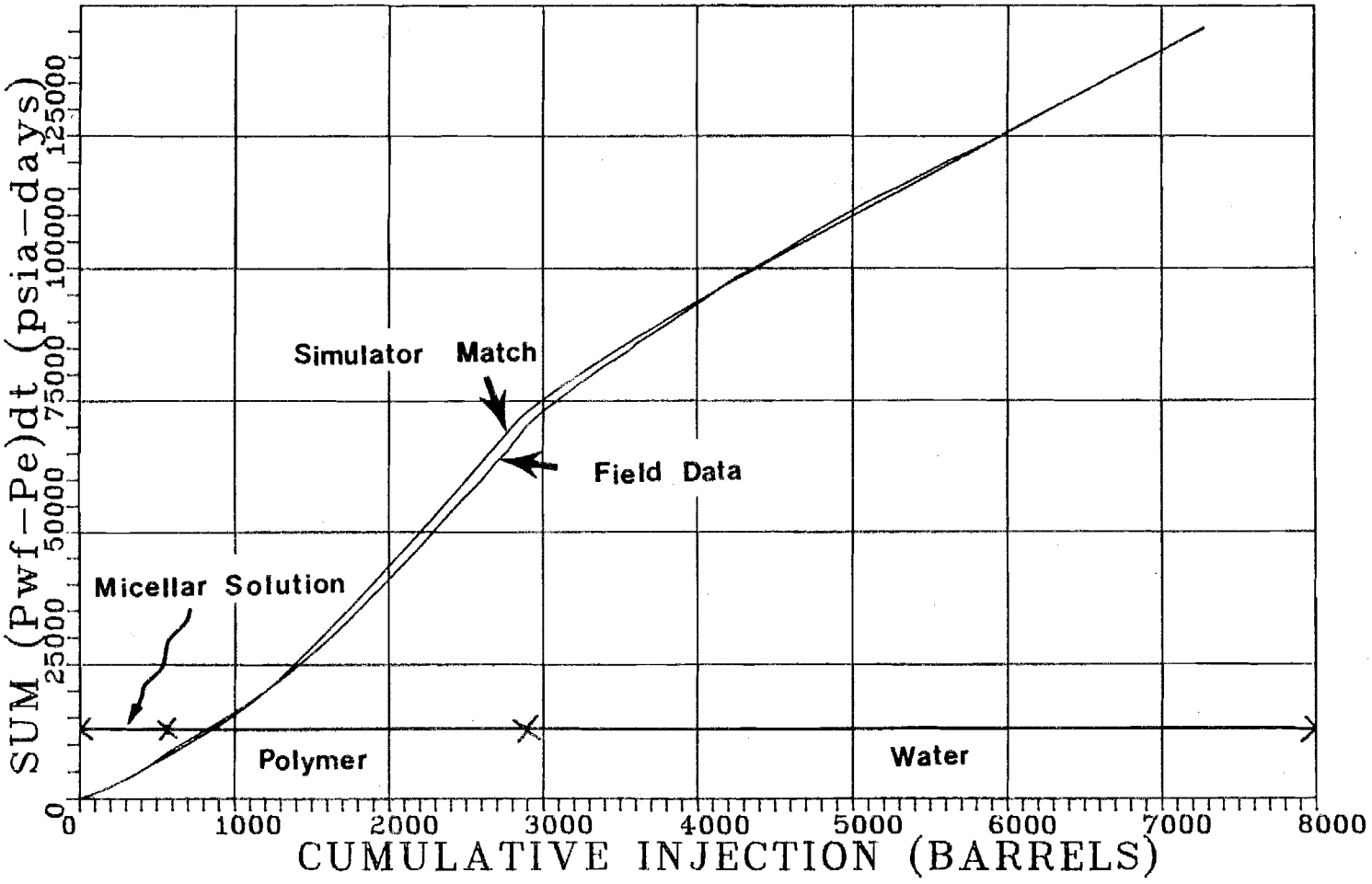

Figure 5.12

Hall Plot, Rate Control History Match, Well C

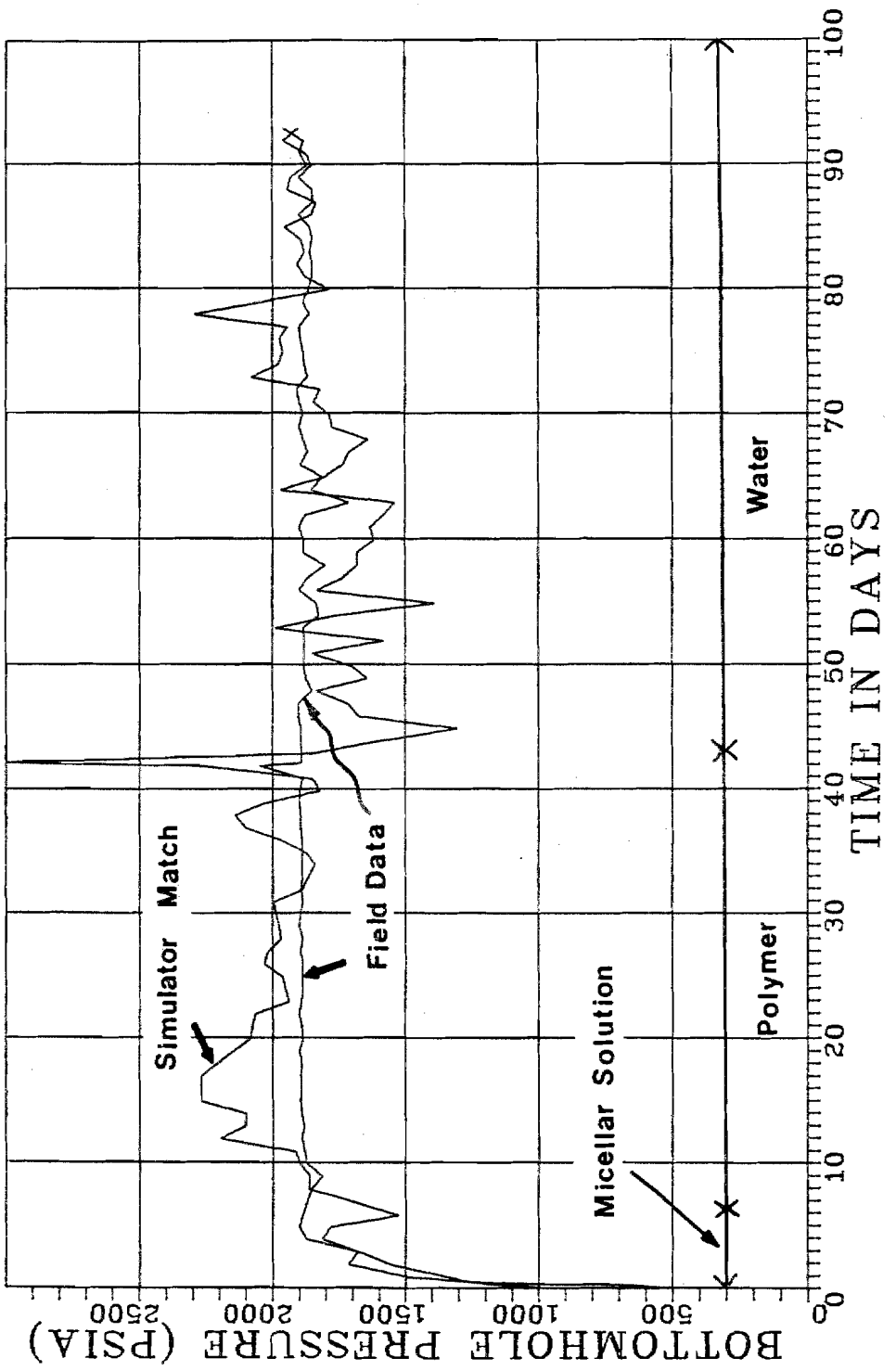

Figure 5.13

Bottomhole Pressure Versus Time, Rate Control History Match, Well C

varied plus or minus 10 percent, significant changes in viscosity could occur. There could also be inaccuracies in the recorded rates and pressures, which would result in a poorer match. Some of the data is suspect because as the injection rate is increased, and all other things remaining equal, there is no change in pressure. The amount of permeability reduction was much larger than for Well B. The maximum residual resistance factor used in the best match was 11.3. The history match using the pressure control boundary condition is shown in Figures 5.14 and 5.15. The match using the pressure control boundary condition is about the same as the match obtained using the rate control boundary condition. This can be seen when Figures 5.12 and 5.14 are compared. Reasons for problems with the match are the same as with the Neumann boundary condition. The maximum residual resistance factor used on the best match was 11.5. The rheology given in Tables B.3 and B.4 was used. Using the rate control boundary condition, cases were run with varying levels of adsorpton/retention. The results, as with Well B, were found to be very insensitive to the amount of adsorption/retention.

Figure 5.16 compares three different methods of integrating the Hall plot. For each method of integration, the slopes of the curves are quite different, as in the

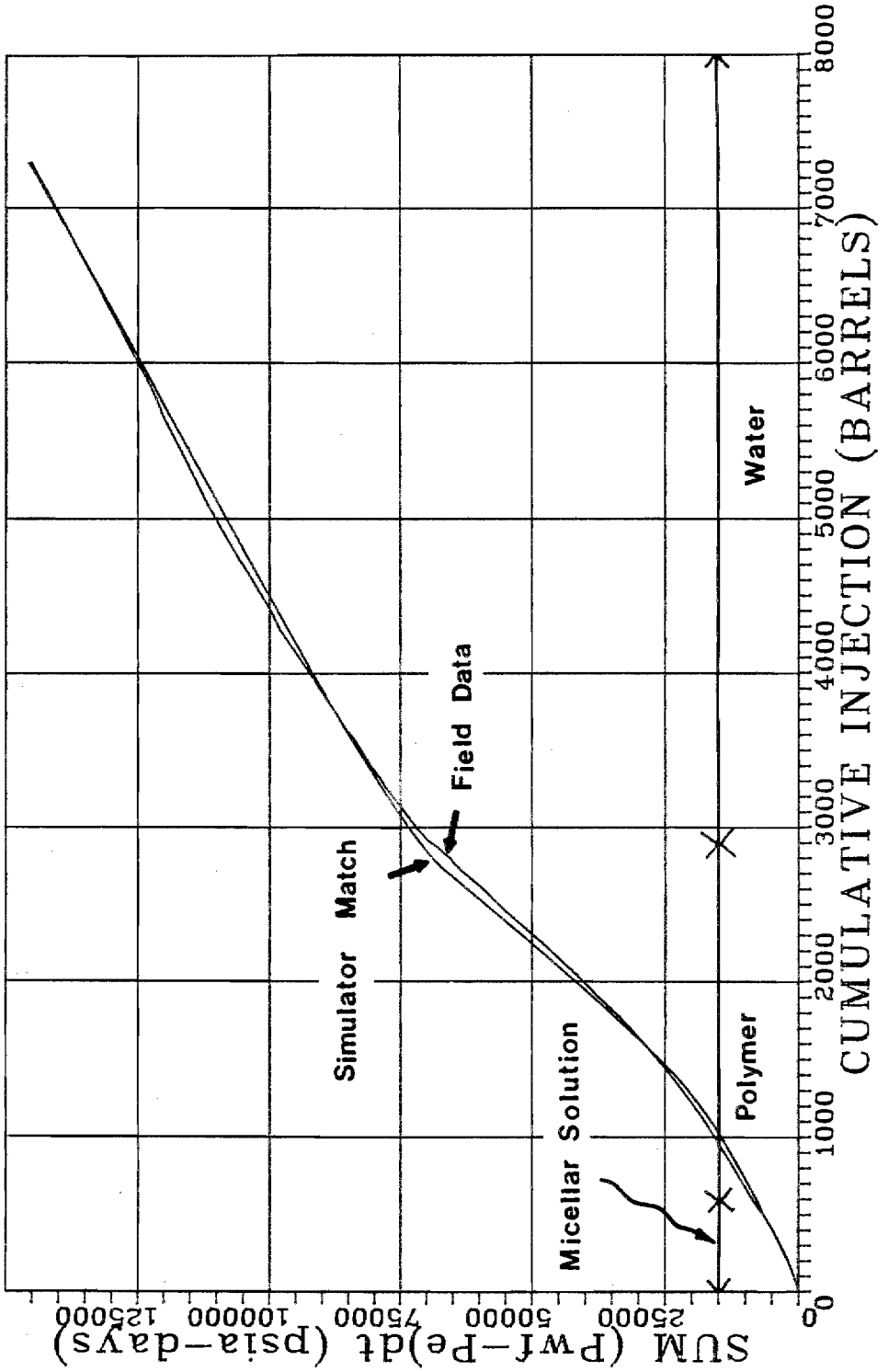

Figure 5.14

Hall Plot, Pressure Control History Match, Well C

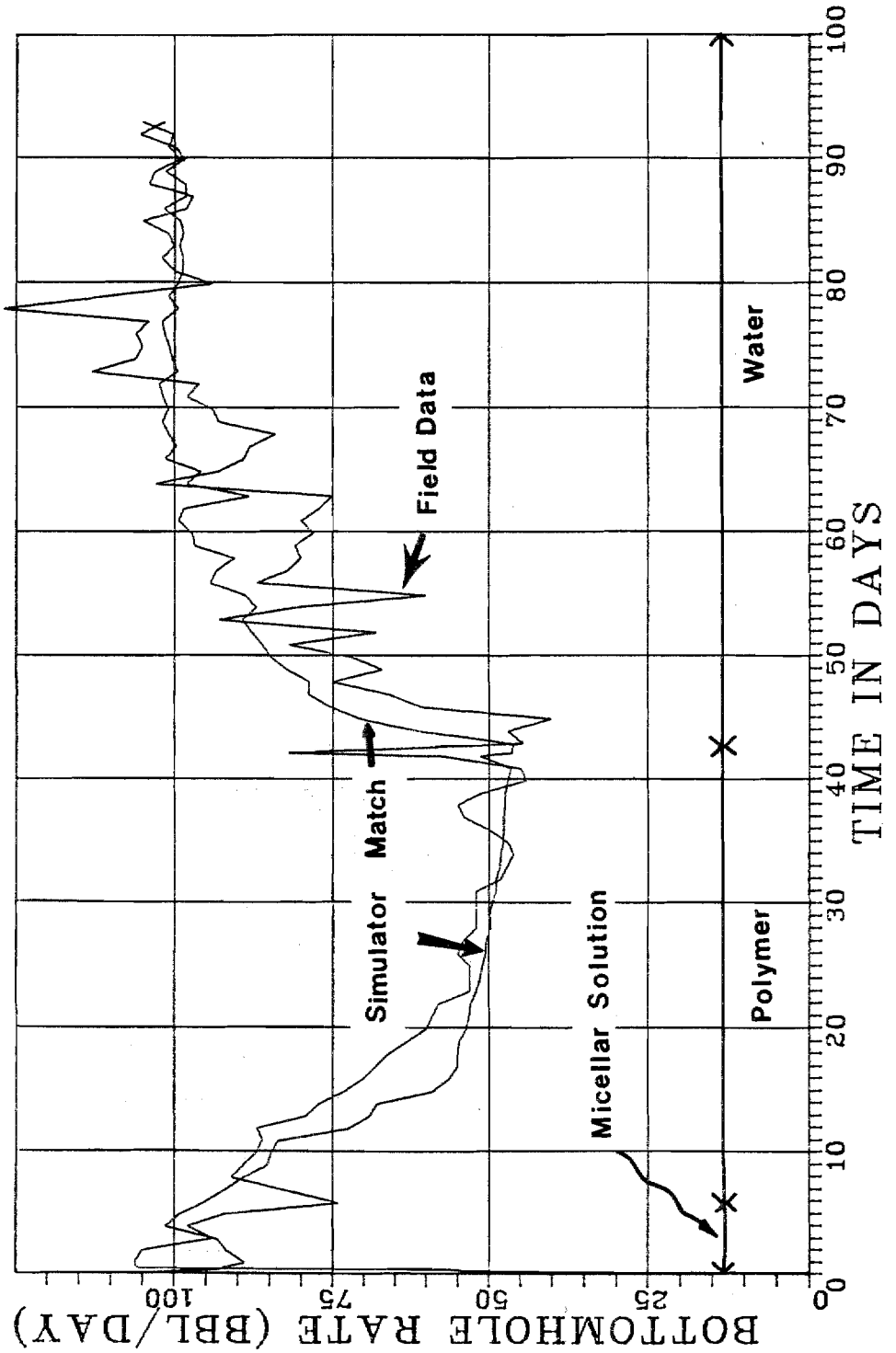

Figure 5.15

Bottomhole Rate Versus Time, Pressure Control History Match, Well C

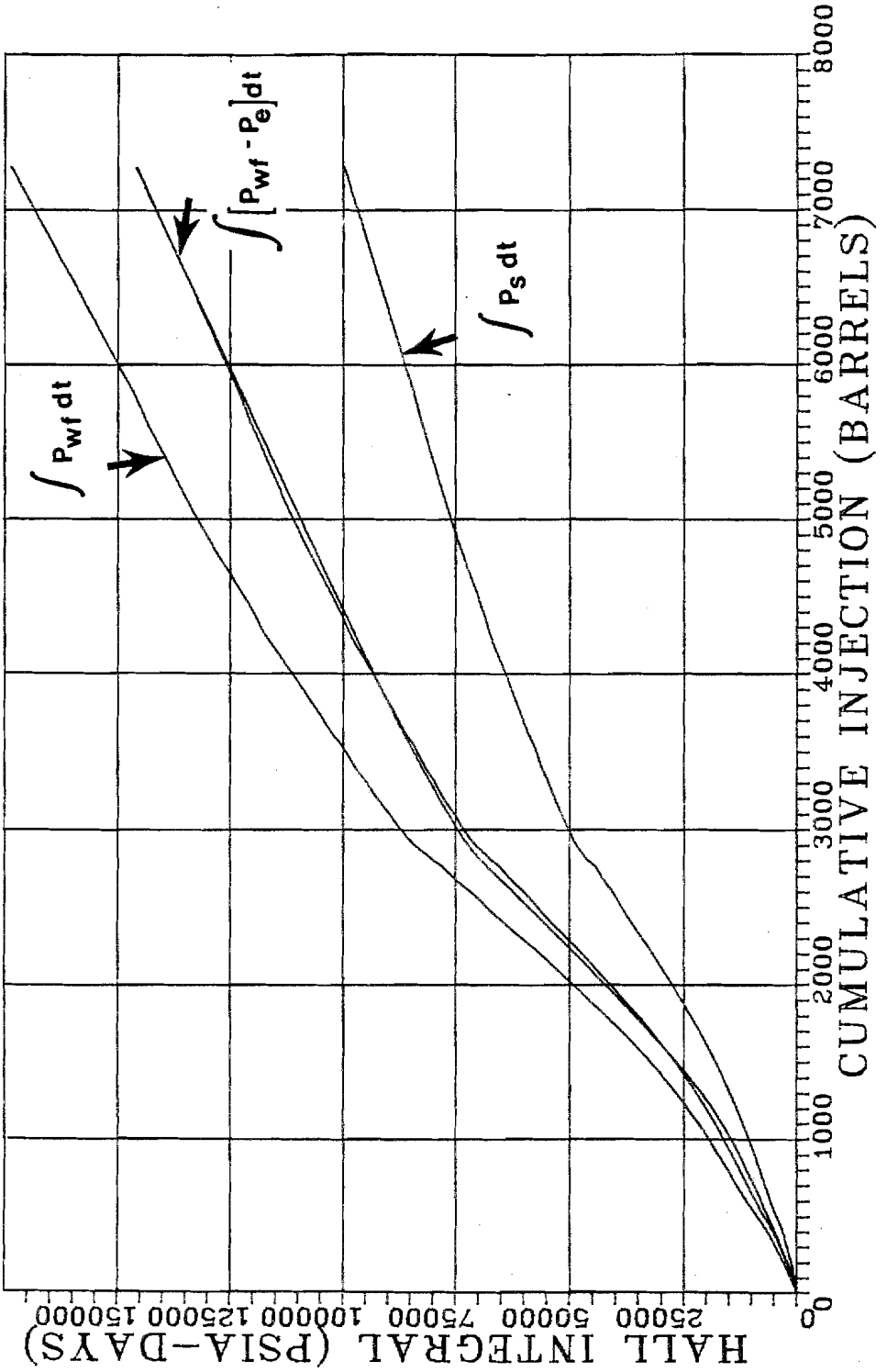

Figure 5.16

Comparison of Hall Integration Methods, Well C

previous section. An example correction will be done, as was performed in the previous section, on the water injection period given in Figure 5.16. The corrected slope of the Hall plot will be calculated using two points, one at a cumulative injection of 5000 STB and another at 7000 STB. The pressure at the external drainage radius is constant at 300 psia. The combined hydrostatic head and the pressure loss due to friction is equal to 800 psi. The data for the Hall plot corrections are given in Tables 5.6 and 5.7. When the corrections have been applied to the other integrations, the corrected values should agree closely with the slope of 16.50 (psia-days)/STB when using $\int(p_{wf}-p_e)dt$. The integral $\int p_s dt$ is corrected to calculate a Hall plot slope of 16.60 (psia-days)/STB, and $\int p_{wf} dt$ is corrected to calculate a Hall plot slope of 16.45 (psia-days)/STB. The difference in the corrected slopes and the slope from $\int(p_{wf}-p_e)dt$ is due to the accuracy with which values can be picked from Figure 5.16. Once the slopes have been corrected, all calculations proceed exactly the same.

Equations (4.9) and (4.10) can also be used to correct the slope directly. When the integral plotted is $\int p_{wf} dt$, equation (4.9) is used. Using the data given in Table 5.7, the slope using $\int p_{wf} dt$ is 19.50 (psia-days)/STB and the slope correction is 3.06. The corrected Hall plot slope,

Table 5.6

Hall Plot Integration Correction Example for $\int p_s dt$, Well C

Cum. Injection (STB)	Time (days)	$\int p_s dt$ (psig-days)	$(p_e - \rho gL + \Delta p_f)$ (psia-days)	Corr. Integral (psia-days)
7000.0	87.8	96,000	-43,900	139,900
5000.0	67.4	73,000	-33,700	106,700

$$m_H = \frac{139{,}900 - 106{,}700}{7000.0 - 5000.0} = 16.60 \text{ (psia-days)/STB}$$

Table 5.7

Hall Plot Integration Correction Example for $\int p_{wf} dt$, Well C

Cum. Injection (STB)	Time (days)	$\int p_{wf} dt$ (psig-days)	$p_e \Delta t$ (psia-days)	Corr. Integral (psia-days)
7000.0	87.8	166,000	26,300	139,700
5000.0	67.4	127,000	20,200	106,800

$$m_H = \frac{139{,}700 - 106{,}800}{7000.0 - 5000.0} = 16.45 \text{ (psia-days)/STB}$$

m_H, is calculated to be 16.44 (psia-days)/STB. If the integral $\int p_s dt$ is plotted equation (4.10) is used to correct the slope. The slope m'_H is equal to 11.50 (psia-days)/STB when the integral $\int p_s dt$ is used. The slope correction is calculated to be -5.10 (psia-days)/STB using equation (4.10), which yields a corrected slope of 16.60 (psia-days)/STB.

The Hall plot for Well C can be analyzed in a manner similar to what was done for Well B. There was no initial water injection data for this well. However, the slope prior to polymer and micellar solution injection, can be calculated since the skin and transmissibility are known. The Hall plot slope for water injection is calculated to be 1.6844 (psia-days)/STB based on the falloff testing data prior to polymer injection. The slope for the late water injection period is 16.50 (psia-days)/STB. Equation (5.7) can now be used to calculate a residual resistance factor of 9.80. The in situ residual resistance factor calculated in the simulator is 11.10 for this case. Table 5.8 compares the analytical solutions with the simulator results.

Equations (5.4) and (5.5) can now be used to calculate the average resistance factor of the polymer-micellar solution banks. At the end of polymer-micellar solution injection, the bank is at 54 feet and the Hall plot has a

slope of 35.3 (psia-days)/STB. The average resistance factor using equation (5.4) is 29.53. The average resistance factor can also be approximated by assuming a single bank which extends to the drainage radius, which results in an average resistance factor of 20.95. The pressure drop across the polymer bank is 1541 psi at a rate of 44.5 STB/day when the bank has reached a radius of 54 feet. The average resistance factor when applying Darcy's law is 29.4.

After water injection, the polymer-micellar bank is between 48 and 95 feet. The pressure drop across the bank is 325 psi at a rate of 105 STB/day. Applying Darcy's law again, an average resistance factor of 14.7 is calculated. Using equation (5.5), a resistance factor of 16.6 is calculated.

Table 5.9 illustrates the effect of shear thinning rheology. The apparent viscosity is given as a function of radial distance, concentration, and interstitial velocity. As can be seen in Table 5.9, the change in the apparent viscosity within the polymer bank is small. This indicates that the effect due to non-Newtonian rheology is relatively small on the Hall plot for Well C. Small changes in apparent viscosity within the polymer bank also occurred with Well B. Based on the history matching of Wells B and

C, it appears that the non-Newtonian flow effect is relatively small.

Table 5.8

Comparison of-Analytical Method with Simulator Results, Well C

Parameter	Analytical Method Multiple Banks	Analytical Method Single Bank	Simulator
R_{rf}	9.80	9.80	11.10
R_{f1}	29.53	20.95	29.40
R_{f2}	16.63	--	14.73

Table 5.9

Apparent Viscosity as a Function of Concentration and Radial Distance, Well C

Profile at 42.875 days, Cumulative Injection = 2807 BBL

Node No.	Distance (feet)	Concentration (ppm)	Inter. Vel. (ft/day)	App. Visc. (cp)
1	0.59	3430.0	22.06	2.47
2	0.99	3430.0	18.02	2.49
3	1.25	3430.0	13.53	2.52
4	1.40	3430.0	12.07	2.54
5	1.57	3430.0	10.77	2.55
6	1.75	3430.0	9.61	2.57
7	1.97	3430.0	8.57	2.59
8	2.20	3430.0	7.65	2.56
9	2.47	3430.0	6.82	2.55
10	2.77	3430.0	6.09	2.56

Table 5.9 (continued)

Node No.	Distance (feet)	Concentration (ppm)	Inter. Vel. (ft/day)	App. Visc. (cp)
11	3.10	3430.0	5.43	2.58
12	3.48	3430.0	4.84	2.60
13	3.90	3430.0	4.32	2.62
14	4.37	3430.0	3.85	2.65
15	4.90	3430.0	3.44	2.67
16	5.49	3430.0	3.07	2.69
17	6.15	3430.0	2.74	2.72
18	6.89	3430.0	2.44	2.75
19	7.72	3430.0	2.18	2.78
20	8.66	3430.0	1.94	2.81
21	9.70	3430.0	1.73	2.85
22	10.87	3430.0	1.55	2.89
23	12.18	3430.0	1.38	2.93
24	13.66	3430.0	1.23	2.97
25	15.30	3430.0	1.10	3.01
26	17.15	3430.0	0.98	3.06
27	19.22	3430.0	0.87	3.11
28	21.54	3427.4	0.79	3.17
29	24.15	3410.7	0.69	3.24
30	27.06	3346.2	0.62	3.31
31	30.33	3181.3	0.55	3.41
32	33.99	2867.3	0.49	2.79
33	38.09	2365.6	0.44	1.77
34	42.69	1684.3	0.39	1.72
35	47.85	965.5	0.35	1.55
36	53.62	421.6	0.31	1.31
37	60.10	135.7	0.28	1.11
38	67.35	31.8	0.25	1.03
39	75.49	5.4	0.22	1.00
40	84.60	0.7	0.20	1.00
41	94.81	0.1	0.18	1.00
42	106.26	0.0	0.16	1.00
43	119.09	0.0	0.14	1.00
44	133.47	0.0	0.13	1.00
45	149.58	0.0	0.11	1.00
46	167.65	0.0	0.10	1.00
47	187.89	0.0	0.09	1.00
48	210.57	0.0	0.08	1.00
49	235.99	0.0	0.07	1.00
50	264.99	0.0	0.06	1.00

CHAPTER 6

CONCLUSIONS

Using a numerical reservoir simulator, it has been demonstrated that quantitative analysis can be performed on the Hall plot when non-Newtonian solutions are injected into petroleum reservoirs. The best method for analyzing the Hall plot would be to use a reservoir simulator as developed for this study. However, for the practicing engineer a simulator may not be available. The simulator is also the most time-consuming type of analysis. Two approximate analysis methods for the Hall plot have been developed which can be implemented easily by the practicing petroleum engineer.

One analysis method is based on a single-fluid bank that extends to the drainage radius, and a second method is based on multiple-fluid banks. While neither analysis method will yield results as accurate as those obtained from the simulator, the appropriate method will yield results which are of acceptable accuracy for most oilfield engineering computations. The methods developed can be used to calculate permeabilities, resistance factors, and residual resistance factors.

The conclusions of this study are now summarized.

1. The Hall plot will generate the correct qualitative

response when the Hall integral $\int p_s dt$ is used, if the rates are relatively constant and/or the integral $\int(p_e+\Delta p_f-\rho gL)dt$ is neglible. The Hall plot will generate the correct qualitative response when the Hall integral $\int p_{wf} dt$ is used, if the rates are relatively constant and/or the integral $\int p_e dt$ is neglible. The correct qualitative response will always be generated when the Hall integral $\int(p_{wf}-p_e)dt$ is used. The slope of the Hall plot will increase when the mobility of the injected fluid decreases, and the slope will decrease when the mobility of the injected fluid increases.

2. To perform quantitative analysis using the Hall plot, the integral plotted should be $\int(p_{wf}-p_e)dt$. It is possible to perform quantitative analysis using $\int p_s dt$ or $\int p_{wf} dt$, but it is necessary to correct the integrals such that they are equivalent to $\int(p_{wf}-p_e)dt$. In some situations, it may be possible to make a quantitative analysis of the Hall plot when the Hall integral is $\int p_s dt$, if the quantity $\int(p_e+\Delta p_f-\rho gL)dt$ is approximately equal to zero. In general, the quantity $\int(p_e+\Delta p_f-\rho gL)dt$ will not be negligible. The Hall integral $\int p_{wf} dt$ can be used for quantitative calculations only when the $\int p_e dt$ can be considered to be zero or the appropriate correction is made to the Hall plot slope.

3. In general, the multibank analysis method will yield more accurate answers than the single-bank method. When the fluid bank in contact with the wellbore has moved out a short distance, the multibank analysis method should be used. When the fluid bank in contact with the wellbore has moved out a substantial distance, the single-fluid bank analysis method can be used with good accuracy. The single-bank analysis method has problems when fluid banks of very different properties exist in the reservoir.
4. It is possible to calculate the resistance factor of a polymer bank as it moves away from the wellbore, but the calculated resistance factor is very sensistive to small errors in the Hall plot slope.
5. The non-Newtonian rheology effect is small based on the two wells which were history matched; that is, the change in the in-situ apparent viscosity of the polymer solutions through space is relatively small.
6. The amount of permeability reduction has a significant effect on the Hall plot and simulator results. The Hall plot and simulator results are very insensistive to the amount of polymer adsorption/retention.
7. The transient flow period has little effect on the Hall plot because, in most field situations, the transient

period rarely lasts more than a few days. During the transient flow period, the Hall plot slope rapidly approaches the steady state slope; therefore, the slope during the transient period is usually quite close to the steady state slope after a short period of time. Since most Hall plot data is usually recorded on a daily basis, it is usually not possible to observe the transient flow period on the Hall plot.

8. In a reservoir which has been extensively waterflooded prior to polymer injection, that is, the reservoir is close to residual oil saturation in the vicinity of the wellbore, multiphase flow is not significant. A good history match was obtained for Wells B and C, ignoring multiphase flow where the reservoir had been extensively waterflooded. For a reservoir that is initially oil saturated, the importance of considering multiphase flow is dependent on the difference in the mobility of the two flowing phases. For example, if water is displacing a high viscosity oil, then multiphase flow is very important. As the injected fluid displaces oil away from the well, multiphase flow will become less significant. The shape of the relative permeability curves can also have an important effect on the importance of multiphase flow.

9. When history matching field injectivity data, there was no significant difference found in assuming that field rates were correct and matching pressures (Neumann), or assuming field pressures were correct and matching rates (Dirichlet). The history match obtained using the field recorded rates to control the wellbore boundary condition yields basically the same polymer solution parameters as using the field recorded pressures to control the wellbore boundary condition.
10. Comparing the in-situ apparent viscosities for the polyacrylamide solutions used in Wells B and C, the polymer used in well B performed better. Using approximately 25 percent of the polymer concentration as used in Well C, the Well B polymer solution developed more apparent viscosity. The in-situ apparent viscosities of the two polymer solution can be seen in Tables 5.1 and 5.9. It should be noted that the molecular-weight distributions were different for each polymer. The Well B reservoir was also at a higher temperature than the Well C reservoir.
11. The number of cells required to obtain convergence of the numerical solution generated by the simulator is a function of the residual resistance factor. As the the residual resistance factor becomes larger, more cells

are required to obtain convergence of the numerical solution. More cells are required to obtain convergence at higher resistance factors because a small amount of numercial dispersion in the concentration front, can result in large permeability changes in the cells in which the dispersion occurs.

There are several areas in which additional research could be performed to extend the work done in this study. A more elaborate reservoir simulator could be developed. Multiple communicating layers and fracturing occur frequently in field situations. The simulator used for this study is not designed to handle multiple communicating layers or fractured wells in a rigorous manner. The reservoir is assumed to be above the bubble point at all times for this study. However, a three-phase simulator could be used to consider the presence of a gas saturation when the reservoir pressure dropped below the bubble point. The simulator used for this study considers only three components. A more elaborate simulator would allow consideration of additional components such as: sodium, calcium, and magnesium ions. The influence of other components such as sodium and calcium ions was demonstrated

in the analysis of Well B, with the differing injectivity of brine and fresh water. Another useful extension of this work is the development of dimensionless Hall type curves as a method of analysis.

REFERENCES CITED

Bird, R. B.; Stewart, W. E.; and Lightfoot, E. N., 1960, Transport Phenomena, John Wiley and Sons, New York.

Blair, P. M. and Weinaug, C. F., 1969, "Solution of Two-Phase Flow Problems Using Implicit Difference Equations," Soceity of Petroleum Engineers Journal, December, pp. 417-424.

Bondor, P. L.; Hirasaki, G. J.; and Tham, M. J., 1973, "Mathematical Simulation of Polymer Flooding in Complex Reservoirs," Society of Petroleum Engineers Reprint Series No. 11, Numerical Simulation, pp. 394-407.

Buckley, S. E. and Leverett, M. C., 1942, "Mechanism of Fluid Displacement in Sands," Transactions A.I.M.E., vol. 146, p. 107.

Carreau, J. P., 1968, Rheological Equations from Molecular Network Theories, Ph.D. Thesis, University of Wisconsin, Madison.

Chauveteau, G., 1981b, "Molecular Interpretation of Several Different Properties of Flow of Coiled Polymer Solutions Through Porous Media in Oil Recovery Conditions," Society of Petroleum Engineers, paper no. 10060.

Christopher, R. H. and Middleman, S., 1965, "Power-Law Flow Through a Packed Tube," I&EC Fundamentals, vol. 4, no. 4, pp. 422-426.

Cohen, Y. and Christ, F. R., 1984, "Polymer Retention and Adsorption in the Flow of Polymer Solutions Through Porous Media," Society of Petroleum Engineers, paper no. 12942.

Cohen, Y. and Christ, F. R., 1986, "Polymer Retention and Adsorption in the Flow of Polymer Solutions Through Porous Media," Society of Petroleum Engineers Reservoir Engineering, March, pp. 113-118.

Collins, R. E., 1961, Flow of Fluids Through Porous Materials, Petroleum Publishing, Tulsa.

Craig, F. F., 1971, The Reservoir Engineering Aspects of Waterflooding, Monograph no. 3, Society of Petoleum Engineers, Dallas.

Dawson, R. and Lantz, R. B., 1974, "Inacessible Pore Volume in Polymer Flooding," Society of Petroleum Engineers, paper no. 3522.

DeMarco, M., 1968, "Simplified Method Pinpoints Injection Well Problems," World Oil, pp. 95-100.

Earlougher, Jr., R. C., 1977, Advances in Well Test Analysis, Monograph no. 5, Society of Petroleum Engineers, Dallas.

Fanchi, J. R., 1985, "CHEM2D: A Two Dimensional, Three-Phase, Nine Component Chemical Flood Simulator, Volumes I, II, and III," Department of Energy, DOE/BC 10033, April.

Gencer, C. S. and Ikoku, C. U., 1984, "Well Test Analysis for Two-Phase Flow of Non-Newtonian Power-Law and Newtionian Fluids," Journal of Energy Resources Technology, June, vol. 106, pp. 295-305.

Gogarty, W. B., 1967a, "Rheological Properties of Pseudoplastic Fluids in Porous Media," Society of Petroleum Engineers Journal, June, pp. 149-160.

Hall, H. N., 1963, "How to Analyze Waterflood Injection Well Performance," World Oil, October, pp. 128-130.

Hawkins, M. F.,Jr., 1965, " A Note on the Skin Effect," Journal of Petroleum Technology, December, p. 65.

Hirasaki, G. J. and Pope, G. A., 1974, "Analysis of Factors Influencing Mobility and Adsorption in the Flow of Polymer Solution Through Porous Media," Society of Petroleum Engineers Journal, August, pp. 337-346.

Horner, D. R., 1951, "Pressure Buildup in Wells," Proceeding of the Third World Petroleum Congress, The Hague, section II, p. 503-523.

Huh, C. and Snow, T. M., 1985, "Well Testing with a Non-Newtonian Fluid in the Reservoir," Society of Petroleum Engineers, paper no. 14453,

Ikoku, C. U. and Ramey Jr., H. J., 1979, "Transient Flow of Non-Newtonian Power-Law Fluids in Porous Media," Society of Petroleum Engineers Journal, June, pp. 164-174.

Ikoku, C. U. and Ramey Jr., H. J., 1980, "Wellbore Storage and Skin Effects During the Transient Flow of Non-Newtionian Power-Law Fluids in Porous Media," Society of Petroleum Engineers Journal, February, pp. 25-38.

Ikoku, C. U. and Ramey Jr., H. J., 1982, "Pressure Behavior During Polymer Flow in Petroleum Reservoirs," Journal of Energy Resources Technology, June, vol. 104, pp. 149-156.

Jennings, R. R.; Rogers, J. H.; and West, T. J., 1971, "Factors Influencing Mobility Control by Polymer Solutions," Journal of Petroleum Technology, March, pp. 391-401.

Lecourtier, J. and Chauveteau, G., 1984, "Propagation of Polymer Slugs Through Porous Media," Society of Petroluem Engineers, paper no. 13034.

Lee, J., 1982, Well Testing, Society of Petroleum Engineers, Dallas.

Lund, O. and Ikoku, C. U., 1980, "Pressure Transient Behavior of Non-Newtonian/Newtonian Composite Reservoirs," Society of Petroleum Engineers, paper no. 9401.

Maerker, J. M., 1975, "Shear Degradation of Partially Hydrolyzed Polyacrylamide Solutions," Society of Petroleum Engineers Journal, August, pp. 311-322.

Maerker, J. M., 1976, "Mechanical Degradation of Partially Hydrolyzed Polyacrylamide Solutions in Unconsolidated Porous Media," Society of Petroleum Engineers Journal, 1976, August, pp. 172-174.

Marshall, R. J. and Metzner, A. B., 1966, "Flow of Viscoelastic Fluids Through Porous Media," Society of Petroleum Engineers, paper no. 1687.

Marshall, R. J. and Metzner, A. B., 1967, "Flow of Viscoelastic Fluids Through Porous Media," I&EC Fundamentals, August, vol. 6, no. 4, pp. 393-400.

Matthews, C. S. and Russell, D. G., 1967, Pressure Buildup and Flow Tests in Wells, Society of Petroleum Engineers, Dallas.

Milton Jr., H. W.; Argabright, P. A.; and Gogarty, W. B., 1983, "EOR Prospect Evaluation Using Field Manufactured Polymer," Society of Petroleum Engineers, paper no. 11720.

Moffitt, P. D. and Menzie, D. E., 1978, "Well Injection Tests of Non-Newtonian Fluids," Society of Petroleum Engineers, paper no. 7177.

Morris, C. W. and Jackson, K. M., 1978, "Mechanical Degradation of Partially Hydrolyzed Polyacrylamide Solutions in Porous Media," Society of Petroleum Engineers, paper no. 7064.

Mungan, N., 1972, "Shear Viscosities of Ionic Polyacrylamide Solutions," Society of Petroleum Engineers Journal, December, pp. 469-472.

Nowak, T. J. and Lester, G. W., 1955, "Analysis of Pressure Fall-Off Curves Obtained in Water Injection Wells to Determine Injective Capacity and Formation Damage," Petroleum Transactions, AIME, pp. 96-102.

Odeh, A. S. and Yang, H. T., 1979, "Flow of Non-Newtonian Power-Law Fluids Through Porous Media," Society of Petroleum Engineers Journal, June, pp. 155-163.

Poettmann, F. H., 1983, Improved Oil Recovery, Interstate Oil Compact Commission, Oklahoma City

Poettmann, F. H., 1985, Lecture notes, Colorado School of Mines.

Sadowski, T. J. and Bird, R. B., 1965, "Non-Newtonian Flow Through Porous Media. I. Theoretical," Transactions of the Society of Rheology, pp. 243-250.

Sadowski, T. J., 1965, "Non-Newtonian Flow Through Porous Media. II. Experimental," Transactions of the Society of Rheology, pp. 251-271.

Savins, J. G., 1969, "Non-Newtonian Flow Through Porous Media," Industrial and Engineering Chemistry, October, vol. 61, no. 10, pp. 18-47.

Seright, R. S., 1980, "The Effects of Mechnical Degradation and Viscoelastic Behavior on Injectivity of Polyacrylamide Solutions," Society of Petroleum Engineers, paper no. 9297.

Smith, J. T., 1982, Pressure Transient Analysis, Texas Tech., Lubbock, Texas.

Truesdell, C., 1964, "The Natural Time of a Viscoelastic Fluid: Its Significance and Measurement," Physics of Fluids, August, pp. 1134-1142.

Van Everdingen, A. F. and Hurst, W., 1949, "The Application of the Laplace Transformation to Flow Problems in Reservoirs," Petroleum Transactions of the AIME, December, vol. 186, pp. 305-324.

Van Poollen, H. K. and Jargon, J. R., 1969, "Steady-State and Unsteady-State Flow of Non-Newtonian Fluids Through Porous Media," Society of Petroleum Engineers Journal, March, pp. 80-88.

Vogel, P. and Pusch G., 1981, "Some Aspects of the Injectivity of Non-Newtonian Fluids in Porous Media," edited by F. John Fayers, Enhanced Oil Recovery, Elsevier, New York, pp. 179-196.

Vongvuthipornchai, S. and Raghavan, R., 1984, "Pressure Falloff Behavior in Vertically Fractured Wells: Non-Newtonian Power-Law Fluids," Society of Petroleum Engineers, paper no. 13058.

Vongvuthipornchai, S. and Raghavan, R., 1985, "Well Test Analysis of Data Dominated by Storage and Skin: Non-Newtionian Power-Law Fluids," Society of Petroleum Engineers, paper no. 14454.

Welge, H. J., 1952, "A Simplified Method for Computing Oil Recoveries by Gas or Water Drive," Transactions of the A.I.M.E., vol. 91, p.195

Weinstein, H.; Nolen, J. S.; and Chappelear, J. E., 1986, "Second Comparative Solution Project: A Three-Phase Coning Study," Journal of Petroleum Technology, March, pp. 345-353.

UNCITED REFERENCES

Al-Fariss, T. and Pinder, K. L., 1985, "Flow Through Porous Media of a Shear-Thinning Liquid with Yield Stress: A Friction Factor Correlation," Society of Petroleum Engineers, paper no. 14683.

Appleyard, J. R.; Cheshire, I. M.; and Pollard, R. K., 1981, "Special Techniques for Fully Implicit Simulators," edited by F. John Fayers, Enhanced Oil Recovery, Elsevier, New York, pp. 395-408.

Argabright, P. A.; Rhudy, J. S.; and Phillips, B. L., 1982, "Partially Hydrolyzed Polyacrylamides with Superior Flooding and Injection Properties," Society of Petroleum Engineers, paper no. 11208.

Aziz, K. and Settari, A., 1979, Petroleum Reservoir Simulation, Elsevier Applied Science, New York.

Aziz, K., 1981, "Numerical Modelling of EOR Processes," edited by F. John Fayers, Enhanced Oil Recovery, Elsevier, New York, pp. 367-379.

Baijal, S. K., 1980, Flow Behavior of Polymers in Porous Media, Pennwell, Tulsa.

Benson, S. M. and Bodvarsson, G. S., 1982, "Nonisothermal Effects During Injection and Falloff Tests," Society of Petroleum Engineers, paper no. 11137.

Bird, R. B., 1976, "Useful Non-Newtionian Models," Annual Review of Fluid Mechanics, vol. 8, Annual Reviews, Palo Alto, pp. 13-35.

Bird, R. B.; Armstrong, R. C.; and Hassager, O., 1982, Dynamics of Polymeric Liquids, vol. 1, John Wiley, New York, pp. 270-273.

Carnahan, B.; Luther, H. J.; and Wilkes, J. O., 1969, Applied Numerical Methods, John Wiley, New York.

Castagno, R. E.; Shupe, R. D.; Gregory, M. D.; and Lescarboura, J. A., 1984, "A Method for Laboratory and Field Evaluation of a Proposed Polymer Flood," Society of Petroleum Engineers, paper no. 13124.

Chauveteau, G. and Zaitoun, A., 1981a, "Basic Rheological Behaviour of Xanthan Polysaccharide Solutions in Porous Media: Effects of Pore Size and Polymer Concentration," edited by F. John Fayers, Enhanced Oil Recovery, Elsevier, New York, pp. 197-212.

Claridge, E. L., 1979, "A Layered Pattern Simulator for Non-Newtonian Fluids in Graded Viscosity Banks," Society of Petroleum Engineers, paper no. 7691.

Crichlow, H. B., 1977, Modern Reservoir Engineering - A Simulation Approach, Prentice-Hall, Englewood Cliffs, New Jersy.

Crochet, M. J. and Walters, K., 1983, "Numerical Methods in Non-Newtonian Fluid Mechanics," edited by Van Dyke, Milton; Wehausen, J. V.; and Lumley, John L., Annual Review of Fluid Mechanics, Annual Reviews, Palo Alto, pp. 241-260.

Dake, L. P., 1978, Fundamentals of Resevoir Engineering, Elsevier Scientific Publishing, New York.

Daubin, D. L. and Menzie, D. E., 1967, "Flow of Polymer Solutions Through Porous Media," Journal of Petroleum Technology, August, pp. 1065-1073.

Doe, P. H.; Carey, B. S.; and Helmuth, E. S., 1984, "The National Petroleum Council EOR Study: Chemical Processes," Society of Petroleum Engineers, paper no. 13240.

Dominguez, J. G. and Willhite, G. P.; 1977, "Retention and Flow Characteristics of Polymer Solutions in Porous Media," Society of Petroleum Engineers Journal, April, pp. 111-121.

Ershaghi, I. and Handy, L. L., 1971, "Mobility of Polymer Solutions in Porous Media," Society of Petroleum Engineers, paper no. 3683.

Ewing, R. E., 1983, The Mathematics of Reservoir Simulation, Frontiers in Applied Mathematics no. 1, Society of Industrial and Applied Mathematics, Philadelphia.

Ferrer, J., 1972, "Some Mechansitic Features of Flow of Polymers Through Porous Media," Society of Petroleum Engineers, paper no. 4029.

Foulser, R. W. S., 1981, "Some Considerations Concerning the Efficiency of Chemical Flood Simulators," edited by F. J. Fayers, Enhanced Oil Recovery, Elsevier, New York, pp. 409-424.

Gaitonde, N. Y. and Middleman, S., 1966, "Flow of Viscoelastic Fluids Through Porous Media," Society of Petroleum Engineers, paper no. 1685.

Gencer, C. S., 1982, Well Test Analysis for Two-Phase Flow of Viscoelastic and Newtonian Fluids, Masters Thesis, University of Tulsa.

Gogarty, W. B., 1967b, "Mobility Control With Polymer Solutions," Society of Petroleum Engineers Journal, June, pp. 161-173.

Gogarty, W. B.; Levy, G. L.; and Fox, V. G., 1972, "Viscoelastic Effects in Polymer Flow Through Porous Media," Society of Petroleum Engineers, paper no. 4025.

Harvey, A. H. and Menzie, D. E., 1970, "Polymer Solution Flow in Porous Media," Society of Petroleum Engineers Journal, June, pp. 111-118.

Heemskerk, J.; Janssen-van Rosmalen, R.; Holtslag, R. J.; and Teeuw, D., "Quantification of Viscoelastic Effects of Polyacrylamide Solutions," Society of Petroleum Engineers, paper no. 12652.

Ikoku, C. U., 1978, Transient Flow of Non-Newtonian Power-Law Fluids in Porous Media, Doctoral Dissertation, Stanford University.

Ikoku, C. U. and Ramey Jr., H. J., 1978, "Numerical Solution of the Nonlinear Non-Newtonian Partial Differential Equation," Society of Petroleum Engineers, paper no. 7661.

Ikoku, C. U., 1982, "Well Test Analysis for Enhanced Oil Recovery Projects," Journal of Energy Resources Technology, June, vol. 104, pp. 142-148.

Jones, R. S.; Pope, G. A.; Ford, H. J.; and Lake, L. W., 1984, "A Predictive Model for Water and Polymer Flooding," Society of Petroleum Engineers, paper no. 12653.

Jones, W. M. and Maddock, J. L., 1966, "Flow of Viscoelastic Liquids: Comparison of Departures from Laminar Flow in Porous Beds and in Tubes," Society of Petroleum Engineers, paper no. 1686.

Kazemi, H.; Merrill, L. S.; and Jargon, J. R., 1972, "Problems in Interpretation of Pressure Fall-Off Tests in Reservoirs with and without Fluid Banks," Journal of Petroleum Technology, September, pp. 1147-1156.

Klein, J. and Kulicke, W. M., 1980, "Polymer-Polymer and Polymer-Solid Interaction and Their Relevance for Polymer Application in Enhanced Oil Recovery," Society of Petroleum Engineers, paper no. 8980.

Koning, E. J. L. and Niko, H., 1985, "Fractured Water-Injection Wells: A Pressure Falloff Test for Determining Fracture Dimensions," Society of Petroleum Engineers, paper no. 14458.

Letkeman, J. P. and Ridings, R. L., 1970, "A Numerical Coning Model," Society of Petroleum Engineers Journal, December, pp. 418-424.

MacDonald, R. C. and Coats, K. H., 1970, "Methods for Numerical Simulation of Water and Gas Coning," Society of Petroleum Engineers Journal, December, pp. 425-436.

McDonald, A. E., 1979, "Approximate Solutions for Flow of Non-Newtonian Power Law Fluids Through Porous Media," Society of Petroleum Engineers, paper no. 7690.

McKinley, R. M.; Jahns, H. O.; Harris, W. W.; and Greenkorn, R. A., 1966, "Non-Newtonian Flow in Porous Media," A.I.Ch.E. Journal, January, vol. 12, no. 1, pp. 17-20.

Meister, J. J.; Pledger Jr., H.; Hogen-Esch, T. E.; and Butler, G. B., 1980, "Retention of Polyacrylamide by Berea Sandstone, Baker Dolomite, and Sodium Kaolinite During Polymer Flooding," Society of Petroleum Engineers, paper no. 8981.

Merrill Jr., L. S.; Kazemi, H.; and Gogarty, W. B., 1974, "Pressure Falloff Analysis in Reservoirs with Fluid Banks," Journal of Petroleum Technology, July, pp. 809-818.

Moradi-Arghi, A. and Doe, P. H., 1984, "Stability of Polyacrylamides in Hard Brines at Elevated Temperatures," Society of Petroleum Engineers, paper no. 13033.

Mungan, N.; Smith, F. W.; and Thompson, J. L., 1966, "Some Aspects of Polymer Floods," Journal of Petroleum Technology, September, pp. 1143-1150.

Mungan, N., 1969, "Rheology and Adsorption of Aqueous Polymer Solutions," The Journal of Canadian Petroleum Technology, April-June, pp. 45-50.

Murtha, J. A. and Ertekin, T., 1983, "Numerical Simulation of Power-Law Fluid Flow in a Vertically Fractured Reservoir," Society of Petroleum Engineers, paper no. 12011.

Nouri, H., H. and Root, P. J., 1971, "A Study of Polymer Solution Rheology, Flow Behavior, and Oil Displacement Processes," Society of Petroleum Engineers, paper no. 3523.

Omar, A. E., 1983, "Effect of Polymer Adsorption on Mobility Ratio," Society of Petroleum Engineers, paper no. 11503.

Park, H. C.; Hawley, M. C.; and Blanks, R. F., 1973, "The Flow of Non-Newtonian Solutions Through Packed Beds," Society of Petroleum Engineers, paper no. 4722.

Pirson, S. J.; Boatman, E. M.; and Nettle, R. L., 1964, " Prediction of Relative Permeability Characteristics of Intergranular Reservoir Rocks from Electrical Resistivity Measurements," Journal of Petroleum Technology, May, pp. 561-570.

Pope, G. A., 1980, "The Application of Fractional Flow Theory to Enhanced Oil Recovery," Society of Petroleum Engineers Journal, June, pp. 191-205.

Pye, D. J., 1964, "Improved Secondary Recovery by Control of Water Mobility," Journal of Petroleum Technology, August, pp. 911-916.

Sandiford, B. B., 1964, "Laboratory and Field Studies of Water Floods Using Polymer Solutions to Increase Oil Recoveries," Journal of Petroleum Technology, August, pp. 917-922.

Sarem, A. M., 1970, "On the Theory of Polymer Solution Flooding Process," Society of Petroleum Engineers, paper no. 3002.

Schneider, F. N. and Owens, W. W., 1980, "Steady-State Measurements of Relative Permeability for Polymer-Oil Systems," Society of Petroleum Engineers, paper no. 9408.

Settari, A. and Aziz, K., 1975, "A Computer Model for Two-Phase Coning Simulation," Society of Petroleum Engineers Journal, June, pp. 221-236.

Slater, G. E. and Farouq-Ali, S. M., 1970, "Two-Dimensional Polymer Flood Simulation," Society of Petroleum Engineers, paper no. 3003.

Slattery, J. C., 1966, "Flow of Viscoelastic Fluids Through Porous Media," Society of Petroleum Engineers, paper no. 1684.

Smith, F. W., 1968, "A Rapid Method of Determining Characteristics of Liquid Flow in Porous Media," Journal of Petroleum Technology, November, pp. 1219-1220.

Smith, F. W., 1970, "The Behavior of Partially Hydrolyzed Polyacrylamide Solutions in Porous Media," Journal of Petroleum Technology, February, pp. 148-156.

Sonier, F.; Besset, P.; and Ombret, O., 1973, "A Numerical Model of Multiphase Flow Around a Well," Society of Petroleum Engineers Journal, December, pp. 311-320.

Sorbie, K. S. and Roberts, L. J., 1984, "A Model for Calculating Polymer Injectivity including the Effects of Shear Degradation," Society of Petroleum Engineers, paper no. 12654.

Sosa, A.; Raghavan, R.; and Limon, T. J., 1981, "Effect of Relative Permeability and Mobility Ratio on Pressure Falloff Behavior", Journal of Petroleum Technology, June, pp. 1125-1135.

Stalkup Jr., F. I., 1983, Miscible Displacement, Monograph no. 8, Society of Petroleum Engineers, Dallas.

Szabo, M. T., 1972, "Molecular and Microscopic Interpretation of the Flow of Hydrolyzed Polyacrylamide Solution Through Porous Media," Society of Petroleum Engineers, paper no. 4028.

Teeuw, D. and Hesselink, F. T., 1980, "Power-Law Flow and Hydrodyanmic Behaviour of Biopolymer Solutions in Porous Media," Society of Petroleum Engineers, paper no. 8982.

Tinker, G. E.; Bowman, R. W.; and Pope, G. A., 1976, "Determination of In-Situ Mobility and Wellbore Impairment from Polymer Injectivity Data," Journal of Petroleum Technology, May, pp. 586-596.

Van Domselaar, H. R., 1982, "The Apparent Viscosity of Power-Law Fluids and Its Application in Polymer Drive Simulations," Society of Petroleum Engineers, paper no. 10613.

Vela, S.; Peaceman, D. W.; and Sandvik, E. I., 1976, "Evaluation of Polymer Flooding in a Layered Reservoir with Crossflow, Retention, and Degradation," Society of Petroleum Engineers Journal, April, pp. 82-96.

Wang, F. H. L.; Duda, J. L.; and Klaus, E. E., 1979, "Influences of Polymer Solution Properties on Flow in Porous Media," Society of Petroleum Engineers, paper no. 8418.

Ward, J. S. and Martin, F. D., 1980, "Prediction of Viscosity for Partially Hydrolyzed Polyacrylamide Solutions in the Presence of Calcium and Magnesium Ions," Society of Petroleum Engineers, paper no. 8978.

APPENDIX A

SIMULATOR DEVELOPMENT

A.1 Governing Equations

The simulator built for this study was designed to model the injectivity of non-Newtonian solutions. In the general case, the flow of three substances - oil, water, and polymer solutions, are of interest. The surfactant concentration in a micellar solution will be treated in the same way as polymer in solution. Three analytical flow equations are therefore required to describe the flow of the three substances. The equations for radial axisymmetric flow are as follows:

Oil Phase

$$\frac{1}{r}\frac{\partial}{\partial r}\left\{\frac{r\, kk_{ro}}{R_{rfo}\mu_o B_o}\frac{\partial p_o}{\partial r}\right\} = \frac{\partial}{\partial t}\left\{\frac{\phi S_o}{B_o}\right\} \qquad (A.1)$$

Water Phase

$$\frac{1}{r}\frac{\partial}{\partial r}\left\{\frac{r\, kk_{rw}}{R_{rfw}\mu_w B_w}\frac{\partial p_w}{\partial r}\right\} = \frac{\partial}{\partial t}\left\{\frac{\phi S_w}{B_w}\right\} \qquad (A.2)$$

Polymer Species

$$\frac{1}{r}\frac{\partial}{\partial r}\left\{\frac{rCkk_{rw}}{R_{rfw}F_c\mu_w B_w}\frac{\partial p_w}{\partial r}\right\} = \frac{\partial}{\partial t}\left\{\frac{\phi C S_w}{B_w}\right\} + (1-\phi_o)\gamma_r\left\{\frac{\partial A}{\partial t}\right\} \qquad (A.3)$$

In equation (A.3) ϕ_o is a base porosity which is not a

function of pressure, and γ_r is the specific gravity of the rock. For these three coupled, second-order, partial differential equations, there are five unknowns. The unknowns are water and oil pressure, water and oil saturation, and surfactant/polymer concentration. It is necessary to introduce two additional relations related to two-phase flow to solve the flow equations. One equation is related to capillary pressure and the other to the sum of the saturations (equations [A.4] and [A.5]).

$$S_o + S_w = 1.0 \qquad (A.4)$$

$$p_o - p_w = p_{cwo}(S_w) \qquad (A.5)$$

Equations (A.1)-(A.5) result in five equations and five unknowns. When a problem is discretized in space and time, these five equations must be solved at each node. Before equations (A.1)-(A.5) can be solved, it is necessary to put equations (A.1)-(A.3) in finite-difference form. The development of the finite difference equations is discussed in the next section. In equation (A.3) there is no dispersion term. The transport of the surfactant/polymer is assumed to completely dominate dispersion.

To be able to simulate pressure injectivity and falloff tests, another expression for the wellbore is needed. The flow in and out of the wellbore can be described as follows:

$$q_s = q_{sf} + \frac{C_s}{B}\frac{dP_{wf}}{dt} \qquad (A.6)$$

(surface rate) (sand face rate) (wellbore accumulation)

Where C_s is the wellbore storage coefficient.

4.2 Finite Difference Equations

The finite difference equations are based on a block-centered grid. In a block centered geometry the blocks are selected first, and then the nodes are centered in the blocks. The alternative method to the block centered grid is the point centered grid. The point centered grid is mathematically more rigorous, but for almost all petroleum engineering problems the type of grid makes no practical difference. The block centered geometry is the standard geometry used in the petroleum industry for simulators in radial coordinates (Weinstein, Nolen, and Chappelear 1986). Figure A.1 illustrates the geometry of the simulator. The finite difference equations can be thought of as a statement of the material balance on each cell, which is expressed by equation (A.7).

(Rate of Material In) - (Rate of Material Out)

+ (Sources + Sinks) = (Rate of Accumulation) (A.7)

We use the central-difference approximation for the left hand sides of equations (A.1)-(A.3). For instance, the left hand side of the water equation takes the form given by

equation (A.8), with the exception of being multiplied by the formation thickness h.

$$\frac{1}{r}\frac{\partial}{\partial r}\left\{\frac{rhkk_{rw}}{R_{rfw}\mu_w B_w}\frac{\partial p_w}{\partial r}\right\} = \frac{T^n_{i+1/2}(p^{n+1}_{i+1} - p^{n+1}_i) - T^n_{i-1/2}(p^{n+1}_i - p^{n+1}_{i-1})}{\pi\,(r^2_{i+1/2} - r^2_{i-1/2})} \qquad (A.8)$$

The n superscript denotes the current known time level, while the n+1 superscript denotes the unknown time level. The transmissibilities for oil, water, and polymer are given in equations (A.9) through (A.11), respectively. The radii are as given in Figure A.1.

$$T_{o,i+1/2} = \left[\frac{2\pi\, kk_{ro}\, h}{B_o R_{rfo}\mu_o}\right]_{i+1/2} \frac{r_{i+1/2}}{(r_{i+1} - r_i)} \qquad (A.9)$$

$$T_{w,i+1/2} = \left[\frac{2\pi\, kk_{wo}\, h}{B_w R_{rfw}\mu_w}\right]_{i+1/2} \frac{r_{i+1/2}}{(r_{i+1} - r_i)} \qquad (A.10)$$

$$T_{p,i+1/2} = \left[\frac{2\pi\, kk_{rw}\, h}{F_c B_w R_{rfw}\mu_w}\right]_{i+1/2} \frac{r_{i+1/2}}{(r_{i+1} - r_i)} \qquad (A.11)$$

All relative permeabilities, resistance factors, and viscosities in the transmissibilites are calculated at the upstream location to ensure convergence to the Buckley-Leverett solution. The right hand sides of equations

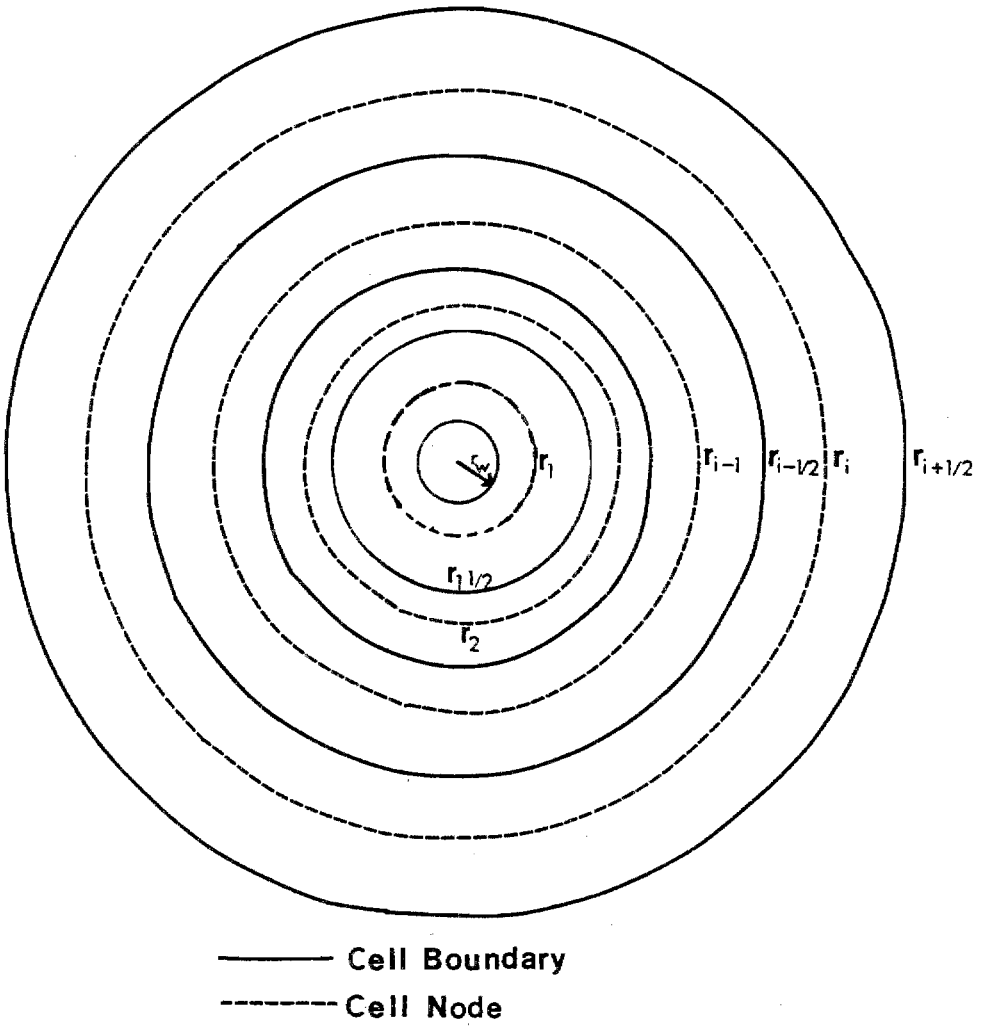

Figure A.1

Simulator Geometry

(A.1)-(A.3) can be approximated as in equation (A.12). The subscript i indicates the cell number. The rock compressibility is assumed to be negligible and the porosity can therefore be assumed to be constant.

$$\frac{h\partial}{\partial t}\left\{\frac{\phi S_w}{B_w}\right\} = \frac{h\phi}{\Delta t}\left[\left\{\frac{S_{w,i}}{B_{w,i}}\right\}^{n+1} - \left\{\frac{S_{w,i}}{B_{w,i}}\right\}^{n}\right] \qquad (A.12)$$

The pore volume of a cell is given by equation (A.13).

$$VP_i = h\phi\pi\,(r^2_{i+1/2} - r^2_{i-1/2}) \qquad (A.13)$$

Using the definition of pore volume for a cell, and equation (A.11) and (A.12), equation (A.2) can be written in the compact, finite-difference form of equation (A.14), with the addition of a source/sink term.

$$T^n_{w,i+1/2}(p^{n+1}_{w,i+1} - p^{n+1}_{w,i}) - T^n_{w,i-1/2}(p^{n+1}_{w,i} - p^{n+1}_{w,i-1}) + q_{w,i} = \frac{VP_i}{\Delta t}\left[\left\{\frac{S_{w,i}}{B_{w,i}}\right\}^{n+1} - \left\{\frac{S_{w,i}}{B_{w,i}}\right\}^{n}\right] \qquad (A.14)$$

The development of finite difference equations for oil and polymer is exactly the same as for water. The source term in equation (A.14) is used to implement the boundary conditions. The transmissibilities of the reservoir are taken as zero at the external drainage radius and at the wellbore. Any flow in or out of the reservoir is then controlled by the source term. The source term at the

wellbore is written as in equation (A.15).

$$q_{sf} = \left[\frac{k_{ro}}{\{R_{rfo}\mu_o\}} + \frac{k_{rw}}{\{R_{rfw}\mu_w\}}\right] * \frac{0.007082\ kh(p_{wf}^{n+1} - p_1^{n+1})}{B_w\ (\ (r_{1\,1/2}^2/(r_{1\,1/2}^2-r_w^2))\ \ln(r_{1\,1/2}/r_w) - 0.5 + s\ )} \quad (A.15)$$

The injectivity at the well must be written in terms of total mobility. If a negative skin exists at the wellbore, that is a stimulated condition; it is possible for the apparent wellbore radius to exceed the outer radius of the first cell in contact with the wellbore. The apparent wellbore radius due to skin is equal to $r_w e^{-s}$. When the apparent wellbore radius exceeds the outer radius of the first cell, a negative pressure drop results. To overcome the problem of the negative pressure drop in a stimulated well, the skin factor is set to zero, and the permeability of the first few cells is increased. The permeability in the first few cells is increased using a relation developed by Hawkins (1965) to yield an equivalent skin factor, which is given in equation (A.16).

$$s = (k/k_s - 1.0)\ \ln(r_s/r_w) \quad (A.16)$$

The subscipt s denotes the radius and permeability of the skin zone, and k is the permeability of the virgin

formation.

The productivity at the external drainage radius is written only in terms of the mobility of the phase. The water boundary condition at the external drainage is given in equation (A.17). The subscript I denotes the last cell at the drainage radius.

$$q_{w,re} = \left[\frac{k_{rw}}{\{R_{rfw}B_o\mu_w\}}\right] \frac{0.007082\ kh\ (p_I^{n+1} - p_{re}^{n+1})}{((r_{I1/2}^2/(r_e^2-r_I^2))\ \ln(r_I/r_{I-1/2}) - 0.5 + s)} \qquad (A.17)$$

Equations (A.15) and (A.17) are used for either the Neumann or Dirichlet boundary conditions. For the Neumann boundary condition the rate is specified and for the Dirichlet boundary condition the pressure p_{wf} or p_{re} is specified. The final finite difference equation to develop is for wellbore storage. The finite difference form of equation (A.6) is given in equation (A.18).

$$q_s = q_{sf} + \frac{C_s}{B}\frac{(p_{wf}^{n+1} - p_{wf}^{n})}{\Delta t} \qquad (A.18)$$

Equation (A.15) would be substituted for q_{sf} in equation (A.18).

A.3 Solution Procedure

The solution of equations (A.1)-(A.5) uses a sequential IMPES (implicit in pressure--explicit in saturation) procedure. Water and oil equations are combined to obtain a pressure equation in terms of water pressure only. This pressure equation, having a parabolic form, is solved to obtain the pressure surface. This pressure is substituted in the water equation to calculate the water saturation explicitly. Finally, water pressure and saturation are used in the surfactant/polymer flow equation to obtain the polymer concentration implicitly. Performing the manipulations as outlined and putting the result in the form of a tridiagonal matrix results in equations (A.19)-(A.22). The coefficient α_i is equal to $B_{w,i}/B_{o,i}$. All transmissibilities, capillary pressures, and α_i are calculated at the n time level. The inclusion of wellbore storage simply adds one more equation to the matrix, based on equation (A.18).

Superdiagonal:

$$B_i = \alpha_i T_{w,i+1/2} + T_{o,i+1/2} \qquad (A.19)$$

Main Diagonal:

$$A_i = -B_i - C_i - \frac{VP_i}{\Delta t} \left[\alpha_i S^{n}_{w,i} c_w + (1-S^{n}_{w,i}) c_o\right] \qquad (A.20)$$

Subdiagonal:

$$E_i = \alpha_i T_{w,i-1/2} + T_{o,i-1/2} \qquad (A.21)$$

Right Hand Side Vector:

$$D_i = -\left[\frac{VP_i}{\Delta t}\right]\{\alpha_i S^n_{w,i} c_w + (1-S^n_{w,i})c_o\} - T_{o,i+1/2}(P_{cwo,i+1}-P_{cwo,i})$$

$$+ T_{o,i-1/2}\,(P_{cwo,i}-P_{cwo,i-1}) + \alpha_i q_w + q_o \qquad (A.22)$$

The values E_i, A_i, and B_i are the coefficients for the pressures $p_{w,i-1}$, $p_{w,i}$, and $p_{w,i+1}$, respectively. This system of equations is easily solved directly using the Thomas algorithim for the implicitly unknown water pressures. The water saturations can then be calculated explicitly at the n+1 time level using equation (A.14). Using equations (A.4) and (A.5), the oil pressures and saturations can be calculated at the n+1 time level, if the water pressures and saturations are known. At this point all pressures and saturations are known.

The polymer flow equation can now be solved. When originally formulated the polymer equation (A.3) was solved explicitly. The explicit solution of the polymer equation becomes unstable when more than one pore volume is injected into a cell during a time step; the concentration profile then begins to oscillate. To alleviate this problem, the polymer equation was solved implicitly. The implicit solution of the polymer equation allows much larger time

steps. The implicit formulation of the polymer equation results in a bi-diagonal matrix, since the polymer equation is solved with a backward difference formulation. The bi-diagonal matrix can be solved by either back substitution or by the Thomas algorithim. The form of the bidiagonal matrix is:

Main diagonal:

$$A_i = \left[\frac{\phi S_w}{B_w}\right]^{n+1} \frac{VP_i}{\Delta t} + (1-\phi_o)\gamma_r \frac{A_i^{n+1} - A_i^n}{C_i^{n+1} - C_i^n} - T_{p,i+1}\left[p_{w,i+1}^{n+1} - p_{w,i}^{n+1}\right] \quad \text{(A.23)}$$

Subdiagonal:

$$E_i = T_{p,i-1}\left[p_{w,i}^{n+1} - p_{w,i-1}^{n+1}\right] \quad \text{(A.24)}$$

Right Hand Side Vector:

$$D_i = C_i^n\left[\frac{\phi S_w}{B_w}\right]^{n+1} \frac{VP_i}{\Delta t} + C_i^n(1-\phi_o)\gamma_r \frac{A_i^{n+1} - A_i^n}{C_i^{n+1} - C_i^n} \quad \text{(A.25)}$$

The values A_i and E_i are the coefficients for the concentrations C_i^{n+1} and C_{i-1}^{n+1}, respectively. The quantity $(A_i^{n+1}-A_i^n)/(C_i^{n+1}-C_i^n)$ is the chord slope of the adsorption/retention curve, and is taken to be a constant for the time step. If the concentration in a cell starts to drop, the chord slope is set to zero, and the concentration is recomputed. Setting the cord slope to zero for decreasing concentrations makes the adsorption/retention

irreversible.

Having reached this point, equations (A.1) through (A.5) have been solved. The interstitial velocity, apparent viscosity, adsorption, and resistance factor are now updated for all cells. The next time step can now be computed.

A.4 Capabilities, Limitations and Assumptions of the Simulator

Based on the discussions of Chapters 2 and Appendix A thus far, the capabilities of the simulator have been stated. Table A.1 briefly reviews the capabilities of the simulator. What the simulator is not designed to consider will also be discussed. With a simulator formulated in radial coordinates, there are some limitations and advantages. The radial coordinate system is well suited to transient radial well testing. The radial coordinate system cannot rigorously handle fractured wells. If the fracture length is quite small then appreciable error will probably not result using this simulator; however, no testing has been done to verify the amount of error.

The radial system does not rigorously handle the boundary condition at the external drainage radius for many situations. For example, in a five- or nine-spot pattern, there will be fingering toward the sinks (producing wells). Fingering towards the sinks is not accounted for in the

Table A.1

Summary of Simulator Features

Geometry

One dimensional, radial coordinate system. Block centered nodes, logarithmically distributed.

Boundary Conditions

1. Wellbore - pressure specified (Dirichlet) or rate specified (Neumann)
2. Drainage radius - pressure specified or closed

Completion Effects

1. Skin
2. Wellbore Storage - a. full fluid column
   b. rising/falling fluid level

Phase Options

1. Single phase, water-polymer flow
2. Two phase, oil and water-polymer flow

Relative Permeability

1. Pirson's equations
2. Tabular input of relative permeability

Polymer Flow Effects

1. Langmuir adsorption isotherms
2. Residual resistance factor - permeability reduction
3. Inaccessible pore volume
4. Polymer concentrations

Rheology

1. Carreau fluids
2. Modified power law fluids
3. Newtonian fluids
4. Viscosity table as a function of interstitial velocity

Shear-Rate, Velocity Relations

1. Savins
2. Jennings, Rogers, and West
3. Christopher - Middleman

simulator. The simulator is a single-layer radial simulator. In a reservoir which is highly stratified, the effect of multiple layers could cause the simulator to be significantly in error. It is not possible to handle gravity effect for a tilted reservoir in a meaningful way using a radial coordinate system; therefore, the effects of underrunning or override are not considered in the simulator.

The simulator is designed for single-phase (water polymer) or two-phase (oil and water-polymer) flow. This obviously assumes that the reservoir is above the bubble point, and there is no free gas saturation. The upstream weighting built into the simulator is currently designed only for injection. Erroneous results will be obtained if production occurs. For micellar solutions, only the rheology is modelled and not the interfacial tension effects. Capillary pressure is not considered in the model, other than to relate the oil and water pressures. Degradation is not directly considered in the model; rheological data is assumed to be appropriately corrected for all types of degradation. All adsorption/retention is considered to be irreversible; in some cases, adsorption/retention may have some reversibility.

Simulators in radial coordinates can have stability

problems if the time steps are too large, unless the simulator is fully implicit. Since this simulator is not fully implicit, some caution must be exercised in selecting time-step size. The principal source of instability is the small size of the near wellbore cells. Once the near wellbore cells have stabilized at some condition, larger time steps can be taken. What this means is that whenever there is a shock to the system, small time steps should be taken. Examples of shock include, when water injection is commenced in a reservoir at irreducible water saturation or when polymer injection is commenced.

After a short period of time, the near wellbore cells have stabilized at residual oil saturation for water injection. In the polymer injection case, concentrations in the near wellbore cells stabilize rapidly. Usually a day of injection is enough to stabilize the near wellbore cells. Time steps are distributed logarithmically to minimize any stability problems at early times.

After the initial stabilizing period, time steps can typically be taken as large as 5 days with no instability. The number of time steps required to see virtually no change in the results depends on the changes in concentrations and injection rates. If the rates and concentrations do not change on a day to day basis, one or two time steps per day

is adequate, with additional time steps causing no change in the result. Significant changes in the day to day rates and concentrations will require additional time steps; typically, 5 to 10 time steps per day is adequate.

The simulator is currently dimensioned to handle 100 radial cells. Runs were made for the same cases at 10, 20, 50 and 100 cells. The number of cells required to obtain convergence of the numerical solution is a function of the residual resistance factor. Small amounts of numerical dispersion in the polymer concentration front can cause large reductions in the reservoir permeability when the residual resistance factor is large. When the residual resistance factor is close to 1.0, improved answers were obtained when going from 10 to 20 cells; however, no significant change was obtained between 20 and 50 cells when comparing wellbore pressures and rates. Figure A.2 compares 20 and 50 cells for Well B, when the residual resistance factor is 1.35. When the residual resistance factor was 11.3, as for Well C, 50 cells were required to for convergence of the wellbore pressures and rates. Figure A.3 compares 20, 50, and 100 cells for Well C. The more radial cells, the better the identification of the flood front location for any displacement process. If flood front location is of importance,the maximum number of cells should

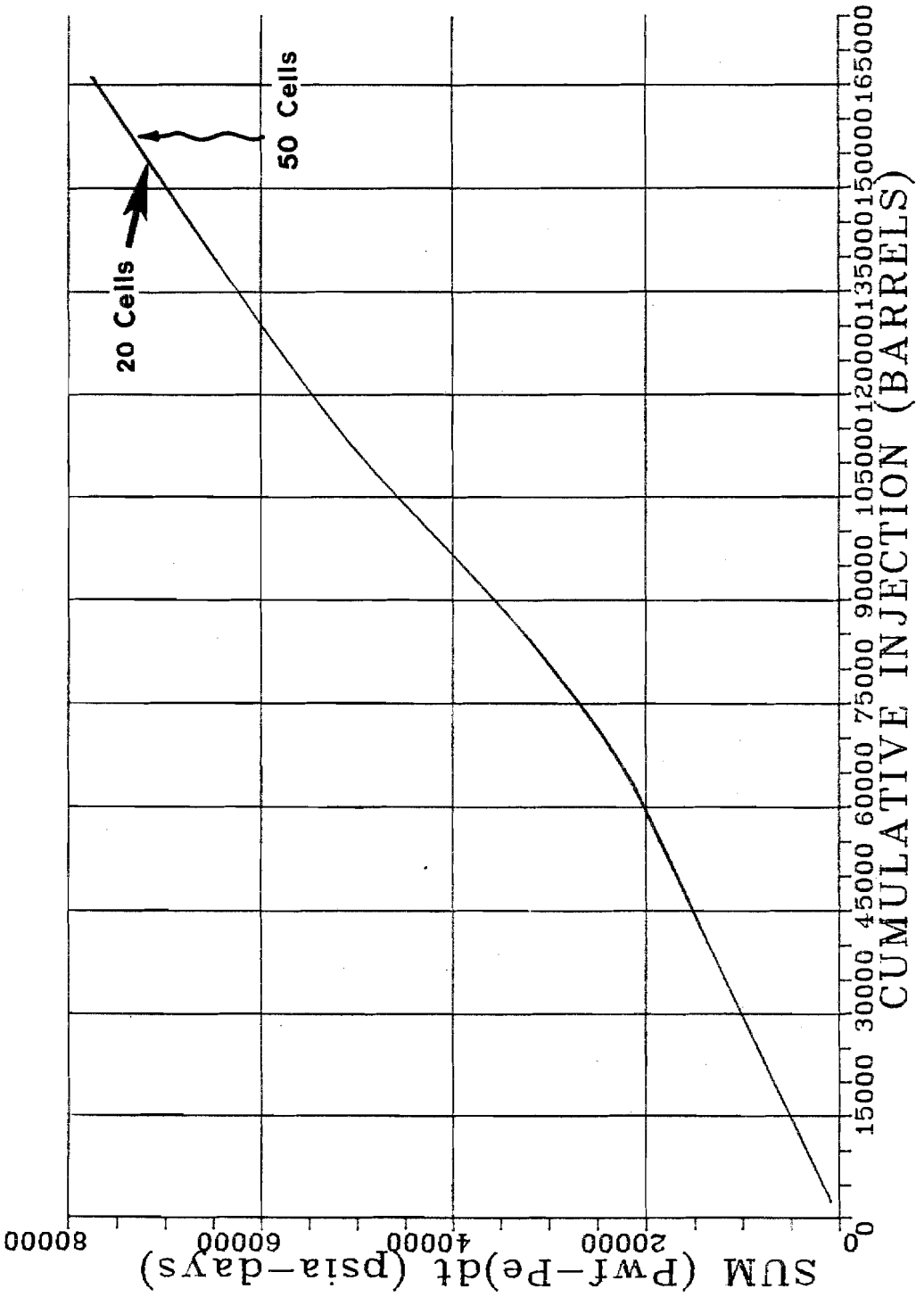

Figure A.2

Comparison of 20 and 50 Cells, Well B

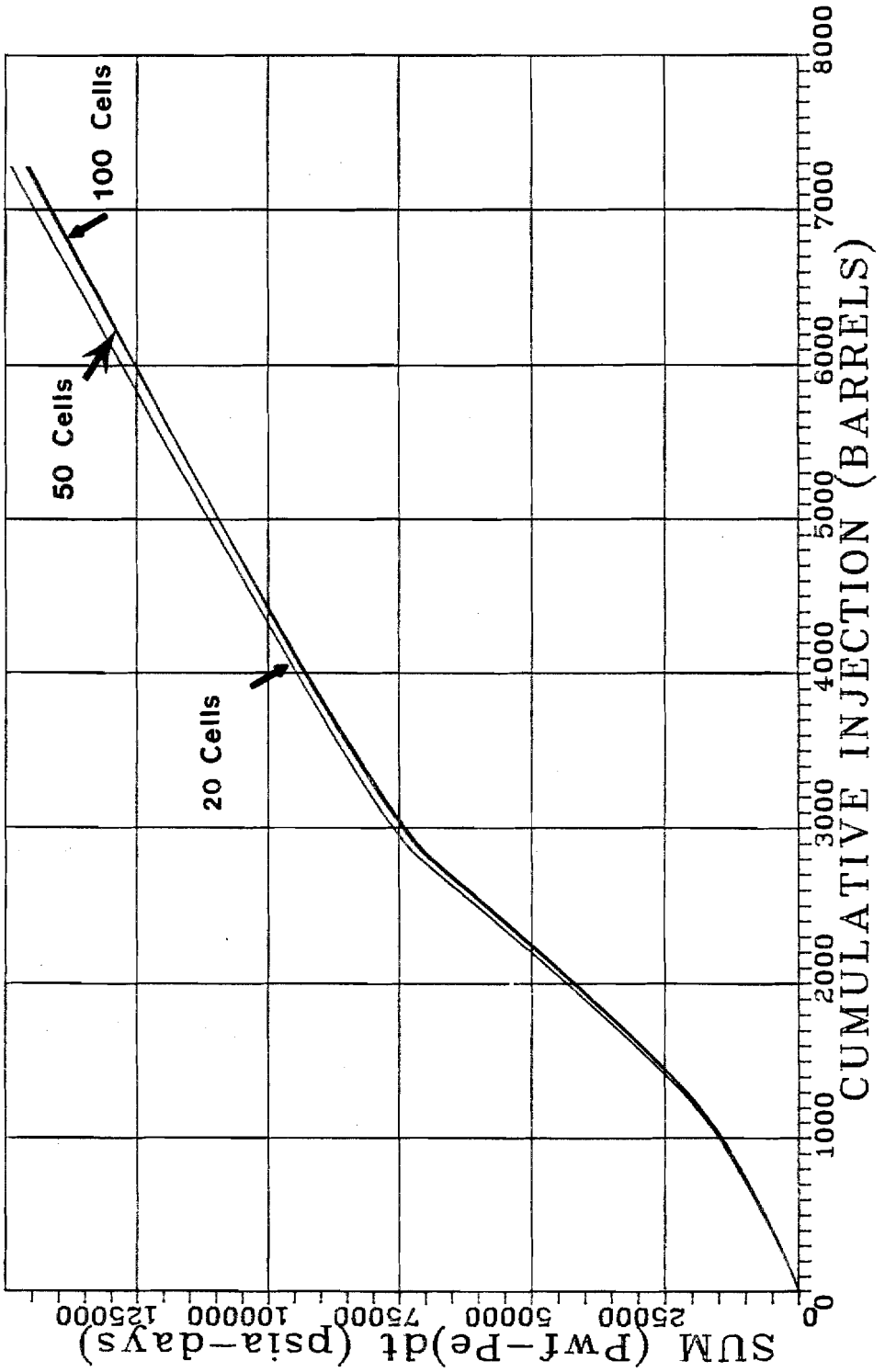

Figure A.3

Comparison of 20, 50, and 100 Cells, Well C

be used. If just wellbore pressures and rates are important, between twenty and fifty cells is adequate.

A.5 Simulator Verification

The principal method of testing the simulator was the comparison of simulator results with analytical solutions. The simulator results were compared to analytical solutions for the following situations:

1. Injection test
2. Falloff test
3. Steady-state flow
4. Hall plot
5. Wellbore storage
6. Buckley-Leverett displacement
7. Miscible polymer-water displacement

The comparison of simulator results with analytical solutions was done using a hypothetical data set, called Well A. The data for Well A is given in Appendix B. The data for Well A was applied to single- and two-phase flow. A brief review of a portion of the tests run follows.

Figure A.4 gives the simulator results for a falloff test using 20 cells. The input skin and permeability is 3.0 and 100 md. respectively. Based on the slope of the falloff test plot, a permeability of 99.7 md is calculated. The skin is calculated to be 3.030. Figure A.5 is for the same

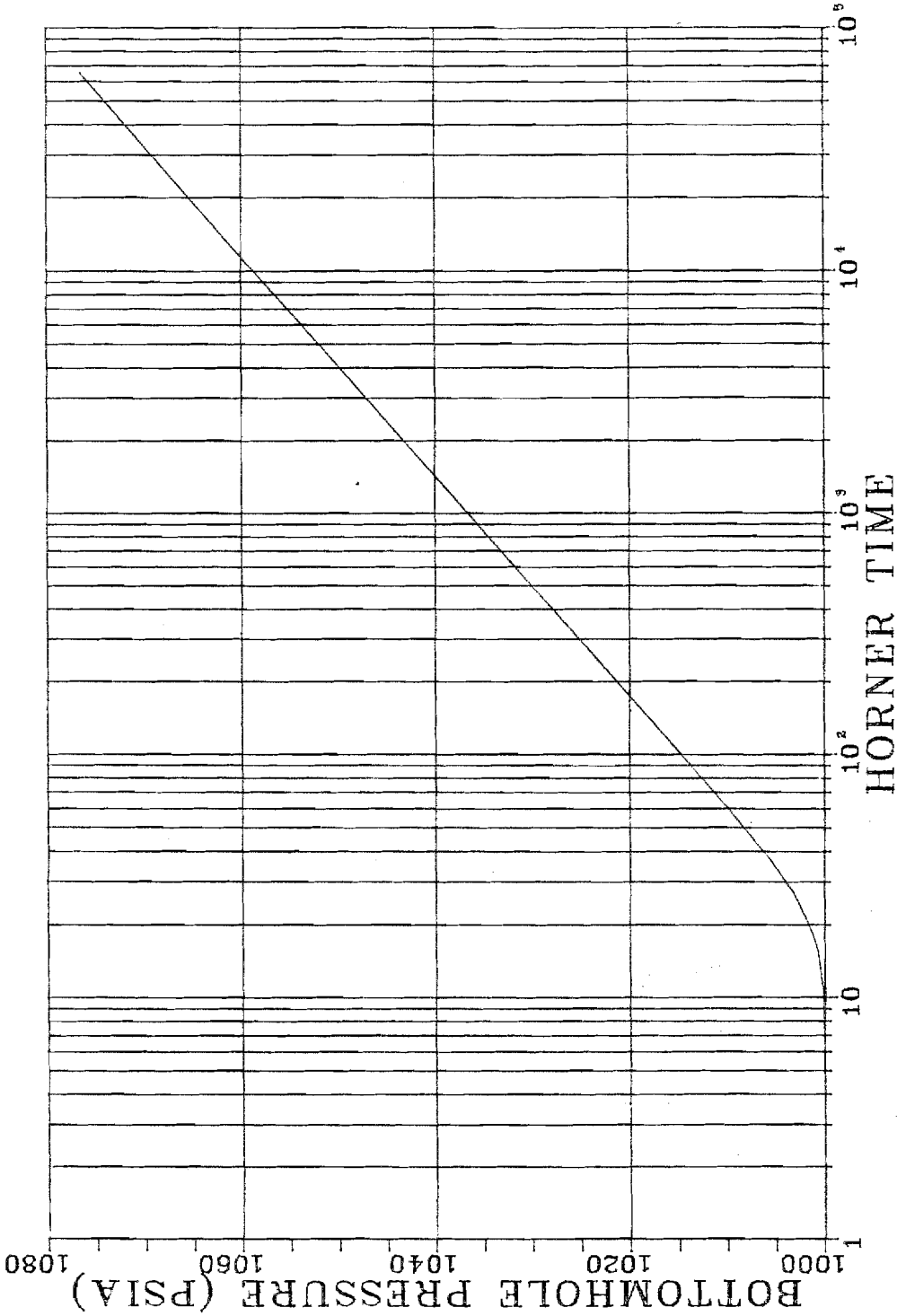

Figure A.4

Well A, Falloff Test Case

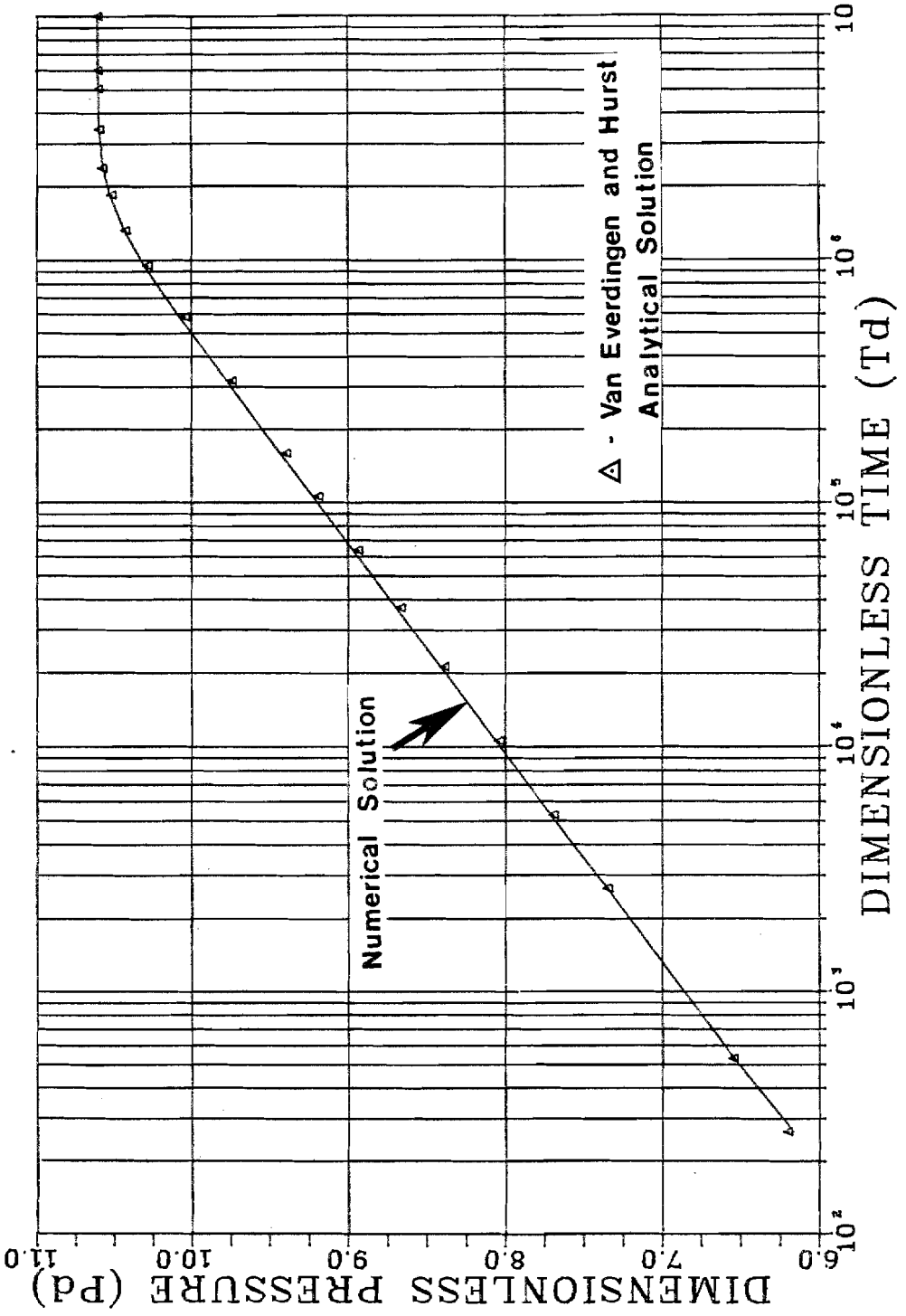

Figure A.5

Well A, Falloff Test, Dimensionless Type Curve Match

data plotted in Figure A.4, but the results are plotted in a dimensionless form. Dimensionless pressure is plotted versus dimensionless time. The dimensionless plot in Figure A.5 compares the analytical solutions of Van Everdingen and Hurst (1949) with the simulator results. The definition of dimensionless pressure and time are as follows.

$$t_D = \frac{0.000264\ kt}{\phi\mu\ c_t\ r_w^2} \tag{A.26}$$

$$p_D = \frac{0.007082\ kh\ \Delta p}{qB\mu} \tag{A.27}$$

Figure A.6 illustrates an injection test run with using 20 cells. The input skin and permeability are 3.0 and 100.0 md respectively. The calculated skin is 3.030 and the calculated permeability is 99.6 md based on the injection plot. Figure A.7 is a comparison with the Van Everdingen and Hurst dimensionless solutions. Figure A.8 is for the same data as in Figures A.6 and A.7, except the outer boundary has been closed. The closed outer boundary case serves as a material balance check. Based on the amount of material added to the reservoir, the simulator should converge to a new stabilized reservoir pressure. The new stabilized reservoir pressure calculated by the simulator when the well is shutin was used to verify material balance. In Figure A.8 1000 barrels of water was injected during two

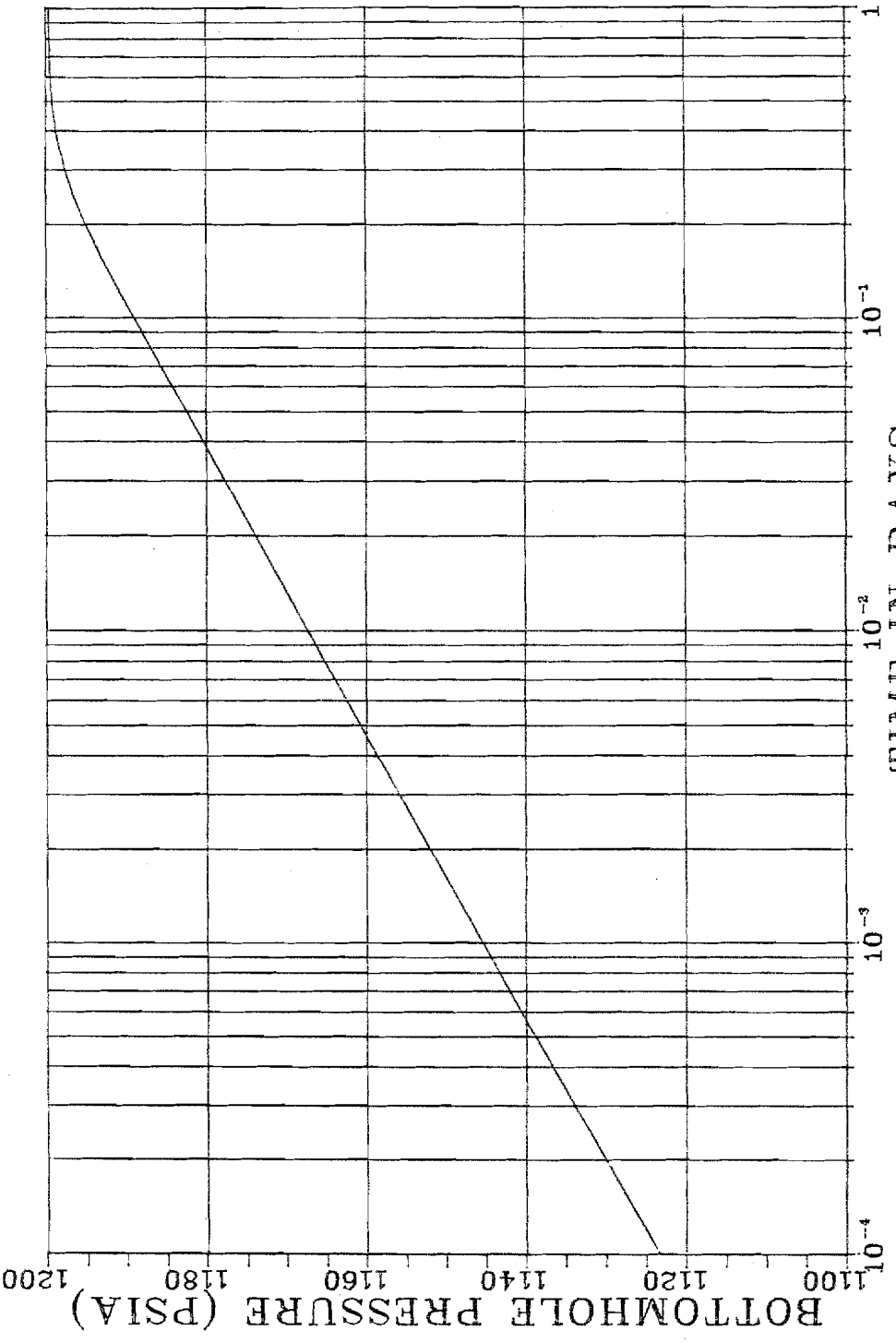

Figure A.6

Well A, Injection Test Case

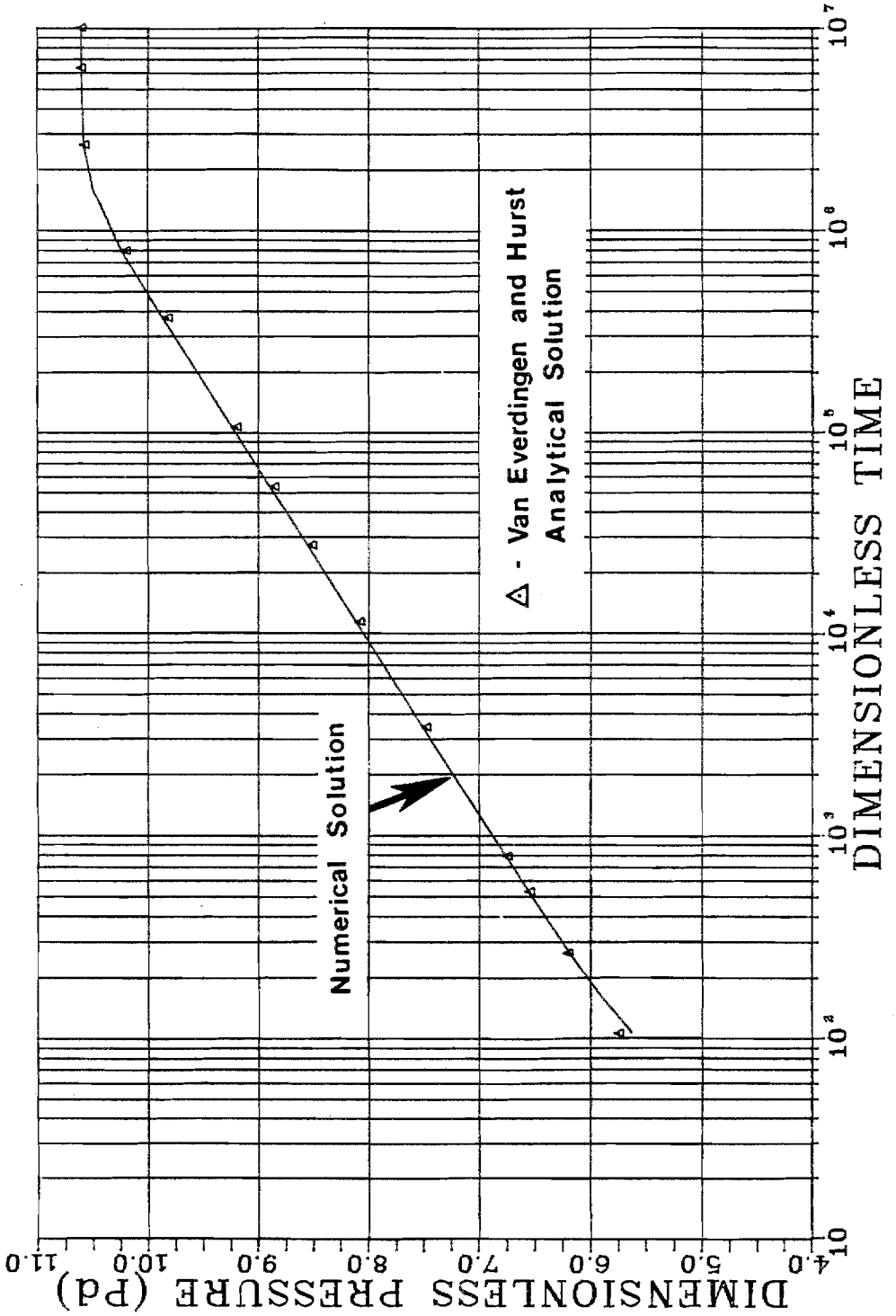

Figure A.7

Well A, Injection Test, Dimensionless Type Curve Match

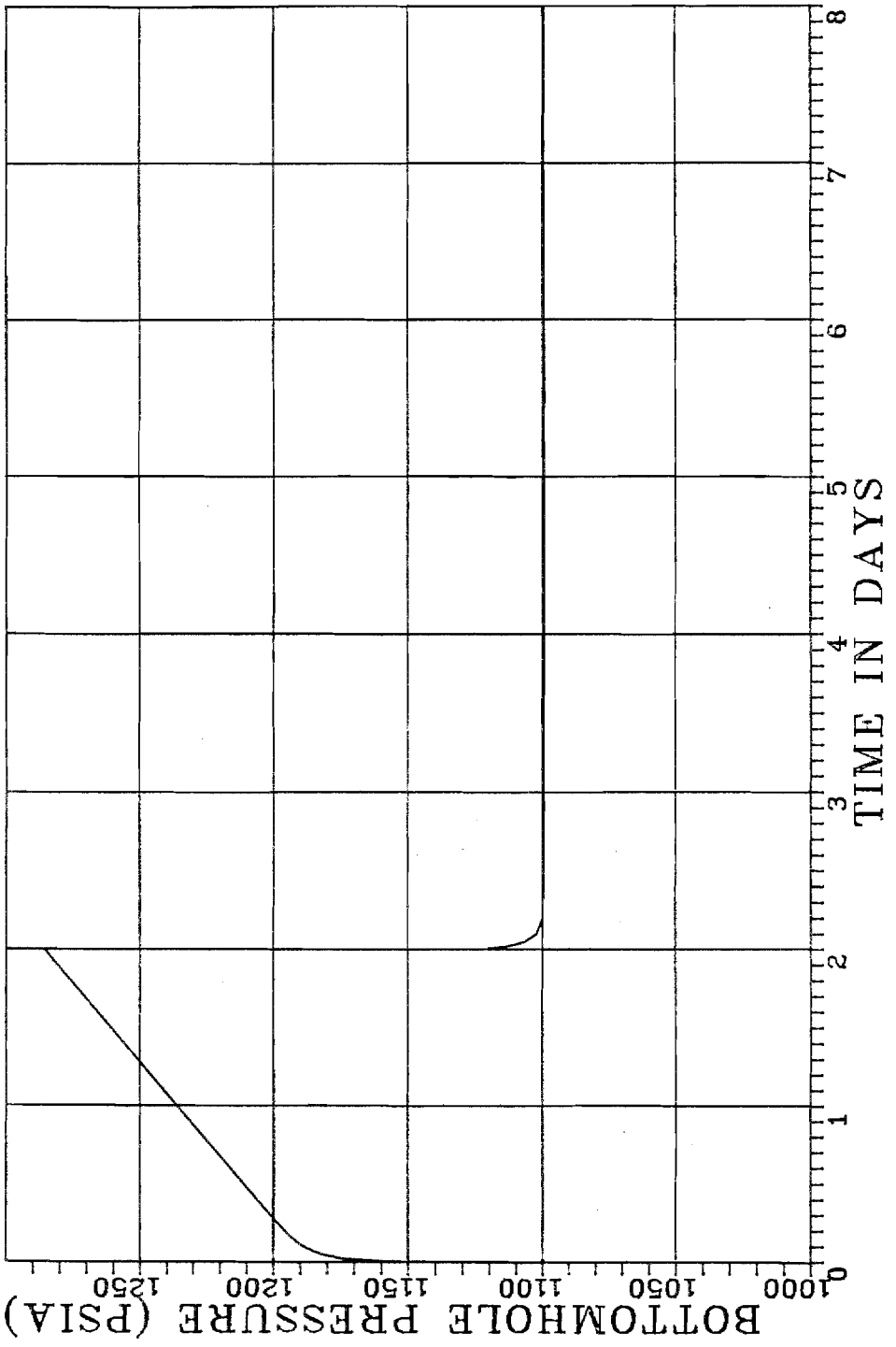

Figure A.8

Well A, Injection Test Case, Closed Outer Boundary

days. The new average reservoir pressure calculated by the simulator after shutin is 1099.3 psia. Based on material balance and the compressibility relationship the new average reservoir pressure is 1099.3 psia. Tests like those mentioned above, and others, were used to verify the transient behavior of the simulator. The equations as developed in section 3.1 were used to calculate skin and permeability.

It was also necessary to verify the steady state solution of the simulator. Water injection was maintained at a constant rate for a single phase to establish steady state flow. The simulator will calculate the same solution as the steady state Darcy equation. Hall plots were also prepared and analyzed using equations (4.8) and (4.12). The simulator matches the slope of the Hall plot as calculated using equation (4.8). Figure A.9 illustrates a Hall plot test case. The Hall slope based on simulator input is 0.400 (psia-days)/STB and the slope from the Hall plot is 0.399 (psia-days)/STB.

The two phase flow calculations made by the simulator were verified by comparison with the Buckley-Leverett solution. The Buckley-Leverett equation for a linear system is given in equation (A.28).

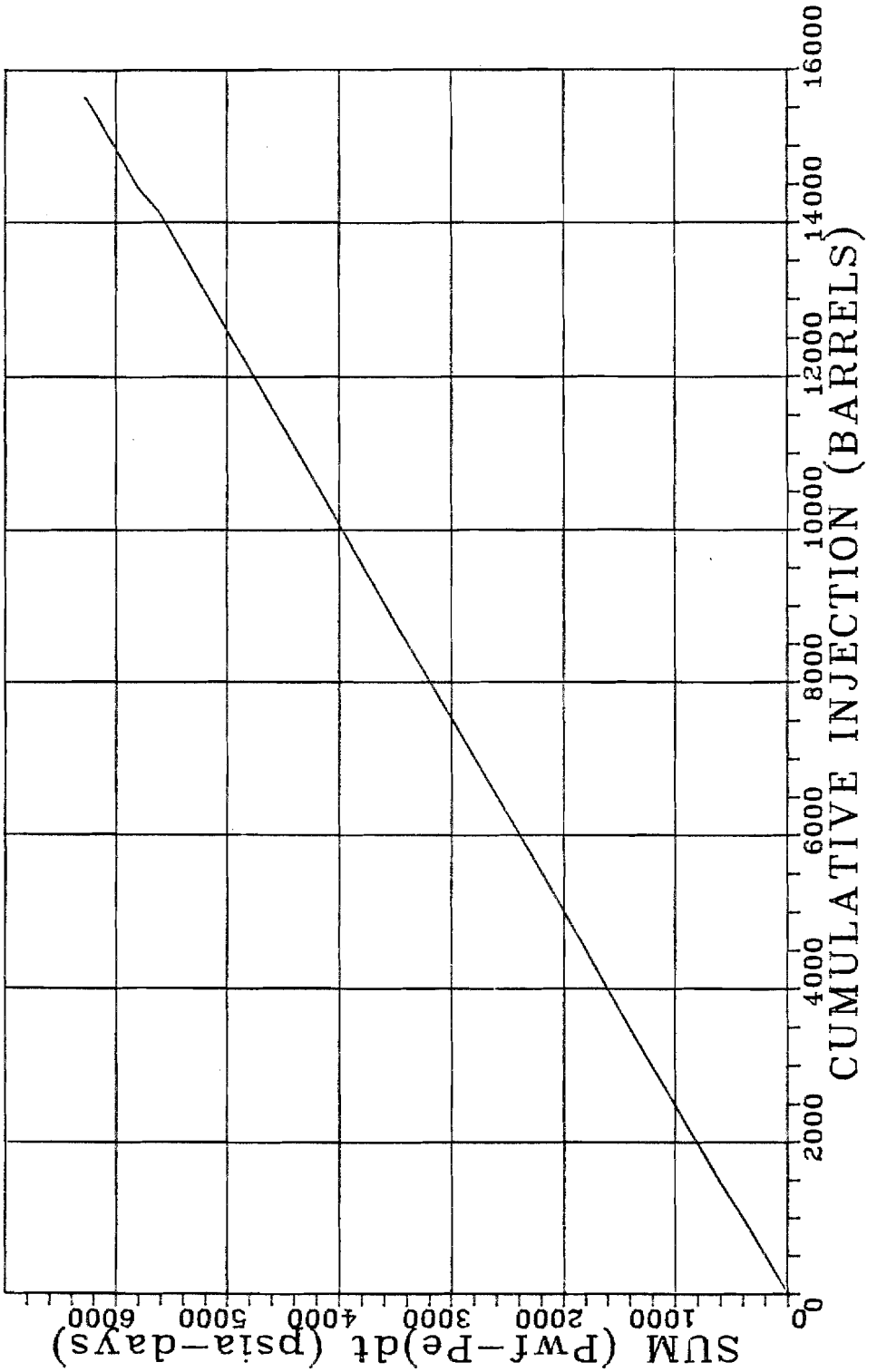

Figure A.9

Well A, Hall Plot Test Case, Water Injection

$$\left(\frac{dx}{dt}\right)_{S_w} = \frac{5.615\ q}{A\phi}\ \left(\frac{df_w}{dS_w}\right)_{S_w} \qquad (A.28)$$

Where the value A is the cross sectional area of the linear system. Equation (A.28) can also be solved for flow in radial coordinates, when the space coordinate is changed to r, and A is set equal to $2\Pi\phi h$. Equation (A.28) changed for radial coordinates is given equation (A.29).

$$\left(\frac{dr}{dt}\right)_{S_w} = \frac{5.615\ q}{2\Pi\phi h\phi}\ \left(\frac{df_w}{dS_w}\right)_{S_w} \qquad (A.29)$$

The solution to equation (A.29) for tracking a particular saturation in radial coordinates, is given by equation (A.30) (Collins 1976, p. 149).

$$\phi\Pi h\ [r_t^2 - r_0^2]_{S_w} = 5.615[Q_t - Q_0]\ \left\{\frac{df_w}{dS_w}\right\}_{S_w} \qquad (A.30)$$

The subscript 0 denotes time zero, and the subscript t denotes some time in the future. The subscript S_w is for some constant saturation. Figure A.10 illustrates a comparison of the Buckley-Leverett analytical solution with the simulator using 20, 50, and 100 cells. In Figure A.10 15644.3 barrels of water has been injected, which yields a theoretical flood front of 99.2 feet.

The accuracy of the wellbore storage calculations was verifed by making log-log plots. Figure A.11 is a test case for wellbore storage with a rising liquid level and a full

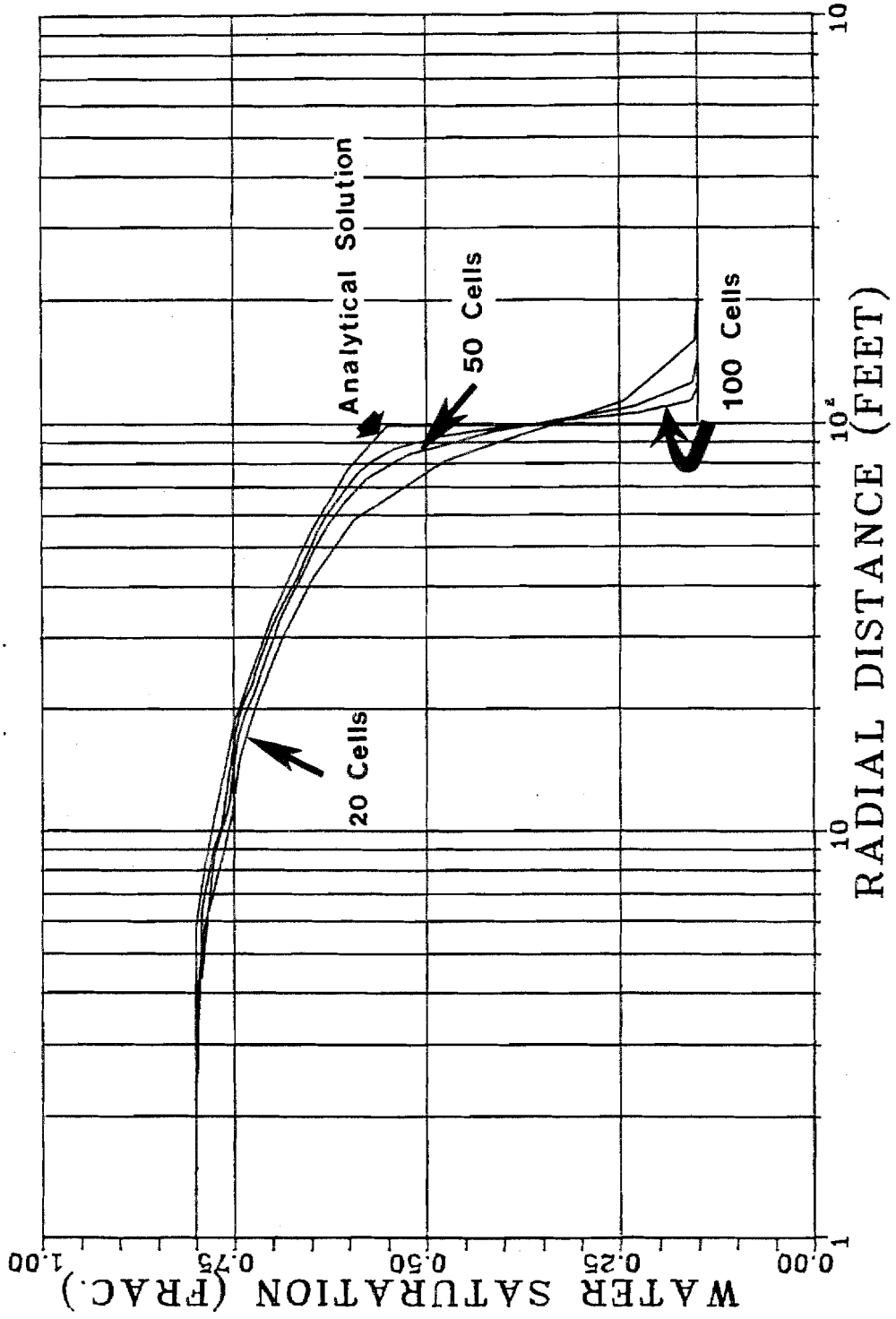

Figure A.10

Well A, Buckley-Leverett Test Case

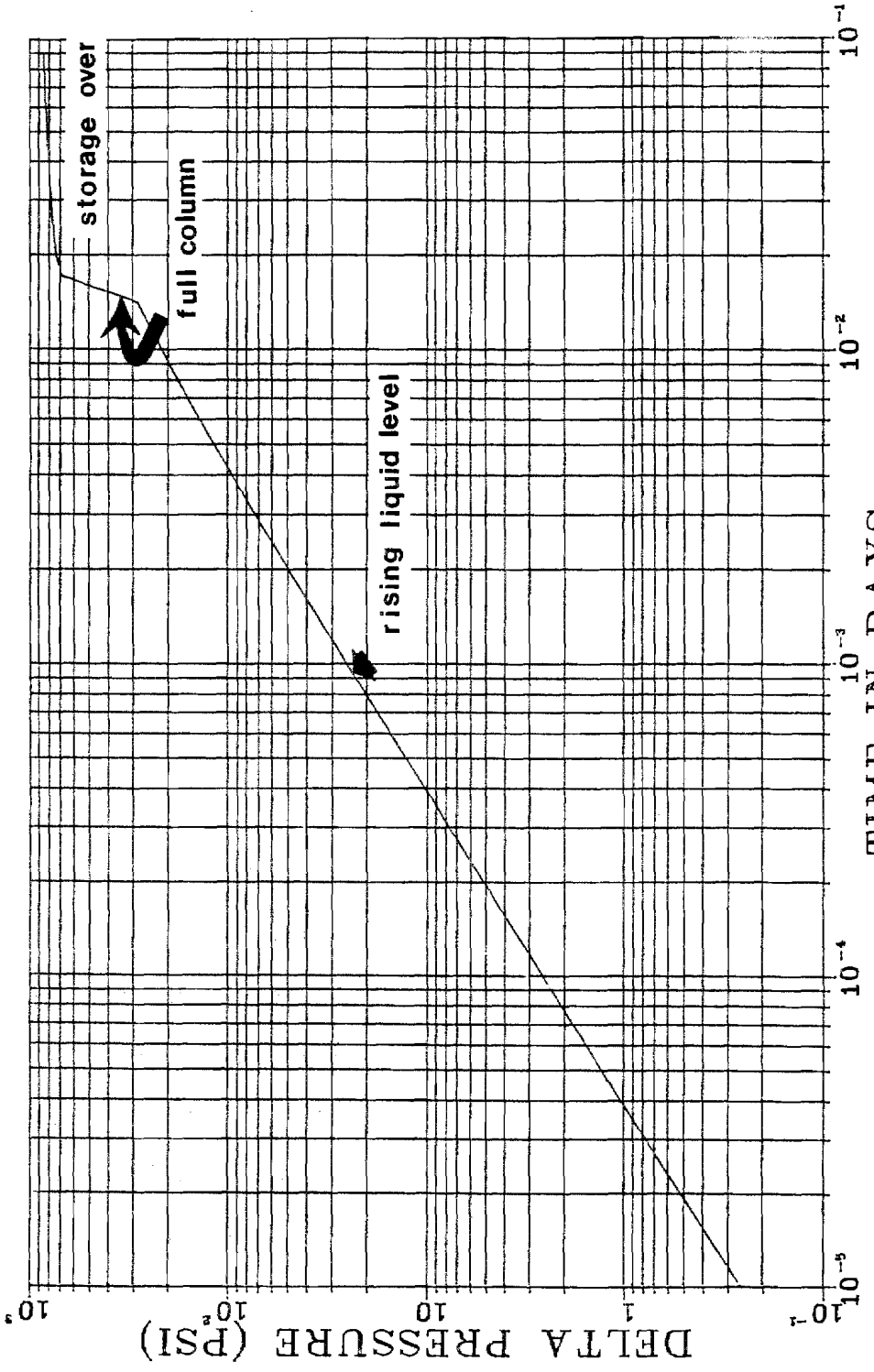

Figure A.11

Well A, Wellbore Storage Plot Test Case

fluid column. The wellbore storage coefficient (C_s) for a full fluid column of water is equal to $c_w V_{wb}$, where V_{wb} is the volume of the wellbore. The wellbore storage coefficient put into the simulator is 0.108 ft^3/psi for a rising liquid level. The wellbore storage coefficient calculated from figure A.11 is 0.110 ft^3/psi.

The solution of the concentration equation was tested against analytical solutions also. When an aqueous polymer solution displaces water, the displacement process is miscible, and therefore piston-like displacement occurs if molecular dispersion and diffusion, and adsorption are ignored. The concentration distribution in space can easily be calculated for piston-like displacement based on volumetric considerations. Figure A.12 compares the analytical solution with the simulator calculated concentrations for Well A, when 20, 50, and 100 cells are used. In Figure A.12 adsorption has been set to zero. The amount of polymer injection is 19225.0 barrels in Figure A.12, which yields a theoretical flood front of 75.6 feet. It can be seen that there is some numerical dispersion in the concentration front, addition of more cells to the simulator reduces the numerical dispersion in the flood front.

In addition to testing with analytical solutions, the material balance error was calculated at the end of every

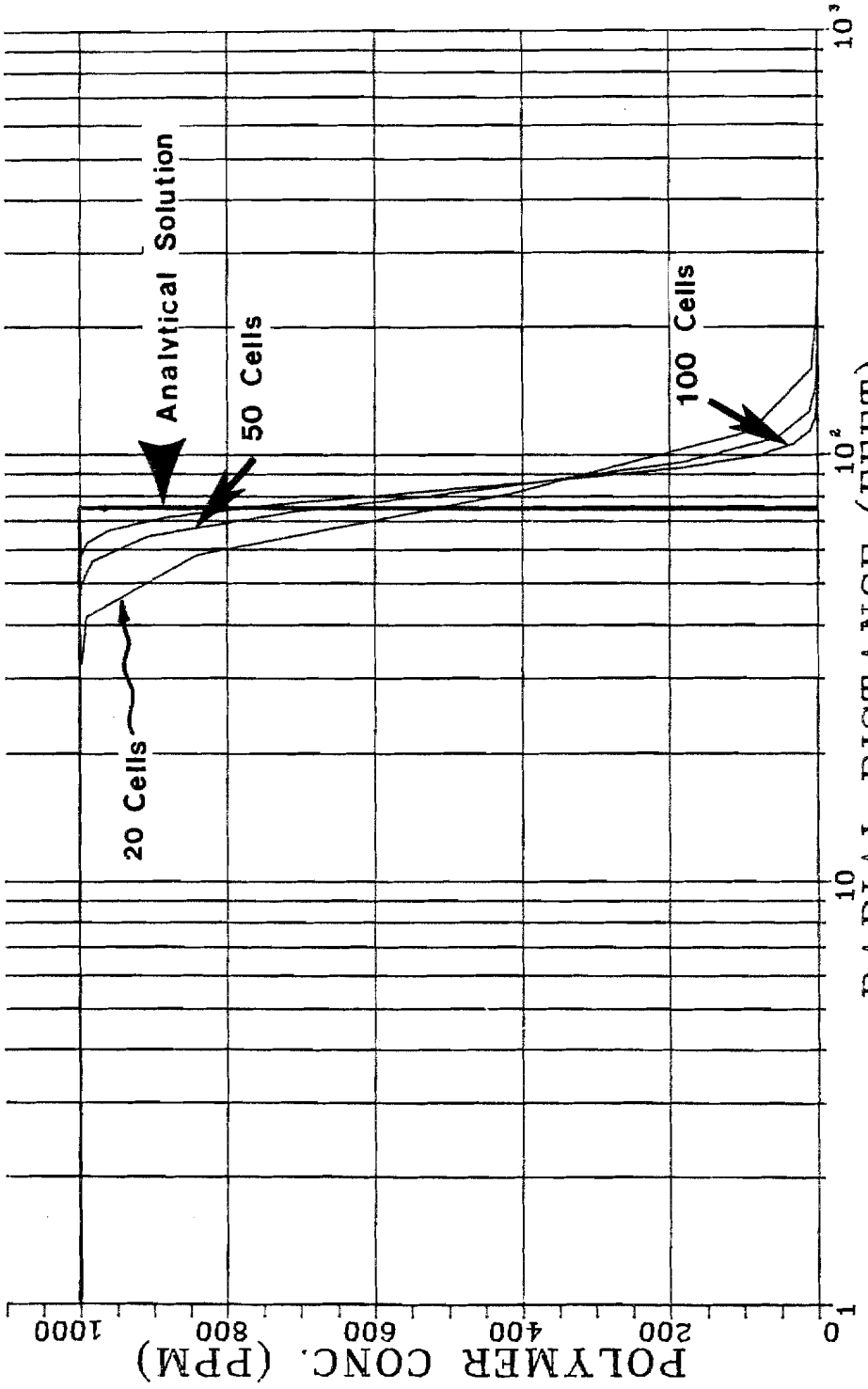

Figure A.12

Well A, Polymer Concentration Profile
Test Case, No Adsorption/Retention

time step, and the cumulative material balance error was recorded. Typical material balance error is $1 * 10^{-6}$ percent; that is, after injecting a million barrels of fluid, a material balance error of 1.0 barrels would be expected. Material balance tests were also done with the external drainage radius closed. When fluid was injected and the outer boundary was closed, the average reservoir pressure was calculated after the reservoir had stabilized. Using the compressibility and the material balance equations, the calculated pressures agree with the simulator for six significant figures.

APPENDIX B

WELL A DATA

Table B.1

Well A, Data and Reservoir Properties

L = Depth = 3000 feet

V_w = Wellbore volume = 25.0 barrels

C_{sr} = Rising/Falling fluid wellbore storage coefficient = 0.1081 $feet^3$/barrel

C_{sf} = Full wellbore storage coefficient = 0.00042 $feet^3$/barrel

h = Reservoir thickness = 30.0 feet

k = Absolute permeability = 100 md.

ϕ = Porosity = 0.20

r_e = External drainage radius = 1000.0 feet

r_w = Wellbore radius = 0.50 feet

p_e = Pressure at the external drainage radius = 1000.0 psia

p_i = Initial reservoir pressure = 1000.0 psia

μ_o = Oil viscosity = 5.0 cp

c_o = Oil compressibility = $15.0 * 10^{-6}$

B_o = Oil formation volume factor = 1.2 res. bbl/STB at 1000 psia

μ_w = Water viscosity = 0.80 cp

c_w = Water Compressibility = $3.0 * 10^{-6}$ psi^{-1}

B_w = Water formation volume factor = 1.0 res. bbl/STB at 1000 psia

γ_f = Rock specific gravity = 2.68

Table B.2

Adsorption/Retention - Resistance Factor Data, Well A

R_{rfw} = residual resistance factor to water = 5.00

R_{rfo} = residual resistance factor to oil = 1.20

A_{max} = maximum polymer adsorption/retention = 0.020 mg/g

F_c = inaccessible pore volume = 1.00

Langmuir Adsorption Isotherm

Concentration (PPM)	Adsorption/Retention (mg/g)
0.0	0.000
10.0	0.005
100.0	0.010
500.0	0.015
1000.0	0.019
5000.0	0.020

Table B.3

Carreau Rheological Data, Well A

Concentration(PPM)	n	λ	μ_0	μ_∞
0.0	1.00	0.50	0.80	0.80
100.0	0.50	0.50	1.50	0.80
500.0	0.50	0.50	6.00	0.80
750.0	0.50	0.50	8.00	0.80
1000.0	0.50	0.50	10.00	0.80
2000.0	0.50	0.50	15.00	0.80
5000.0	0.50	0.50	20.00	0.80

Table B.4

Apparent Viscosity as a Function of Interstitial Velocity, Well A

Savins shear rate-velocity relation used

	Interstitial Velocity (feet/day)					
Conc.(PPM)	0.01	0.10	1.00	10.00	100.0	1000.0
0.0	0.80	0.80	0.80	0.80	0.80	0.80
100.0	1.50	1.50	1.45	1.09	0.89	0.83
500.0	6.00	6.00	5.63	2.93	1.48	1.01
750.0	8.00	7.99	7.49	3.75	1.74	1.10
1000.0	10.00	9.99	9.34	4.57	2.00	1.18
2000.0	15.00	14.99	13.99	6.62	2.65	1.39
5000.0	20.00	19.98	18.63	8.67	3.31	1.59

Table B.5

Relative Permeability Data, Well A

S_w	k_{ro}	k_{rw}	P_{cow}	f_w	df_w/dS_w
0.000	1.00000	0.0000	∞	0.000	0.000
0.150	0.95000	0.0000	1.20	0.000	0.322
0.200	0.75000	0.0040	0.66	0.032	0.978
0.250	0.58750	0.0102	0.54	0.098	1.564
0.300	0.44620	0.0166	0.47	0.189	2.058
0.350	0.33250	0.0232	0.42	0.304	2.489
0.400	0.24500	0.0305	0.38	0.438	2.769
0.450	0.17700	0.0392	0.34	0.581	2.837
0.500	0.12000	0.0497	0.30	0.721	2.641
0.550	0.07240	0.0630	0.27	0.845	2.087
0.600	0.03745	0.0797	0.24	0.930	1.299
0.650	0.01627	0.1000	0.20	0.975	0.627
0.700	0.00564	0.1244	0.17	0.993	0.246
0.750	0.00077	0.1525	0.12	0.999	0.073
0.775	0.00038	0.1698	0.08	0.999	0.016
0.788	0.00019	0.1784	0.00	0.999	0.014
0.800	0.00000	0.1870	-0.20	1.000	0.007
1.000	0.00000	1.0000	- ∞	1.000	0.000

(Blair and Weinaug 1969)

APPENDIX C

WELL B DATA

Table C.1

Well B, Data and Reservoir Properties

Data based on Milton, Argabright, and Gogarty (1983)

Location: Big Horn Basin, Wyoming

Formation: Tensleep sandstone

Injected fluids: fresh water, brine, polyacrylamide solution

L = Depth = 4350 feet

V_w = Wellbore volume = 28.0 barrels

C_{sr} = Rising/Falling fluid wellbore storage coefficient = 0.0835 $feet^3$/barrel

C_{sf} = Full wellbore storage coefficient = 0.00047 $feet^3$/barrel

h = Reservoir thickness = 50.0 feet

k = Absolute permeability = 91.0 md.

ϕ = Porosity = 0.15

r_e = External drainage radius = 1320.0 feet

r_w = Wellbore radius = 0.33 feet

p_e = Pressure at the external drainage radius = 1180 psia

p_i = Initial reservoir pressure = 1180 psia

s = Skin = 7.2

μ_w = Water viscosity = 0.70 cp

c_w = Water compressibility = $3.0 * 10^{-6}$ psi^{-1}

B_w = Water formation volume factor = 1.0 res. bbl/STB at 1180 psia

γ_f = Rock specific gravity = 2.68

Table C.2

Adsorption/Retention and Resistance Factor Data, Well B

R_{rfw} = residual resistance factor to water = 1.35

A_{max} = maximum polymer adsorption/retention = 0.020 mg/g

F_c = inaccessible pore volume = 1.00

Langmuir Adsorption/Retention Isotherm

Concentration (PPM)	Adsorption/Retention (mg/g)
0.0	0.000
10.0	0.005
100.0	0.010
500.0	0.015
1000.0	0.019
5000.0	0.020

Table C.3

Apparent Viscosity as a Function of Interstitial Velocity, Well B

	Interstitial Velocity (feet/day)					
Conc.(PPM)	0.01	0.10	1.00	10.00	100.0	1000.0
0.0	0.70	0.70	0.70	0.70	0.70	0.70
250.0	3.50	3.50	2.30	1.40	0.70	0.70
500.0	5.00	5.00	3.00	1.80	0.70	0.70
1000.0	10.00	10.00	5.50	2.00	0.70	0.70
2000.0	45.00	45.00	20.00	6.00	0.70	0.70

Table C.4

Fluid Injection Summary, Well B

Date	Injected Vol. (bbl)	Avg. Rate (bbl/day)	Wellhead Pressure	Fluid Type
7/23-8/18	61700.0	2470.0	360.0	brine
8/18-8/21	2200.0	730.0	0.0	fresh water
8/21-8/26	7400.0	1480.0	160.0	polymer (250 ppm)
8/26-9/4	12500.0	1390.0	250.0	polymer (500 ppm)
9/4-9/14	14100.0	1410.0	380.0	polymer (950 ppm)
9/14-9/21	10200.0	1460.0	385.0	polymer (750 ppm)
9/21-9/23	3200.0	1600.0	370.0	fresh water
9/23-10/17	32800.0	1370.0	200.0	brine
10/17-10/30	22200.0	1710.0	350.0	brine

Table C.5

Summary of Daily Injection Results, Well B

Date	Average Daily Rate (bbl/day)	Average Wellhead Pressure (psig)	Fluid Type
8/19	529.0	0.0	F.W.
8/20	834.0	0.0	F.W.
8/21	776.0	34.0	F.W.
8/22	1132.0	108.0	polymer
8/23	1490.0	123.0	(250 ppm)
8/24	1518.0	140.0	" "
8/25	1505.0	157.0	" "
8/26	1474.0	173.0	polymer
8/27	1475.0	195.0	(500 ppm)
8/28	1472.0	208.0	" "
8/29	1468.0	214.0	" "
8/30	1465.0	226.0	" "
8/31	991.0	137.0	" "
9/1	1439.0	245.0	" "
9/2	1454.0	245.0	" "
9/3	1474.0	252.0	" "
9/4	1474.0	290.0	polymer
9/5	1416.0	310.0	(950 ppm)
9/6	1398.0	325.0	" "
9/7	1424.0	335.0	" "
9/8	1467.0	345.0	" "
9/9	1455.0	370.0	" "
9/10	1464.0	375.0	" "
9/11	1391.0	380.0	" "
9/12	1373.0	380.0	" "
9/13	1398.0	380.0	" "
9/14	1403.0	390.0	polymer
9/15	1471.0	390.0	(750 ppm)
9/16	1454.0	370.0	" "
9/17	1492.0	370.0	" "
9/18	1494.0	380.0	" "
9/19	1473.0	385.0	" "
9/20	1404.0	370.0	" "
9/21	1407.0	365.0	F. W.
9/22	1540.0	370.0	F. W.
9/23	1571.0	370.0	F. W.
10/1	1265.0	230.0	Brine
10/2	1643.0	310.0	" "
10/4	1539.0	260.0	" "
10/8	1381.0	200.0	" "

Table C.5 (continued)

Date	Average Daily Rate (bbl/day)	Average Wellhead Pressure (psig)	Fluid Type	
10/10	1762.0	260.0	"	"
10/12	1416.0	210.0	"	"
10/17	1972.0	380.0	"	"
10/30	1706.0	350.0	"	"

APPENDIX D

WELL C DATA

Table D.1

Well C, Data and Reservoir Properties

Location: Pennsylvania

Formation: Sandstone

Injected fluids: Micellar solution, polyacrylamide, brine

L = Depth = 1800 feet

V_w = Wellbore volume = 50.0 barrels

C_{sr} = Rising/Falling fluid wellbore storage coefficient = 0.3705 $feet^3$/barrel

C_{sf} = Full wellbore storage coefficient = 0.00084 $feet^3$/barrel

h = Reservoir thickness = 17.0 feet

k = Absolute permeability to water = 27.0 md.

ϕ = Porosity = 0.203

p_e = Pressure at the external drainage radius = 300 psia

p_i = Initial reservoir pressure = 445 psia

r_e = External drainage radius = 280.0 feet

r_w = Wellbore radius = 0.375 feet

μ_w = Water viscosity = 1.00 cp

c_w = Water Compressibility = $3.0 * 10^{-6}$ psi^{-1}

B_w = Water formation volume factor = 1.0 res. bbl/STB at 1000 psia

γ_f = Rock specific gravity = 2.68

Table D.2

Adsorption/Retention - Resistance Factor Data, Well C

R_{rfw} = residual resistance factor to water = 11.30

A_{max} = maximum polymer adsorption/retention = 0.020 mg/g

F_c = inaccessible pore volume = 1.00

Langmuir Adsorption Isotherm

Concentration (PPM)	Adsorption/Retention (mg/g)
0.0	0.0000
10.0	0.0001
100.0	0.0010
500.0	0.0050
1000.0	0.0190
5000.0	0.0200

Table D.3

Carreau Rheological Data, Well C

Concentration(PPM)	n	λ	μ_0	μ_∞
0.0	1.00	5.00	1.00	1.00
2300.0	0.55	5.00	3.00	1.30
2800.0	0.55	5.00	5.00	1.70
3100.0	0.55	5.00	7.00	2.20
3430.0	0.42	5.00	8.50	2.30
5000.0	0.30	5.00	20.00	10.00

Table D.4

Apparent Viscosity as a Function of Interstitial Velocity, Well C

Savins shear rate-velocity relation used

	Interstitial Velocity (feet/day)					
Conc.(PPM)	0.01	0.10	1.00	10.00	100.0	1000.0
0.0	1.00	1.00	1.00	1.00	1.00	1.00
2445.0	3.00	2.85	2.01	1.55	1.39	1.33
2800.0	5.00	4.72	3.07	2.19	1.87	1.76
3100.0	6.99	6.59	4.19	2.91	2.45	2.29
3430.0	8.49	7.83	4.30	2.83	2.44	2.34
5000.0	19.98	18.70	12.55	10.51	10.10	10.02

Table D.5

Summary of Daily Injection Results, Well C

Date	Average Daily Rate (bbl/day)	Average Wellhead Pressure (psig)	Fluid Type
2/18	93.0	540.0	micellar
2/19	105.0	755.0	solution
2/20	94.0	875.0	(2300 ppm)
2/21	98.0	1075.0	" "
2/22	82.0	1100.0	" "
2/23	74.0	1085.0	" "
2/24	83.0	1065.0	polymer
2/25	91.0	1050.0	(2300 ppm)
2/26	89.0	1010.0	polymer
2/27	87.0	1070.0	(2500 ppm)
2/28	86.0	1080.0	" "
3/1	87.0	1090.0	polymer
3/2	79.0	1080.0	(2800 ppm)
3/3	77.0	1090.0	" "
3/4	73.0	1095.0	polymer
3/5	70.0	1090.0	(3100 ppm)
3/6	68.0	1095.0	" "
3/7	66.0	1090.0	polymer
3/8	63.0	1100.0	(3430 ppm)
3/9	60.0	1085.0	" "
3/10	59.0	1090.0	" "
3/11	58.0	1100.0	" "
3/12	53.0	1090.0	" "
3/13	53.0	1085.0	" "
3/14	53.0	1090.0	" "
3/15	55.0	1085.0	" "
3/16	54.0	1095.0	" "
3/17	52.0	1085.0	" "
3/18	52.0	1100.0	" "
3/19	52.0	1095.0	" "
3/20	52.0	1085.0	" "
3/21	48.0	1095.0	" "
3/22	47.0	1085.0	" "
3/23	47.0	1090.0	" "
3/24	47.0	1085.0	" "
3/25	50.0	1090.0	" "
3/26	54.0	1095.0	" "
3/27	55.0	1095.0	" "
3/28	51.0	1100.0	" "
3/29	44.0	1095.0	" "
3/30	45.0	1085.0	" "

Table D.5 (continued)

Date	Average Daily Rate (bbl/day)	Average Wellhead Pressure (psig)	Fluid Type
3/31	58.0	1250.0	fresh
4/1	46.0	1090.0	water
4/2	47.0	1095.0	" "
4/3	40.0	1095.0	" "
4/4	61.0	1105.0	" "
4/5	66.0	1100.0	" "
4/6	75.0	1050.0	" "
4/7	67.0	1075.0	" "
4/8	72.0	1085.0	" "
4/9	82.0	1080.0	" "
4/10	68.0	1080.0	" "
4/11	93.0	1085.0	" "
4/12	81.0	1025.0	" "
4/13	60.0	1035.0	" "
4/14	87.0	1100.0	" "
4/15	82.0	1065.0	" "
4/16	80.0	1000.0	" "
4/17	81.0	1085.0	" "
4/18	78.0	1080.0	" "
4/19	80.0	1100.0	" "
4/20	77.0	1075.0	" "
4/21	75.0	910.0	" "
4/22	103.0	1055.0	" "
4/23	93.0	1010.0	" "
4/24	89.0	1095.0	" "
4/25	88.0	1065.0	" "
4/26	84.0	1085.0	" "
4/27	93.0	1100.0	" "
4/28	94.0	1085.0	" "
4/29	98.0	1100.0	" "
4/30	96.0	1110.0	" "
5/1	113.0	1065.0	" "
5/2	106.0	1080.0	" "
5/3	105.0	1085.0	" "
5/4	106.0	1095.0	" "
5/5	104.0	1100.0	" "
5/6	127.0	1060.0	" "
5/7	111.0	1140.0	" "
5/8	94.0	1060.0	" "
5/9	100.0	1050.0	" "
5/10	102.0	1050.0	" "
5/11	100.0	1060.0	" "
5/12	101.0	1050.0	" "

Table D.5 (continued)

Date	Average Daily Rate (bbl/day)	Average Wellhead Pressure (psig)	Fluid Type	
5/13	105.0	1060.0	"	"
5/14	98.0	1100.0	"	"
5/15	97.0	1045.0	"	"
5/16	104.0	1050.0	"	"
5/17	103.0	1100.0	"	"
5/18	99.0	1050.0	"	"
5/19	101.0	1075.0	"	"
5/20	100.0	1060.0	"	"
5/21	105.0	1100.0	"	"